https://doi.org/10.15388/vu.thesis.44

VILNIUS UNIVERSITY
CENTER FOR PHYSICAL SCIENCES AND TECHNOLOGY

Jūratė Jolanta
PETRONIENĖ

Scanning Electrochemical Microscopy for Human Myocardium-Derived Mesenchymal Stem Cells Investigation

DOCTORAL DISSERTATION

Natural Sciences,
Chemistry N 003

VILNIUS 2020

This dissertation was written between 2015 and 2019 at Vilnius University. The research was supported by the Lithuanian Research council, project No. S-MIP-17-13; project No. SEN-21/2015; Project No. 09.3.3-LMT-K-712; Project No. 09.3.3-LMT-K-712-02-0137. 'Research Projects Implemented by World-class Researcher Groups' under Measure No. 01.2.2-LMT-K-7; 'Research Projects Implemented by World-class Researcher Groups' under Measure No. 01.2.2-LMT-K-718 grant No 09.3.3-LMT-K-718-01-0063, "Smart membranes for electrochemical devices", project No. P-MIP-17-490.

Academic supervisor:
Prof. Habil. Dr. Arūnas, Ramanavičius (Vilnius University, Faculty of Chemistry and Geosciences, Institute of Chemistry, Department of Physical Chemistry, Natural Sciences, Chemistry – N 003).

This doctoral dissertation will be defended in a public meeting of the Dissertation Defence Panel:
Chairman – Prof. Habil. dr. Rimantas Ramanauskas (Center for Physical Sciences and Technology, Natural Sciences, chemistry – N 003).
Members:
Dr. Svajus Asadauskas (Center for Physical Sciences and Technology, Natural Sciences, chemistry – N 003),
Prof. Habil. Dr. Eugenijus, Norkus (Center for Physical Sciences and Technology, Natural Sciences, chemistry – N 003),
prof. Habil. dr. Sigitas Tamulevičius (Kaunas University of Technology, Natural Sciences, physics – N 002),
Prof. Dr. Vida Vičkačkaitė (Vilnius University, Natural Sciences, chemistry – N 003)

The dissertation shall be defended at a public meeting of the Dissertation Defence Panel at 13 hour/ on 18 september 2020 in the Inorganic Chemistry Auditorium (141) at the Faculty of Chemistry and Geosciences of Vilnius University.
Address: Naugarduko str. 24.Room 141, LT-03225, Vilnius, Lithuania
Tel. +370 5 219 3105; e-mail: info@chgf.vu.lt.
The text of this dissertation can be accessed at the Vilnius University and Center for Physical Sciences and Technology libraries, as well as on the website of Vilnius University: www.vu.lt/lt/naujienos/ivykiu-kalendorius

https://doi.org/10.15388/vu.thesis.44

VILNIAUS UNIVERSITETAS
FIZINIŲ IR TECHNOLOGIJOS MOKSLŲ CENTRAS

Jūratė Jolanta
PETRONIENĖ

Skenuojančios elektrocheminės mikroskopijos taikymas žmogaus širdies mezenchiminių kamieninių ląstelių tyrimuose

DAKTARO DISERTACIJA

Gamtos mokslai,
Chemija N 003

VILNIUS 2020

Disertacija rengta 2015– 2019 metais [Vilniaus Universitetas, Chemijos ir Geomokslų fakultetas, Chemijos Institutas]

Mokslinius tyrimus rėmė Lietuvos mokslo taryba, ES struktūrinių fondų lėšomis, projektas ‘Nr. 01.2.2-LMT-K-7; ‘projektas Nr. 01.2.2-LMT-K-718 grant No 09.3.3-LMT-K-718-01-0063, “Smart membranes for electrochemical devices”; projektas No. S-MIP-17-13; projektas No. SEN-21/2015; projektas Nr. 09.3.3-LMT-K-712; projektas Nr. 09.3.3-LMT-K-712-02-0137.

„Žmogaus širdies raumens pirminių kardiosferų regeneracinio potencialo ir mechanoptozės tyrimai“ pagal 2017 m liepos 21 d. projekto finansavimo sutartį Nr. P-MIP-17-490.

Mokslinis vadovas:

prof. habil. dr. Arūnas Ramanavičius [Vilniaus universitetas, gamtos mokslai, chemija – P 003].

Gynimo taryba:

Pirmininkas – **prof. habil. dr. Rimantas Ramanauskas** [Fizinių ir technologijos mokslų centras, gamtos mokslai, chemija – N 003].

Nariai:

Dr. Svajus Asadauskas [Fizinių ir technologijos mokslų centras, gamtos mokslai, chemija – N 003],

prof. habil. dr. Eugenijus Norkus [Fizinių ir technologijos mokslų centras, gamtos mokslai, chemija – N 003],

prof. habil. dr. **Sigitas Tamulevičius** [Kauno technologijos universitetas, fiziniai mokslai, fizika – N 002],

prof. dr. Vida Vičkačkaitė [Vilniaus universitetas, gamtos mokslai, chemija – N 003].

Disertacija ginama viešame Gynimo tarybos posėdyje 2020 m. rugsėjo mėn. 18 d. 13 val. Vilniaus universiteto, Chemijos ir Geomokslų fakulteto, Chemijos instituto Neorganinės chemijos auditorijoje (141). Adresas: Naugarduko g. 24, Vilnius, Lietuva, tel. +370 5 219 3105; el. paštas info@chgf.vu.lt.

Disertaciją galima peržiūrėti Vilniaus universiteto, Fizinių ir technologijos mokslų centro bibliotekose ir VU interneto svetainėje adresu: https://www.vu.lt/naujienos/ivykiu-kalendorius

List of original paper by PhD candidate

Paper 1. I. Morkvenaite-Vilkonciene, A. Valiūnienė, J. Petroniene, A.Ramanavicius, Hybrid system based on fast Fourier transform electrochemical impedance spectroscopy combined with scanning electrochemical microscopy, *Electrochemistry Communications*; Volume 83, October 2017, Pages 110-112. https://doi.org/10.1016/j.elecom.2017.08.020

Paper 2. A. Valiūnienė, J. Petroniene, I. Morkvenaite-Vilkonciene, G. Popkirov, A. Ramanaviciene, A. Ramanavicius, Redox-probe-free scanning electrochemical microscopy combined with fast Fourier transform electrochemical impedance spectroscopy, *Physical Chemistry Chemical Physics*, 2019, **21**, 9831 – 9836, DOI: 10.1039/C9CP00187E.

Paper 3. Valiūnienė, A., Petronienė, J., Dulkys, M., Ramanavičius, A. Investigation of Active and Inactivated Yeast Cells by Scanning Electrochemical Impedance Microscopy. *Electroanalysis*. https://doi.org/10.1002/elan.201900414

Paper 4. Jurate Petroniene, Inga Morkvenaite-Vilkonciene, Rokas Miksiunas, Daiva Bironaite, Almira Ramanaviciene, Lina Mikoliunaite, Aura Kisieliute, Kestutis Rucinskas, Vilius Janusauskas, Ieva Plikusiene, Siegfried Labeit, Arunas Ramanavicius, Evaluation of redox activity of human myocardium-derived mesenchymal stem cells by scanning electrochemical microscopy
ID: ELAN4671, https://doi.org/10.1002/elan.201900723, ID: 16687620 Article accepted on 7 February, 2020

Author's contribution to the original papers

Paper 1. The autor designed and performed experiments with synchronized SECM and FFTs devices system for scanning electrochemical impedance microscopy. Also, selected the most suitable materials (sample of conductive and sample of noncoductive) to illustrate hypothesis of events at short distance between the investigated surface and ultramicroelectrode by electrochemical impedance measurements.

Paper 2. The autor planed and performed experiments of electrochemical impedance microscopy with synchronized SECM and FFTs devices, based on natural characteristics of ultramicroelectrodes, to investigate processes in solutions without additional redox mediators at short distances between ultramicroelectrode and surface of interest when hemispherical diffusion is hindered. Author wrote a literature review.

Paper3. The autor observed and proposed an idea for experimentation with activated and de-activated yeast cells; using combination of FFTS and SECM,. presented an action plan for experimentation for undergraduate student, processed results with ZView, plotted graphs, wrote a literature review, actively worked in article writting.

Paper 4. The autor planed and performed an electrochemical experiments on human myocardium-derived mesenchymal stem cells, pathological and healthy cells using redox mediators pair menadione/ menadiol by SECM aproaching curves using different SECM modes. Autor noticed and recorded differences in the data of results depending of cell pathologicity by SECM. Autor wrote a literature review, expermental and other parts of article. Actively worked on correcting manuscript with co-authors.

TABLE OF CONTENTS

INTRODUCTION

Living cell naturally became an object of electrochemical research. The clinical research is raising some questions, that can be answered with active cooperation of other scientific disciplines like an electrochemistry. Electrochemical investigation of a human left verticular mesenchymal stem cells are important and consistent part of cell study and can help medical researchers to improve therapeutic research. Electrochemical non-invasive methods of alive cell investigation are usually directed to processes occouring across the cell membrane. Most important part of such investigation is to keep the cell alive during all time of experiment. A simplified idea for such study would be a surface investigation experiments. Thus, more detailed electrochemical surface investigation is a natural step of traditional electrochemistry, because the surface plays a key role in electrochemical processes, expecially in alive cell investigation.

Requirement to immobilize the object for electrochemical investigation is common due to the properties of many substrates. Electrical conductivity of surface, selected for immobilization, is most important property leading the choise of material as surface for immobilization. As miniaturization is going in all fields of science and industry, a specific needs arise for surface investigation in electrochemistry too. Microelectrochemical methods become a powerful techniques for studying localised processes on/near small objects when processes are lasting a short time. Ultramicroelectrodes, commonly used for scanning electrochemical microscopy reserach, have a large diffusion layer, small overall currents, allow to achieve stable steady-state conditions and are more sensitive to numerous environmental status. The object/surface under investigation can be characterized by electrochemical activity with positive or negative feedback effects in feedback loop, which extends ability to measure the effect with a small disturbance. Reduced time for experiment leads to ability of measurements of short term processes occouring on surface. Electrochemical impedance spectroscopy (EIS) is one of convenient and efficient methods of surface investigation in electrochemistry. EIS measured response of system resistive and capacitive/dielectric properties can be analyzed as a sum of sinusoidal functions (a Fourier series). EIS method is interesting for analysis in electrochemistry because the molecules can be detected without a redox active mediator in the system. Among many convenient EIS measuring devices, fast Fourier Transform (FFT) EIS impedansometer can perform whole EIS spectrum in very short time (less than 2 seconds) in comparison to the capabilities of other popular devices applied for EIS measurements. The scanning electrochemical microscopy (SECM) usually has it‘s own software for EIS measurement, but the time required

for registering EIS is about ten minutes. So, SECM combined with FFT-EIS can be used for redox-probe free investigation in rapidly changing system. The surface analysis by SECM combined with FFTS enabled to register EIS, with controled distance of working electrode, with maximum recording speed of incoming information. An additional feature of FFTS is the ability to get information of electrochemical cell‘s conditions before the experiment, and enables to avoid errors in constructing experiment and increases the data reliability. The combination of these two devices enabled to investigate diffusion processes in a moment of touch a substrate by UME. Scanning electrochemical impedance microscopy (SEIM) using FFTS and SECM combination is reliable way to examine processes close to the living cell surface. An improved non-invasive methods are relevant for living cells investigation.

The yeast *Saccharomyces cerevisiae* cells are well known as suitable for electrochemical investigations like a model of living. They were selected as model in testing the combination’s of FFTS and SECM reliability. More environmentally sensitive are cultivated human heart. left ventricle myocardium-derived mesenchymal stem cells (hmMSC). The SECM is reseach-friendly even for a such sort of soft cells. Looking for ways to extend the methods of SECM usage, investigation of healthy and pathological hmMSC is appropriate sample of cells for SECM measurements.

Menadione or vitamin K is well known and well studied compound. It is important in processes ongoing in tissues and individual cell. Menadione as a redox mediator is well studied and it is easy to attribute electrochemical signals for this compound. So, menadione for investigation and sorting of hmMSC by pathologicity is reliable choise in our investigation. Successful results of a few last years in hmMSC SECM measurements are leaving a space for further development of this method.

Keywords: Scanning electrochemical microscopy, Scanning Electrochemical impedance spectroscopy, fast Fourier Transform electrochemical impedance spectroscopy, ultramicroelectrode, active and inactivated yeast, *Saccharomyces cerevisiae,* left ventricle myocardium-derived mesenchymal stem cells (hmMSC), redox mediator, menadione, menadiol, polytetrafluoroethylene, graphite.

List of Symbols and Abbreviations

AC - alternating current
a -UME's tip conducting part radius
$\mathbf{a_s}$ – radius of substrate
AFM - Atomic force microscopy
C - counter electrode
CPE - constant phase element
CV - cyclic voltammogram
d - distance from surface (tip / substrate distance)
d/a - where d distance between the tip and the substrate and a-tip radius.
EIS - electrochemical impedance spectra
EDL - electric double layer
FFT - fast Fourier transform
FFT-EIS - Fourier transform based EIS technique
FFT-EIS/SECM - EIS method in combination devices FFT with SECM
FRA - frequency response analyzers
G/C-mode-Generaton/ Collection mode
i_T - measured current
$i_{T,\infty}$ - current in volume solution
L - function tip-substrate separation or normalized distance
MD - or Vit-K_3- menadione or **2-Methyl-1,4-naphthoquinone, Vitamin K_3**
MDNaS- 2-Methyl-1,4-naphthoquinone sodium bisulfite
n(W) - exponential number, the phase shift of impedance *vs* applied perturbation.
N - number of transfered electrons
n(CPE) - exponential number of constant phase element
PTFE - polytetrafluoroethylene
PBS - phosphate buffer
O - oksidized form
R - reduced form
$\mathbf{R_{ct}}$ - charge transfer resistance
RG - tip and size of insulating glass sheath surrounding the tip
$\mathbf{r_g}$ - the radius of the insulating sheath around the conducting part
Ref. - reference electrode
RC-SECM - Redox competition mode
Vit-K_1- 2-Methyl-3-phytyl-1,4-naphthoquinone sodium bisulfite
$\mathbf{R_s}$ - electrolyte solution resistance,
(SG/TC)-mode Substrate generation/ tip collection mode
TG/SC mode-Tip generation/substrate collection mode
SECM - scanning electrochemical microscopy
SEIM - scanning electrochemical impedance microscopy
SG/TC - substrate generation/tip collection
UME - ultramicroelectrode
W - Warburg impedance
$\mathbf{W_R}$ - Warburg element, diffusion based resistance
Z - direction- the vertical moving of UME

THE AIM OF THE STUDY:

To synchronize Fast Fourer transform impedansometer and Scanning Electrochemical microscope, for reducing a time of EIS measurements by SECM, with distance control from the substrate, for applicability of unstable and sensitive systems investigation with redox mediators. To demonstrate a possibility to apply FFT-EIS in SECM measurements by this hybrid system for fast/localized registration of EIS spectra at a several distances from conductive and non-conducting surfaces without redox mediators and convenience of this system for living cells by electrochemical activity measurements. To evaluate a possibility of recognition differences of human myocardium-derived mesenchymal stem cells (hmMSC) by pathologicity using SECM approach curves.

THE OBJECTIVES OF THE STUDY

1. To synchronize Fast Fourier Transform Impedansometer and Scanning Electrochemical Microscope for electrochemical impedance measurements with aproach conductive and insulating surfaces by SECM, using redox mediator pair in phosphate buffer pH6.8, to find ways to reduce time of EIS measurement at several distances from conducting (graphite) and non-conducting (polytetrafluoroethylene (PTFE)) surfaces in the presence of $[Fe(CN)_6]^{3-}/[Fe(CN)_6]^{4-}$ (hexacyanoferrate) as a redox-couple.
2. To demonstrate the possibility to apply FFT-EIS in SECM measurements (FFT-SEIM) for fast/localized registration of EIS spectra at several distances (0 to 200μm) from conducting (graphite) and non-conducting (polytetrafluoroethylene) surfaces in a redox-probe-free mode (without any additional redox probes), which will open new applicability for this hybrid method in investigations of such samples that are sensitive to redox compounds (*e.g.* living tissues, cells and some other biological samples). than EIS measurements are registered at distances from 10μm to minimum possible from the surface.
3. To demonstrate the possibility to apply FFT-EIS in SECM measurements (FFT-SEIM) for fast/localized registration of EIS spectra at several distances from yeast *Saccharomyces cerevisiae* surfaces with purpose to show possibility to observe differences in measurments depending on cell‘s viability.
4. To demostrate ability to measure the redox activity differences in cell’s reaction to menadione, using healthy and pathological hmMSC, by different SECM modes. To demonstate the ability of SECM for developing a new model for the investigation of hmMSC intracellular redox status depending on cell pathologicity

SCIENTIFIC NOVELTY:

1. Electrochemical impedance spectra (EIS) were performed at points then cyclic voltammetry curves dynamic is changing from Faradaic process to nonfaradaic, using Fast Fourier Transform Impedansometer combined with Scanning Electrochemical Microscopy for distance control.
2. EIS spectra were performed in redox-probe free, nonstable conditions, when oxygen participates as redox mediator, when UME is at distance from substrate less than 10 mikrometers or 2 d/a to 0 using samples of carbon materials with different electroconductivity: Polytetrafluoroethylene (PTFE or Teflon) as an insulator and graphite as a conductor.
3. EIS spectra were performed near the surface of immobilized active and deactivated yeast *Saccharomyces cerevisiae,* for investigation differencies of living (active) and died (deactivated) yeast cells samples electrochemical properties.
4. SECM measurements were performed on patological and healthy human heart mesenchymal stem cells for identification of membrane permeability in close to a natural for cells enviroment, using redox mediator menadione/menadiol.

STATEMENTS FOR DEFENCE:

1. The combination of devices Fast Fourier Transform Impedansometer and Scanning Electrochemical Microscope can be used for Electrochemical Impedance measurements in short distances between ultramicroelectrode and surface for investigation (conductive and insulator) in redox probe free conditions and also in using redox mediators pair, when Faradaic processes are observed.
2. The proper distance for surface investigation by SECM combined with FFTS in redox probe free conditions is not more than 2 d/a.
3. EIS performed by FFTS combination with SECM can be applied for yeast *Saccharomyces cerevisiae* viability measurements using redox mediators menadione/ menadiol pair. The maximum distance from gold ultramicroelectrode and yeast sample appropriate for determination of electrochemical activity of yeast cells is 2 d/a, which is still suitable for efficient investigation of yeast cell activity by FFT-SEIM.
4. SECM aproaching curves measurements performed using menadion/menadiol redox mediator couple, applied for patological and healthy human heart mesenchymal stem cells is suitable as method to register a differences of cell's interaction with menadione depending on pathologicity of cells, when the distance between UME and cell is not more than 3d/a.

1. LITERATURE REVIEW

As the science is going on progress, it is necesarry to expand existing methods for investigation of a small objects [1]. The concept of microelectrode, as working electrode, was defined in early of 20th century and opened a new posibbility for analysis of processes on the electrode surface [2, 3] and arround it. The idea to create smaller electrodes adapted for studies *in vivo* for biological objects were published first in 1942 [4] by P.W. Davies and F. Brink Jr. Over the decade after this publication, various electrochemical techniques has been developed, including voltamperometry [5] for a small value signaling. Almost at the same time, ultramicroelectrodes (UME) [2, 6] were proposed to be used for opening up new possibilities for the electrochemical analysis and electrode processes. A new era in electrochemistry started when A. Bard [7] a positioning table of optical microscope adapted for the ultramicroelectrode position control [8, 9]. A new class of microscopy emerged. It was named a scanning electrochemical microscopy (SECM) [7]. This technique is still developing and have widely applications for any electrochemical research object: corrosion processes [10, 11], alive cells and tissues investigation [12], surface mapping [13, 14] and etc. Various experimental techniques were aplied for SECM: scanning vibrating electrode technique [15], scanning reference electrode technique [16], local electrochemical impedance technique [17]. SECM was conbined with other devices to expand posibilities of experiment: with Atomic force microscopy [13, 18, 19], surface plasmon resonance [20].

The Fast Fourier Transformation method for electrochemical impedance microscopy (EIS) was applied by Smith [21] is still developing. The main possibility of this setup is to obtain EIS at any point in the cyclic voltammogram. G. Popkirov and Schindler [22] measured simultaneously in two electrochemical cells at constant potential in one and constant current in the second found a method to separate the incoming signal. A new electrochemical impedance spectrometer developed and announced in 1992 year [23] and was succesfully applied [24-27]. Synchronization of SECM and FFTS devices leads to improving posibbilities of existing devices with additional features [28].

1.1 Study of electrode processes

Faradaic and nonfaradaic processes represents two different modes on electrode. Both processes, Faradaic and nonfaradaic,were discussed by many authors but some uncertainties are left [29]. The volume solution around the ultramicroelectrode (UME) is serving as reservoirs in which can be established a constant chemical potential (activity) of the ionic, atomic or molecular species

participating in redox reaction. When reactants are coming from volume phase to electrode and after the products are going back and the charge is transfering out of UME- it is a Faradaic process. Reactants and products are parcitipating in charge transfer reaction, they also can act in chemical steps without charge transfer, they can adsorb or desorb, dissociate or react in other ways. The main requirement for a process to be Faradaic is electronic charge transferring away from electrode, which demands involvement of reactants and products moving in and out a volume solution. An oxidation/reduction processes presenting in charge transfer is ruling by Faraday‘s law and it is faradaic process too. In non Faradaic or capacitive processes the charge stays at the electrode [30, 31]. This is then is no real charge transfer across the electrode interface. The volume phase around the electrode is serving the redox spieces for electrode processes and guarantees a stability of system. Poliarization curve (*i*-V) and Cyclic voltammetry is most universal electroanalytical technique for studying electroactive spieces and for characterizing processes on electrode [5, 32]. Not only charge transfer reaction is going on electrode, but a chemical steps without charge transfer such as adsorb/desorb surface can take place in parallel. In summary, nonpolarizable and ideally polarizable electrodes terms line up with differences between a Faradaic and Non Faradaic processes [29, 30]. On ideal polarized electrode no charge transfer accross interface can occour. Only nonfaradaic processes can occour on ideal polarized electrode. Adsorbtion presented in electrical double layer changes is not described by Faraday‘s law and it is non Faradaic.The real electrode is with all Faradaic processes. They are two categories: an activation energy is too high when Faradaic process is insignificant or activation energy is low. Electrodes at which Faradaic processes occur are named charge transfer electrodes [30]. Process, then electric current pasage is changing the potential of the electrode- is the polarization [29, 30]. The polarization causes changes in double layer on electrode surface [33]. In slow charging process the double layer can be equated as a capasitor with some leakage because of resistance presented in paralell. Current whitch is passing across the two phase boundary but did not involved in changing charge of double layer is the Faradaic current [30, 34]. The uncompensated resistance is the resistance of solution left between working electrode surface and reference electrode probe [35]. It is a serious problem when electrolyte is low concentration and it can arise from inherent resistivity of material of which a working electrode is constructed or inadequate electrochemical instrumentation. Uncompensated resistance depends on distance separating working and reference electrodes. It limits a choise of electrochemical cell‘s geometry. In electrochemical literature are many publications dedicated to uncompensed resistance problem, solution and ways to avoid it. A geometry of working ultramicroelectrode according authors [35-38] determine registering

signalin electrochemical cells.There exist many experimental methods of measuring systems with uncompensated resistance using ac methods [39] or electronic compensation using positive feedback [40].

1.2 Ultramicroelectrodes for surface investigation

Ultramicroelectrode (UME) is a conductive disc made from platinum,gold or other conductive material and covered arround by insulating part from glass (fig.1). Ideal shape of electrode the conductive part should be in the geometric center of the glass part, but real geometry of electrode is slightly with error. The real UME of our experiments are presented in fig.1.

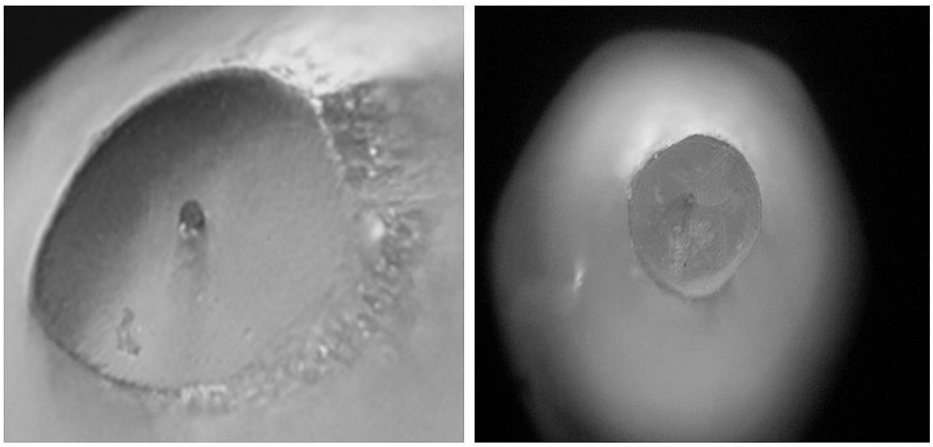

Fig.1. View of UME‘s working part samples. Real electrodes with non-ideal geometry. Photo were did by optical microscope CETI Medline Scientific, (Oxford, United Kingdom) (magnification of CETI microscope is SP 40x / 0.65 / 160 / 0.17) with digital camera.

For SECM measurements as usuall are carried out with a disk-shaped electrodes, because of they best sensitivity in comparison with electrodes having a different geometry.

The ultramicroelectrode [2, 6] geometry can be characterized by dimensionless **RG** value whitch describes a ratio between radius of insulating sheath ($\mathbf{r_g}$) placed around the active electrode part **(a)** is presented in eq.1.[41].

$$\mathbf{RG=r_g/a} \qquad (1)$$

Where $\mathbf{r_g}$ *radius of insulating sheath,* **a-** *the active electrode part*

Some difficulties are appearing than insultating part of UME is very large- it may contact with sample in a short distances. The flux of redox species to a small conductive disc by diffusion is quite large and the convection does not influence the current.. The current on a small disc reaches steady-stateconditions in a very short time. For example a 10μm radius disc will reach a steady-state in a few seconds. As usual the UME‘s aproach curves are provided the normalized current as function of normalized distance (eq.2).

$$\mathbf{I=i_T/i_{T,\infty}\ ;\ L=d/a} \qquad (2)$$

Where $\boldsymbol{i_T}$*-measured current,* $\boldsymbol{i_{T,\infty}}$*- current in volume solution,* ***a****- is radius of tip,* ***d*** *- substrate distance.* ***L****-function tip-substrate separation or normalized distance*

Then an insultating part (**RG** less 10) is very small- it leads to UME damaging. This ojective reason determines the acceptable diameter insulating part of UME. The ideal UME for electrochemical experiments is still developing and with new technologies a nanosize UME‘s are used for SECM experiments. In our experiments the platinum and gold UME‘s were applied, and RG was calculated for every set of experiments.

The behavior of UME in volume solution has been described by many rewievers [42, 43]. Typical cyclic voltammogram (CV) for the UME is a sigmoidal shape. The CV is very informative method to evaluate the cleanliness and cleaning of UME surface.

Than a biological signals are recorded with a standart size electrode, a significant noise component are coming from the elekctrode with limited resolution of biopotential recordings [44]. But SECM with UME‘s enables to investigate differences in less then a micron length scale [45]. The posibility to obtain a steady state currents without a convection allows to use UME as a scanning probe, across the surface for large variety of electrochemical processes [46, 47] without limitation of charging current or uncompensated resistance [7, 48-50]. Size of UME is most important for the investigation of a living cell. Investigation of a single cell can be performed without disturbing a concentration profile of a mediator, formed around the cell by tip reaction [51]. As it was written above, each UME is of individual geometry, due to some imperfections in manufacturing processes. Ussualy the conductive part of electrode is slightly shifted from a geometrical center of insultating part. This geometrical inaccuracy have an influence on all results, expecially for a horizontal scanning. Many authors are investigating this issue, how a geometry of UME affects on results [2, 3, 52-54]. To prevent some artefacts in measurements, for that reason, usually are provided a normalized current in data describing [7, 55]. It is important that the

normalized curves are independent of the mediator concentration [56]. The understanding of electrochemistry at a small electrode surface is very important for understanding of operation Scanning Electrochemical Microscope (SECM). As usual for SECM measurements, a two mediator couple is using for this kind of experiments. A mediator which can not permeable the membrane is using as electron shuttle to UME. In recent year the imaging of biological cells is actively developing.

1.3 Conductive and Insulating Surfaces for EIS Measurements

A carbon is the best for investigation for conductive and insulating properties due to its universality as a chemical element generating multitude of materials. One of natural carbon form is a graphite. Pure graphite (every carbon atom can be bonded to 3 other carbon atoms) is one of most chemically inert material. Natural and artificial graphites have some impurities and defects and dislocations in structure. The surface energy of graphite depends on its cristalographic defects and areas with different directions of layers. So, graphite as material with less defects and large crystals have best chemical resistance. The engineered graphite have amorphous structure with less then natural based disorders [57]. An amourphous carbons have sections of hexagonal carbon layers with some parallel layer in structure. The carbon as a material for electrodes is very atractive. A nonporous carbon electrodes has been well rewieved [58] and can be used for investigation as conductive material sample. Then graphite electrode may contain some narrow pores. The double layer capacity of electrode with unknown number of defects can not be predictable. Carbons with a higher percentage of edge orientations could have higher capacitance [57]. Low capacitance is recorded when a basal layer of the graphite is exposed to a solution [59]. The porous carbons have an extremely large surface areas and are working as supercapacitors. Carbon nanomaterials are applied for energy conversion or storage and sensing. These applications require a fast electron transfer. A carbon/solution interface processes are not well understood completely [60].To measure an electrochemical properties of the carbon is very complicated, because it easily accumulating an organic contaminants. A capasitance of graphite placed into the solution is growing in time depending on structure defectiveness. In our reserarch a low density graphite rod was applied as a sample of conductive material and for investigation of the yeast cell viability.

Polytetrafluoroethylene (PTFE or Teflon) [61, 62] is synthtetic fluoropolymer, nonreactive, noncorrosive, insulating, hydrophobic properties because of high electronegativity of fluorine. PTFE was discovered in 1938 by Roy Plunkett [63]. The fluorine atoms surrounding the carbon chain are working as protective shield,

transforming this material to very inert, relatively dense polimer, with very strong carbon-florine bonds and lowes known a coefficient of smoothness. The porous PTFE films can be positively or negatively charged at room temperatures [64]. In our experiments a 3 milimeter thick graphite plate was used as conductive and PTFE plate as an insulating material sample.

1.4 Investigation of Surfaces by Scanning Electrochemical Microscopy

The Scanning Electrochemical Microscopy (SECM) is technique accetable for quantative investigations of interfacial physicochemical processes [65, 66]. SECM is well reviewed by many authors [45, 67]. Using controlled mobile UME , the SECM is useful for investigation of metal corrosion [68], investigation of charge transfer mechanisms [69], biological systems investigation and imaging of their surface [70-72], for gas/liquid interfaces [73], adsorbtion/desorbtion processes [74] and redox processes. This technique is suitable for the potentiometric or activity/topography investigation, enzyme or biomaterials. The substrate, which can be solid or liquid, perturb the electrochemical response of the working electrode tip. This perturbation provides information about substrate properties. Most informative method of the SECM is aproach to substrate measurements i.e. aproach curves. Aproach curves enables to register a current differences in an vertical direction. A quantitative desription of approaching curves can be obtained by diffusion eguations of a UME and substrate shown in eq.3 [75]. As written above, these curves are presented in dimensionless form by plotting the tip current normalized by current in volume solution *vs* **L=d/a** where tip- substrate separation is normalized by the tip radius. Then the plot is of only normalized dimensionless variables, it did not depend on concentration or diffusion coeficient of redox species [76]. The aproach curves for insulator depend on $\mathbf{r_g}$ (a ratio between radius of insulating sheath. There are major SECM apreometric methods i.e. feedback and generation/ collection modes.

Feedback Mode (fig.2) is most common mode based on a feedback of signal coming from device to system under investigation and coming back to registering device [9]. Aproach curves measured in Feedback mode (FB-mode) are very informative and suitable for determination a distance between UME and sample, for calculations of kinetics reactions, substrate electrochemical activity and etc. The FB- mode is then the electroactive species are reduced or oxidized at the tip, and steady-state current is generating by hemispherical diffusion (fig. 2A) in volume solution. With aproach to a conductive substrate, a reduced species are forming on the tip and are oxidizing on a conductive substrate surface, then a positive feedback is creating. If an electrode is placed very close from substrate,

a diffusion of the solution species to the tip are blocked. The reaction that couses a decreasing in current is a negative feedback. If the substrate is conductive or it is generating conductive species, at a short distance between tip and substrate, the increase of current can be detect (positive feedback). Then tip is approaching to a conductive surface, a reduced species are forming at the tip. They are oxidizing at the conductive surface. The tip current is increasing, the „positive“ feadback appears (fig.2C). Positive and negative feedback effects enable the imaging surface and the reactions on it.

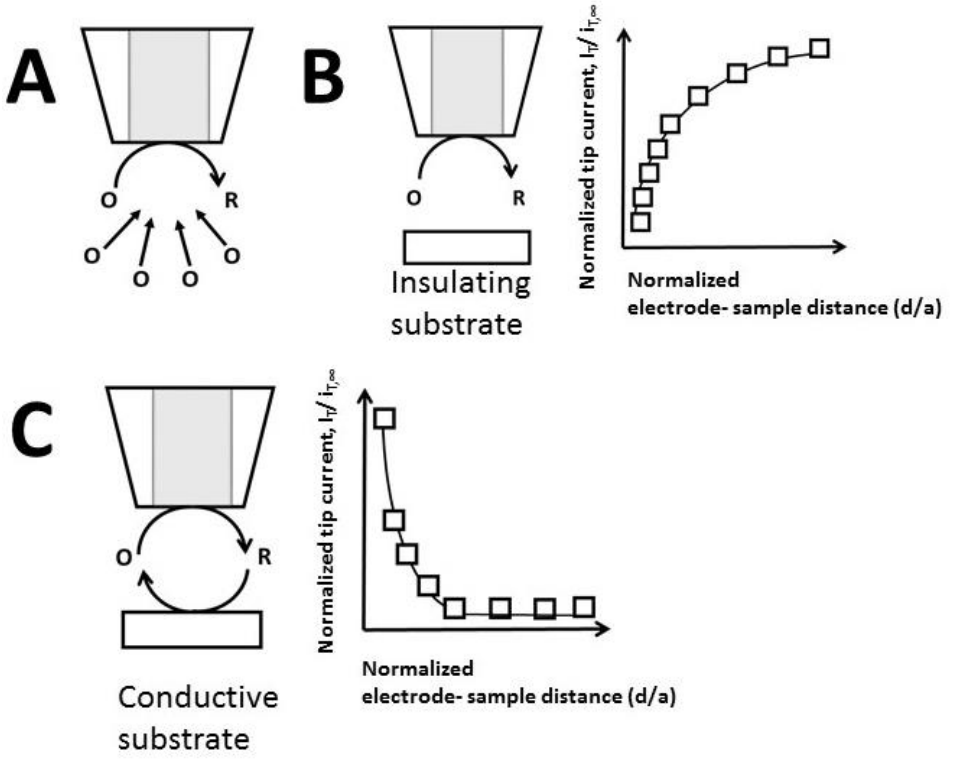

Fig. 2. Hemispherical diffusion at steady-state conditions. B) Approach curve at negative feedback mode C) Aproach curve at positive feedback mode

A different effect is observed when tip is approaching to insulating surface (fig.2B). Then oxidized species can‘t be regenerated and a diffusion to the working electrode is limited- in this situation, a „negative“ feedback is creating. For detecting by UME the reaction which is occoured on surface of the sample, it must be a measureable additional flux of conductive (reduced) species towars the UME. Approaching curve for an insulator surface depends on $\mathbf{r_g}$–value, because the insulating part of UME is blocking a diffusion and a negative feedback is observed. So, the FB- mode allows to investigate conductive or insulating surfaces. A surface imaging and reactions occouring on surface can be registered

by this mode very clearly [77]**.** The FB- mode is widely used to investigate electron transfer kinetic mechanisms [78]. It is a several mathematical models describing results of FB-mode [79, 80] FB-mode can be applied calculation of electrode geometry [8, 76].

Redox competition (RC-SECM) mode- tip and substrate compete/consume for the same electro-active species [81]. This mode developed and desribed by Schumanns group [81] is usefull for investigation of substrates then oxygen is consumed on UME and on surface of substrate at the same time. RC-SECM is very effective technique to investigate hydrogen evolution and hydrogen oxidation processes, local non-homogenic segments on substrate, for evaluation of oxygen reduction reaction [81]. High activity areas on a sample decrease the current measured at the tip. In our work RC-SECM mode was used in stem cell ivestigation.

Generation/ Collection modes. There are few types of this Generaton/ Collection modes (G/C-modes). It is a potentiometric G/C, where the tip is a potentiometric sensor, and two amperometric modes. Generation-Collection modes were developed for investigation of a local chemical properties

Potentiometric G/C mode. In this mode the tip is traveling within a diffusion layer produced by the substrate. A passive sensor-tip did not change concentration profile of the redox species generated on a substrate. This mode is proposed for a steady-state conditions for a small substrate, generating a stable amount of the redox species. In this mode can be measured a concentration gradient by ion-selective tip[82]. The UME positioned at a fixed distance from the substrate can be used as a concentration change sensor for a kinetics measurements, when is proportionality between heterogeneous reaction rate and generated products concentration [83].

Amperometric G/C modes. Tip generation/substrate collection (TG/SC) and **substrate generation/tip collection (SG/TC) modes**. In this SECM-modes species are generated on the one surface and can be collected on a second. In **TG/SC**- mode the UME is generating electroactive species(reactants) and substrate can detect them if it is connected as a second working electrode. If reaction $\mathbf{O}+n\boldsymbol{e}^{-} \rightarrow \mathbf{R}$ occours at the tip, the opposite reaction is detected on substrate-electrode:$\mathbf{R} - n\boldsymbol{e}^{-} = \mathbf{O}$. TG/SC mode is useful in array scanning, for mapping electrocatalysts, for measurement of homogeneous chemical reactions, for measurement of homogeneous chemical reactions. For expample, in an oxygen reduction reaction, one can generate oxygen at the tip at constant current and measure change the substrate current changes, i.e. how much of the oxygen is it collected.

Substrate generation/ tip collection mode (**SG/TC**)-mode is the historically first SECM-type mode. It was applied for a measurements then the tip collects the

reactions products occouring on a substrate. For expample, during the aproach a concentration profile can be found, or during array scan can be identified a different reaction rate on surface.It is useful for investigation concentration gradient near an electrode surface. This method can be used to measure SECM induced adsorption/desorption on substrate, i.e. adsorption/desorption kinetics of a proton in a hydrous metal oxide surface in unbuffered solution then tip is near surface and is reducing the proton to a hydrogen at the tip. [74]. Thus, the UME current in this mode can be used for studying the kinetics of proton desorption and diffusion on the surface.

This UME‘s detection ability is limited in time, i.e. the UME is registering the current changes at a given moment, although the reaction may be continued. Execially this is a problem during experiments with living cells [76]. In SG/TC experiments is important tip size and substrate size. If substrate (**a_s**) is large enough in comparing to tip size (**$a_s \geq a$)**, the resuls may be influenced by thickness of the diffusion layer on tip and on substrate. The teoretical description of this measurement is difficult because of moving of UME stirs a diffusion layer on substrate [76].

Surface imaging by SECM. The main principle of surface imaging is then UME is moving in the X Y directions at constant distance or constant height and acording to measurements is generating a map of surface (fig. 3). There are a several SECM imaging modes: amperometry, potentiometry, constant current, impedance, by aproach curves in every point of surface. Amperometry mode can measure a current of horizontal area at constant height. Potentiometry mode is useful for measuring a potential of probe response *vs* position on constant height from surface. A constant current mode is then the UME position is ajusting by a vertical direction based on a current value. If the substrate is an insulator, this method can be used for surface imaging too. An impedance measurements can be performed at controled probe position or probe in a constant height with specified frequency and amplitude. The AC measurements can get in the one experiment the topography and reactivity of sample.

A horizontal line or array scanning can be performed in constant height or constant distance.The results of horizontal scanning is 3 dimensional image of investigated surface. If a sample contains conductive and nonconductive structures on it, to recognize electroactivity of sample is available by feedback modes. The resolution in SECM investigation of surface depends on tip radius and distance between a tip and sample.Than relief on surface is smaller than UME radius, the constant height is more appropriate. According to SECM theory the current dependence on distance most appropriate resolution of results is than the distance from UME to substrate is less than a distance 5 time longer than UME

radius (d/a). The reliable way to confirm accurate distance UME *vs* substrate is still a qeustion in SECM researchers community. It is some problems, a surfaces tilt.The surfaces roughness have influence on measurement results too. This problems can be solved by “MIRA” mathematical program [84-86]. and Cornut math models [80, 87]. This problem of surface tilt is very important in measurements of living cells. The cells derived from natural tissues are irregular dimensions, they can move out from electrical field generating by UME, they are soft, easily can be damaged by contact with UME. On other hand the cells are sufficiently elastic for pressing.Successful measurement can be performed, if UME is not touching the cell. Imaging processes of molecular flux from membranes,or living cells is decribed by Mirkin, Mauzeroll, Schuhmann and others, but every year a lot of articles are published on biological systems imaging [88-90]. Surface imaging is very appropriate for enzymes and sensors investigation (fig.3).

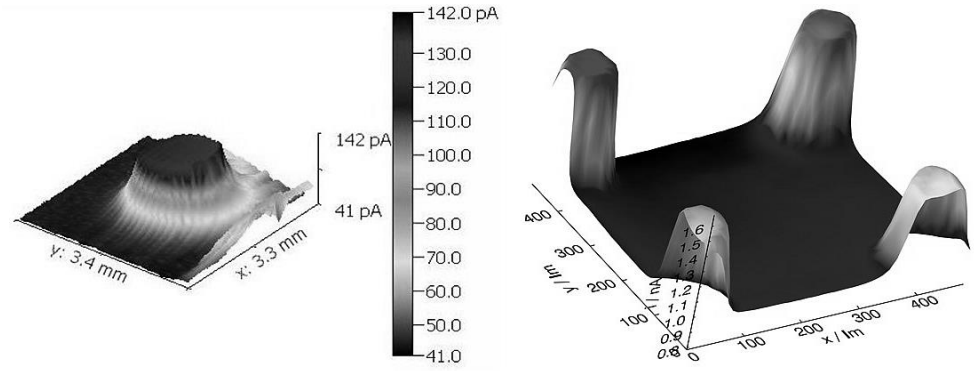

Fig.3. a) Sample array scan of glucosse oksidase (GOx) drop with 0.1mol/L glucosse in PBS immobilized on plastic (non-conductive) Petri dish. **b)** Array scan Gox drop immobilized on gold dots (conductive) with 0.1mol/L glucosse in PBS

Mediators for SECM measurements. Most of a measurement by SECM are applied for a kinetics measurements, very fast processes investigation, double layer events and adsorption [74]. The SECM can be used for surface modification [76]. Redox reactions studies by SECM success depents on selected mediator. The mediator must be stable in both O and R forms at selected pH. Very often decision is determined by redox potential of mediator. For biological experiments the oxygen can serve as a UME reduced species under conditions where negative feedback is expected [76]. Menadione (MD) as mediator for living human cells was desribed by B.Liu, L. Alonso and M.V. Mirkin [89, 91-93]. Menadione or vitamin K_3 is important for living organisms funkcion and cardiocascular health

[94]. Electrochemical investigations of this compound is one of ways to determine its circulation accross the cell membrane. Standard potentials of MD [91] is a parameter regulating a selected potential range for stability during experiments. To analyse correctly SECM measurement results it is necessary to take in account some principle. The Kinetic SECM experiments for macroscopic and microscopic substrates are going different. A size of a substrate is important when the substrate radius/ tip radius dimension is less then 1. Acording to Bard it is possible to identify a particles 10 to 20 times smaller then tip by SECM if this particles are well separated [76].

1.5 Electrochemical Impedance Spectroscopy

In a classical impedance spectroscopy it was usually measured one frequency at a time by a frequency response analyzer (FRA). In 1929 Kramer and Kronig [95] made first step for the realization of a dynamic impedance spectroscopy, than all the frequencies are measured at once. In 1945 the method was developed by Bode and applied to electrochemical impedance spectrum (EIS) finally [96] D.D. Macdonald was published a review of EIS history [97]. Hence, electrochemical impedance spectroscopy (EIS) [98] also called AC impedance spectroscopy [99] allowed a recording of a large data sets, with good accuracy of measurements and analyzed by fast Fourier transform (FFT). But this method is with some limits on a lowest frequency accessibility [100]. A full EIS was done at 1970‘s, with apearance of a potentiostats, a frequency response analyzers (FRA), and become a standard method of results analysis at present moment. EIS data are analyzed by fiting to an equivalent electrical circuit model. The model is containing a common electrical elements: a resistor, a capacitor, an inductor, a Warburg element. The impedance of a resistor is independent of frequency and did not has an imaginary component. The impedance of an inductor is increasing as a frequency increases. The capacitor impedance decreases as the frequency is raising. The resistance of an electrolyte depends on concentration of conductive parts in electrolyte and geometry of UME. A doubler layer capacitance on working electrode depends on electrode potential, electrode rougthness, adsorption and etc. The idealized electrical equivalent circuit containing simplest version is known as a Randles Circuit, the common for EIS, and can be used as a model of a processes with a single electrochemical reaction [101]. This model desribes a solution resistance, a double layer capacitor, charge transfer or polarization resistance. Impedance representation by a Nyquist Plot composed of real and imaginary parts describes a featuresor a system. Another common representation of EIS is a Bode plot, where impedance magnitude and phase angle are ploted angainst a frequency. In summary, the EIS as a method of system analysis is sensitive, non-destructive

technique for an electrical response of chemical system [102]. EIS is suitable to characterize a responce time of chemical system by using an alternating current (AC) voltages over a frequencies range, then a known voltage is passing from the UME through an electrolyte into a counter electrode (C), and ions are acting as a resistors to hinder an electron flow. The electrolyte resistance is determinated by comparing input and output voltages and recorded by reference (Ref) electrode. A polarization resistance gives an information about limitations of charge transfer between the working electrode and an electrolyte interface. Improving of a well known methods, gives a new capabilities for EIS investigation. Hence, improvement of SECM impedance measurement tool by combination with FFTS device, is a powerful technique for the evaluation of a local electrochemical changes on a various surfaces in comparing with publications [28, 30, 98, 103-108].

There are two main strategies described in literature for an impedance data analysis: FFT-EIS and dynamic multi-frequency analysis (DMFA) [109]. Using FFT-EIS method the data are processing in this shedulle: all data are divided in sections and each section is elaborated singulary by Fourier transform, and after a dynamic impedance calculation of Z are performed [110]. So, FFT-EIS method has the advantage in time for determining results.

Non-faradaic EIS method is an excellent technique to capture subtle changes of interactions at the electrode-solution interface without the need of a redox molecules [111-114]. By EIS it is easy to capture changes on the electrode-electrolyte interface [115] when is analysing a conductivity, dielectric constants and capacitance of system. The most imortant in EIS techniques is measurement‘s time and ways to reduce it [102]. The variety of electrode processes are containing the similar stages: a double electric layer, an ohmic resistancem charge transfer resistance of electrochemical reaction, an adsorbed layers, diffusion and etc [98]. EIS enables to distinquish a dialectic and electric properties of every component in an electrochemical system, with time-dependent information about the changes ocouring during the investigation. The localized impedance measurements could be performed in a wide range of frequencies, while the surface of interest is scanned by an UME. The small size of the electrode or UME (<25mm in diameter) allows to observe the fast electro-chemical reactions [116]. The physical modelling of the EIS and fitting to supposed models the experimental spectra enables to extract physico-chemical parameters of the electrode/electrolyte boundary [102, 103]. However, conventional EIS-based techniques represent only an averaged response of the whole electrochemical system. So, to get more advanced mapping of the electrochemical system, the SECM has been merged with EIS. This combined technique is named scanning electrochemical impedance microscopy (SEIM), and can be applied in EIS-based mappingand or other

investigations of surfaces [117-119]. In the SEIM-based technique, a localized impedance measurements can be performed in the range of frequencies when the surface of interest is scanned by UME. Therefore, a detailed electrochemical information can be extracted at each measurement point [103]. The SEIM is an important electrochemical technique, which provides a lot of information about electrochemically active or redox active surfaces parts. The measurements based on SEIM technique, performed by conventional EIS-spectrometers or SECM AC tool, take a very long-time due to point-by-point collection of the data for every EIS spectra [119, 120]. Time is the main limiting factor in the application of SEIM for the investigation of fast processes. Some different generation of Fourier Transform Electrochemical Impedance spestroscopy method were created [102, 121]. The problem related to the slow collection of EIS spectra could be solved by the fast Fourier transform based EIS technique (FFT-EIS) in new way [100, 122, 123] which was developed and advanced by Popkirov and Schindler [23, 124], because FFT-EIS allows the measurement of the EIS spectra simultaneously at 30–50 different frequencies. This device is perturbed electrochemical system not by the consequently applied perturbations at different frequencies, but by the superposition of perturbations applied simultaneously at 30–50 frequencies. All frequencies are multiples of the lowest one, and they increase linearly in a logarithmic scale. This method enables us to reduce the duration of EIS registration by 5–20 times in comparing with conventional EIS-equipment. Therefore, FFT-EIS can be applied in the study of very dynamic electrochemical systems [125] where the data were analyzed by fast Fourier transform (FFT) algorithm[110].

According to A. Valiūnienė [27] the charge transfer resistance (***R**_{ct}*), in a parallel with a constant phase element (***CPE)***, depends on the distribution of insulating and dielectric features at the electrode/electrolyte interface. The constant phase element, (***CPE)***, is attributed to a double electric layer capacitance, in the equivalent circuit and is representing non-ideal capacitor, which matches with an non-homogenity of the interface. The dimensionless parameter **n**, or the exponential number, shows a shift of phase of impedance *vs* applied perturbation. If the UME surface is homogenous, then **n** will be equal to 1 [27]. A low level signal, named a Warburg impedance with linear diffusion, without an adsorption, is characterized by phase angle of 45^{o} [126]. So, the Warburg element, (***W***), is representing the impedance of diffusion [27]. The EIS usually are analyzed by Nyquist and Bode plots [127-129]. As it was mentioned above, the carge transfer is leading Faradaic and nonfaradaic components. The Faradaic component in this case is from an electron transfer of the reaction and is exposed by polarization resistance (**R_p**), with solution resistance (**R_s**). The nonfaradaic current is from charging the double-layer capacitor (**C_d**). The electron transfer rate is

determinated by mass transport of a reactant and a product. The electron transfer registered in EIS, depends on consumption of the oxidants and the production of reactants near the UME surface [102]. The EIS can be used as tool to detect an immunological binding events, occourring on the electrode surface, also for cells toxicology investigation, or monitoring changes in cells morphology [130] with no requirement of a redox mediator.

1.6 Electrochemical Investigation of *Saccharomyces cerevisiae* Cell Surface

Bioelectrochemical methods of investigation the intracellular enzyme activity is very important to understand the cell physiology. The cell viability is important feature of biosensors quality and reliability. So, SECM and EIS investigation of living cells as a noninvasive quantitive analysis method is very actractive. Expecially for intracellular redox enzyme activity, using the redox mediators that shutle electrons between intracellular enzymes and extracellular electrode [51, 131-134]. Mauzeroll and Bard investigated the cellular formation of menadione-S-glutathione conjugate, and the efflux of the conjugate from the cells using GC-SECM mode [90]. A label-free or redox mediator free impedance measurements were studied by several authors [102, 128, 135-139]. In a past few years, the immobilized yeast cell based systems have been widely investigated and used in different fields of biotechnology, pharmacy, biomedicine, food and environmental technologies [28, 140-144]. In these areas *Saccharomyces cerevisiae* (*S. cerevisiae*) cells, well known as a baking yeast, are mostly used as a model for the imitation of eukaryotic cell's behavior. These cells are simple in use as a biological-recognition component in cell-based biosensors or as a 'electrical current generators' in the microbial biofuel cells [131, 145-147]. *S. cerevisiae* is a good living model for the evaluation of cytotoxicity studies[148]. Manipulations with them are uncomlicated. Yeast are low cost and their genome is very well sequenced. A survival rate of *S. cerevisiae* is high enough. They are viable in a different experimental conditions, including aerobic and anaerobic conditions at varying pH [149, 150]. Actually there are some significant differences between *S. cerevisiae* and mammalian cells, but *S. cerevisiae* in many experiments can substitute the mammalian cells, which are very sensitive to environmental factors. There are many reports about manipulations and electrochemical investigations of the yeast cells [90, 151-153]. However, the number of reports on the immobilization and investigations of non-viable *S. cerevisiae* cells islimited, yet [154-158]. Though, non-viable yeast cells are not able to proliferate, but they can contain some active enzymes, therefore they remain important object in bio-systems for the evaluation of living cell properties, as active enzymes can carry out many catalytic functions, actually after the losing cell's viability [159-161].

There are multitude different electrochemical methods, which are appropriate for the investigation of the yeast cells, including the SECM [153, 154, 162] and EIS [155, 156]. The SECM as it was written above, is a useful technique for cell surface analysis of a wide range of processes occuring at electrochemically active interfaces and of course for quantitative investigation [69]. The SECM is rapidly developing technique, ussualy is used in scanning probe electrochemistry, SECM provides ability to analyze and visualize i.e. mapping electrochemical activity of different surfaces [10, 26, 27]. Simultaneously, the EIS is a non-destructive method too, which is providing helpful models on the effect of AC on the living sample. As is known, the EIS enables registering quantitative data of system, which determines properties of electrode/electrolyte boundary [28, 102, 103, 163, 164]. Conventional EIS-based technique are representing only average response of a whole electrochemical system. The SEIM as previous was mentioned enables localised EIS measurements with detailed electrochemical information extracted at each point of measurement [117-119, 153, 165-167]. However, the main problem of combined SECM and conventional EIS techniques (SEIM techniques) is low mapping rate of the SEIM, so, this method is not enough suitable for the investigation of electrochemically active interphases with fast changing properties of samples based on living cells. Therefore, trying to find advanced application of SEIM for the investigation of biological objects, in our researches we were trying to resolve this problem by applying fast Fourier transform based EIS technique (FFT-EIS) [23, 124, 168, 169] which allows to reduce the duration of EIS signal registration by 5-20 times in comparing to time required for conventional EIS equipment. It was demonstrated and desribed in this work, that FFT-EIS can be applied in SECM measurements (FFT-SEIM) [28, 170] for the fast and localized registration of EIS spectra at a several different distances from conducting or non-conducting surface in the presence of the redox mediator couple [2] and in the redox-probe-free mode [170]. The application of FFT-SEIM in SECM measurements enables to reduce significantly the time of measurements because the evaluation of the EIS in the actual frequency range (1.5 Hz to 50 kHz) at any single UME position takes only 1.3 s. The applicability of this combined SECM and FFT-EIS based techniques (FFT-SEIM) was desribed in this research work for the evaluation of redox activity of immobilized the active and inactivated *S. cerevisiae* yeast cells.

1.7 Investigation of Alive Human Cells

In recent years, SECM was applied for biological-modified surfaces including living cells. The living cells as an object of investigation are very sensitive to changes of enviroment. They are unpredictable, not stable and are changing during

experiment. The living human myocardium-derived mesenchymal stem (hmMSC) cells has ability to withdraw from place with unfavorable conditions and can excape from area with electric field generated by UME during experiment. The multiple test are required to ensure the reliability of the results for living cells. The stem cells cultured in a lines are most stable and similar, but today‘s requirement is to find a way to diagnose a disease in any route. A chemical reactivity of a living single cell can be investigated in real time by SECM [45] without invasion on cell. The non invasive SECM measurement respiration activity, of oxigen consumption was done on single bovine embryos in 2001 [171]. A mixed metastatic and nontransformed cells were sucessfuly indetificate by SECM imaging on the basis of their lower reactivity to quinone mediators [172]. The imaging techniques by SECM were developed for mapping cultured neurons [173]. The topographic images of cells usually are obtained using hydrophilic redox mediators, which can not penetrate cell‘s membrane [174]. For that sort of investigation the living cells can be derived from different tissues for different purposes: for diagnosics, for tissue repair and for electrochemical investigation, too. Traditionally, stem cells therapy concept is the isolation of stem cells from patients, differentiation *in vitro,* and susequent re-injection autologous cells into the patient [175]. One of many methods of stem cells processes control can be SECM. Three-dimensional cell culturing conditions, compared to the traditional two-dimensional conditions, have been shown having many positive influences to the cells [176]. Cells grown in spheroid 3D bodies can more tightly interact with each other and influent extra- and -cellular signalling, proliferation and differentiation capacities, energetic status, redox responses and other [177]. The ability to monitor the redox activity of the cells by consumption of different redox mediators have been also shown by other authors [178, 179]. Advantage of GC-SECM modes is that measurements can be performed at higher distance from the investigated surface, since the reaction at the surface of interest occurs independently on the presence of SECM probe (ultramicroelectrode, UME). This helps to ensure that the cells will not be damaged by UME. Additionally, SECM can also register electrically conductive materials secreted by the cells [180]. In SECM measurements, as a redox mediator, very often is used menadione (MD) simulating generation of intracellular $O_2^{\bullet -}$ [181, 182]. MD is a membrane-bound electron carrier with structure similar to that of ubiquinone easy penetrating the cells [183]. Scanning electrochemical microscopy (SECM) is a useful tool for the investigation of cells *in vitro* under their natural growth environment [184, 185].

2. MATERIALS AND METHODS

2.1 Chemicals and materials

All chemicals used in electrochemical experiments were purched from Merck, Fluka, Carl Roth, AppliChem, Alfa Aesar companies and where higest available purity. The 3 mm diameter graphite rod „ultra F purity“ 99.999%, (CAS 7782-42-5) low density, diameter (surface area 0.071 cm^2) as an electrode and a conductive surface sample, was purchased from Carbon Division of Carbon USA, RAVEN-M. and polytetrafluoroethylene (PTFE) (CAS No. 9002-84-0) 3mm thickness sheet from Merk/ Sigma-Aldrich, Berlin, Germany. Phosphate buffer solution (pH 6.8) was prepared in deionized water (with conductivity of 0.05 μS). 24 h before the experiment. $K_3[Fe(CN)_6]$ (CAS No. 13746-66-2), $K_4[Fe(CN)_6]$ (CAS 14459-95-1), NaH_2PO_4 (CAS 7558-80-7), Na_2HPO_4 (CASNo. 10028-24-4) and KCl (CAS 7447-40-7), were purchased from Sigma-Aldrich Chemie GmbH (Taufkirchen, Germany). Hexacyanoferrate-based redox couple was dissolved in PBS buffer, pH 6.8, 1 h before the experiment and stored in a dark room at ambient temperature. *Saccharomyces cerevisiae* (commonly known as baker's yeast) were bought in granular form from food supplier LALLEMAND (Lublin, Poland). Menadione (2-methylnaphthalene-1,4-dione CAS No.: 58-27-5; 98%), Menadione sodium bisulfite (CAS No.: 130-37-0; 95%) from Sigma- Aldrich St.Louis, USA. 2-methylnaphthalene-1,4-dione (MD) was dissolved in 96 % ethanol. The 0.25 mM concentration of MDSNa was prepared in deionized water, 0.25 μM MD was dissolved in 96 % ethanol. Iscove's Modified Dulbecco's Medium (IMDM) and fetal bovine serum (FBS) were purchased from Gibco (Langley, USA). 100x penicillin and streptomycin solution was purchased from Merck Millipore (Carrigtohill, Germany). Fibronectin was purchased from Sigma Aldrich and gelatin from Calbiochem (San Diego, USA). 0.5 mol/L H_2SO_4 (CAS 7664-93-9) solution for UME cleaning by CV was made before every cleaning procedure. An aluminium oxide polishig paper from Sensolytics SECM, code of product 04-01003, 0.3μm ground size, was used a several times for electrodes surfaces cleaning

2.2. Electrodes and electrochemical procedures

a) For insulating and conducting surface investigation, a disk-shaped gold and platinum ultramicroelectrodes (UME) (diameter 10 μm, calculated area 7.85 × 10−7 cm^2) were purchased from Sensolytics (Bochum, Germany). The thickness of the UME glass shield was about 50 μm. Before the experiment the UME consequently was polished with a polishing paper with a grain size of 0.3 μm,

washed in ethanol, UME was electrochemically cleaned in 0.5 M H_2SO_4 by 50 cyclic voltammetry (CV) cycles, the potential range from −0.02 V to +1.7 V *vs.* Ag|AgCl|$KCl_{sat.}$, the scan rate of 0.2 V s^{-1}, step 0,02 V. The quality of cleanliness was checked by CV in PBS: from -0,55 V to +0.6 V, the scan rate of 0.2 V s^{-1}. The sigmoidal form of CV with the same results of anodic and cathodic part of CV was an indication of cleanliness of the UME. For SEIM measurements the UME was positioned at several different distances from the graphite or PTFE surface and FFT-EIS spectra were registered. FFT-EIS experiments were performed in the presence of 0.02 M of hexacyanoferrate at +0.2 mV *vs* Ag|AgCl|KClsat determined from CV based experiments in the potential range at which Faradaic current was observed. The applied frequency range of AC was between 1.5 Hz and 50 kHz, ensuring the registration of the whole EIS at 30 frequencies within 1.3 s. A possible damages of UME were controled by CV in PBS and under the optical microscope after every sequence of experiments.

b) For immobilized yeast cell investigation a disk-shaped platinum ultramicroelectrode (UME) (diameter 23 μm, calculated geometric surface area $4.15x10^{-6}$ cm^2) was used as a working electrode, Ag|AgCl|$KCl_{(sat.)}$ was used as a reference and platinum wire – as a counter electrode. The UME cleaning and cleanleness control procedures were performed as usual

c) The carbon (graphite) rod as an electrode, was sealed into a silicone tube to avoid a contact of electrode side surface with solution i.e. to guarantee a stable area of conducting surface. The prepared electrode was polished by home made polishing mashine to mirror smoothness and washed in deionized water. Before each experiment when graphite was used as an electrode, it was polished with polishing paper and washed in deionized water

d) All microelectrodes for investigation of the living cells were cleaned process in a simmilar way, using an electrochemical and a mechanical cleaning steps After the cleaning procedure of the UME, a steady-state current value was recorded, for calculating an active electrode surface using formula eq. 3. A cooper wire, a conection of UME was polished by emery paper as required.

2.3 Preparation and immobilization of Yeast Cells Sample

Whereas, an active yeast cells are those, which can grow, reproduce and carries out metabolism [169], a suspension of active yeast concentration 0.1 g cm^{-3} was prepared in deionized water according a biochemical protocols[186]. The suspension of active yeast was incubated in 30 °C temperature with constant stirring for 30 minutes. Plastics Petri disch, diameter 50 mm cleaning is desribed below. An activated yeast cells suspension drop was placed on prepardedfor immobilizarion plastics Petri dish and sample was carefully dried. To prepare

inactivated yeast cell sample, the suspension with active cells was stored at 75 °C temperature for two hours [187] and after cooling down to ambient temperature the suspension was immobilized in the same way as a suspension of an active yeast cells. A plastic Petri dish, which was made of poly(methyl methacrylate), was got such cleaning path: it was washed with 96 % ethanol solution at first and dried After it was placed above a glutaroaldehide vapor for 15 mins, dried and washed by deionized water and dried again. Then a drop size 0.5 μL of yeast suspension was placed on the bottom of petri dish and then it was dried out, and fixed by keeping above 25 % glutaroaldehyde solution for 10 minutes. The thickness of yeast sample (fig.4) was measured by Atomic force microscopy (AFM).

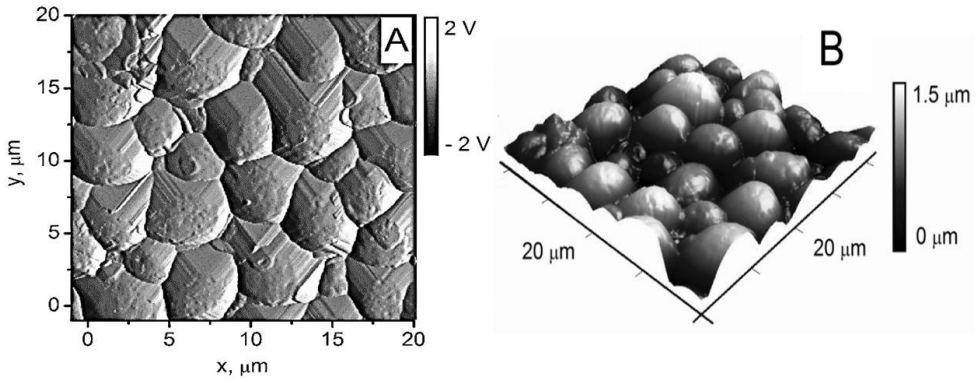

Fig. 4. AFM visualisation of immobilized yeast cell layer, **A** – view from the top, **B** – 'side view'.

The AFM measurements were carried out by Atomic Force Microscope (Bioscope II)/Catalyst from Veeco (Santa Barbara, USA) at room temperature in air. The soft MicroMash silicon probes CSC17/AIBS with nominal elasticity constant of 0.5 N/m and nominal curvature radius of 7 nm were used. The taping mode was used for the imaging. (Author thanks for AFM imaging performed by Assoc. Prof. Dr. Inga Morkvenaite- Vilkonciene)

2.4 The hmMSC preparation for SECM measurements

Isolation of hmMSC from human ventricle myocardium. All samples of hmMSC were got from Department of Regenerative medicine, State Research Institute Centre for Innovative Medicine, Vilnius, Lithuania. The hmMSC cells were completelly prepared for SECM investigation in electrochemical lab and after experiments all biological samples were returned back. Based on information provided by scientist from Department of Regenerative medicine, the cells for electrochemical investigation were prepared for research in this desribed

below in following order. After biopsies the hmMSC were isolated following the publiched protocols with some modifications [188]. The samples of normal (healthy) and pathological hmMSC of cells were seeded on 12 mm cover glass plate in 3 cm diameter Petri dishes in the IMDM with 10 % of FBS, antibiotics. After this procedures, this glass plate with hmMSC cells was placed into an electrochemical SECM cell containing a 3 electrodes and filled by a culture medium. The SECM measurement of one single cell lasted not longer than 30 min, which did not significantly changed cell's viability, as it was noticed by cells provider lab. Information about measurements of cells viability (less than by 5 percent) was done using CCK-8 reagent (data not shown) in Innovative Medicine Center lab.

Ethical statement This investigation on the hmMSC was conducted according to the principles expressed in the declaration of Helsinki. The inveestigation was approved by the local Ethic Committee (license No. 158200-14-741-257). All the patients gave a written informed consent to include their data in the study for each investigational procedure.

2.5 Instrumentation

2.5 1. Electrochemical cell for experiments

A three-electrode based electrochemical cell was applied for all steps of the SECM experiments, where UME (platinum or gold) was connected as a working electrode, Ag |AgCl |KClsat. – as a reference electrode, and platinum wire – as a counter electrode, was applied for electrochemical measurements. Only for FFT EIS measurements 4 electrode electrochemical cell with Pt sense electrode was used. For FFT-SECM EIS measurements a distance from working (UME) electrode and reference (Ag/AgCl in KCl) was set 10 millimeters. Counter (Pt wire) was placed in 10 millimeters from both electrodes (W and Ref.). During measurements of hmMSC's a small homemade Ag|AgCl|KClsat reference electrode was used. For all SECM measurements a „Sensolytics SECM" designed electrochemical cell was placed in grounded Faraday's cage. A tilt of electrochemical cell was investigated by aproach curves at the edges of substrate. The correction of a tilt of the electrochemical cell was based on $\boldsymbol{Z}$ coordinate differences and by adjusting bolts intedrated in the cell's holder. Plastic Petri dish as an electrolyser was used for all experiments on living cells and was incorporated into industrial Sensolytics SECM electrochemical cell for tilt control. A modified structure of plastic Petri dish, for conductive sample and insulator attached into a bottom of it, was applied for the SECM on the same principle.

2.5.2 Scanning electrochemical microscopy

Scanning electrochemical microscopy base model Nr. 03-00002, a nominal resolution of 1 nm (<10 nm repeatability) and software from Sensolytics, Bochum, Germany assembled with potentiostat/galvanostat AUTOLAB PGSTAT 30, managed by NOVA 1.10 was used. The Sensolytics SECM program contains: an electrode 3D positioning, line scan, array scan, AC-measurements, cyclic voltammetry and other. The aproach curves measurements were the first step of all measurements by SECM. The horizontal scan was used for surfaces imaging, as a control step for main investigations. The SECM was applied for all investigation of a redox activity measurements, the positioning of UME and for control of distances for all experiments. The array scan as preliminary study was applied to determine an electrochemical activity of surfaces. In our experiments it was applied the FB-mode, R-C mode, G/C mode.SECM measurements, in combination with fast Fourier transform (FFT) impedance spectrometer, described below [189]. The SECM was applied for all EIS measurements as positioning tool of UME control, replacing a SECM software EIS.

2.5.3 Fast Fourier transformation electrochemical impedance spectroscopy

The EIS were registered using the Impedance Spectrometer EIS-128/16 designed in University of Kiel [124, 189] (Germany), with fast Fourier transform (FFT) function, which enables registration of whole EIS within 1.3 s, with applying AC in the range between 1.5 HZ to 50 kHz range.

FFT-EIS spectra for the redox-probe-free investigation were potentiostatically registered with applied potential of −1.2 V *vs.* Ag|AgCl|$KCl_{sat.}$ in 4 electrodes electrochemical bath, in phosphate buffer (PBS) pH 6.8. At this potential a Faradaic current was observed. The gold UME, (calculated area 7.85 $\times 10^{-7} cm^2$) was positioned at a several different distances from the surface and aproach curves by SECM or FFT-EIS spectra were registered according to the experimental design.

FFT-EIS experiments with a two redox mediator system, in the presence of 0.02 M of hexacyanoferrate, at potential +0.2 mV *vs* Ag |AgCl |KCl_{sat} were performed. The appropriate potential was determined from CV. Measurements were performed in a potential range at which Faradaic current was observed. The applied frequency range of AC was between 1.5 Hz and 50 kHz. The registration of the whole EIS spectrum was at 30 frequencies. The reference electrode and UME were placed as close as it is possible to each other using a Luggin capillary. Every EIS measurement was performed in the frequency range from 1.5 Hz to 50 kHz, applying 3 consecutive

multi-sine signals. The amplitude of the perturbation signal was chosen 10–15 mV in order to avoid non-linearity in the response of signal. The obtained EIS were validated by comparing the power spectra of perturbation and response in the way described in the relevant article [189]. For EIS measurements the UME was placed at a several distances from the surfaces less than 10 radius of the UME. It was expectated to register the impedance spectra with different positive/negative-feedback behavior. In amperometric mode,the positive-feedback can be observed, while approaching the conducting surfaces, because the negative-feedback is mostly obtained when approaching non-conducting surfaces, also on surface with small spots of conductive or with very thin layer of redox species genereating surface

2.5.4 Steps of yeast cells investigation

The potential was set to everyone type of experiments after it was determined from CV in PBS solution, pH 6,75- 6,8, containing 12.5μM of MD and 12.5μM menadione sodium bisulfite, both compounds acting as a redox mediator, in order to adjust the most proper electrochemical parameters, which were applied later to EIS and SEIM based investigation of *S. cerevisiae*. The location of the *S. cerevisiae* cells was revised by an optical microscope CETI Medline Scientific, (Oxford, United Kingdom) (magnification of CETI microscope is SP 40x / 0.65 / 160 / 0.17) with digital camera and by the SECM horizontal scanning. Statistical analysis and calculations of EIS measurement of the yeast cells was done as written in following text. EIS data analysis software "ZView" was used for the determination of electrochemical characteristics under a selected equivalent circuit model. The Nyquist plots of experimentally obtained EIS data and observed fitting results are presented in the corresponding figures below. The thickness of yeast *S. cerevisiae* spot was examined by atomic force microscope, (AFM), (Bioscope II)/Catalyst from Veeco (Santa Barbara, USA) at the room temperature in air, using a tapping mode optical microscope. It was determined that a thickness of yeast *S. cerevisiae* drop is 1.5–2.0 μm, which is in agreement with previuosly published our results [190]. So, the 'zero distance' in SECM measurements of yeast *S. cerevisiae* was set at 1.5 μm from the surface of the Petri dish. Then active yeast *S. cerevisiae* cells were immobilized on a graphite electrode during the same procedure of immobilization as it was applied for the immobilization of yeast cells on the petri dish (as it described in section 2.3). Two vitamins, Vit-K_1 and Vit-K_3, were introduced into an electrochemical cell as the redox mediators, using two different ways and the EIS depending on the selected system were registered at a given time periods:

(i) the 'System 1': 12.5 μM of Vit-K_1 and 12.5 μM of Vit-K_3 were added into the PBS (pH 6.8) solution located in the Petri dish with early immobilized

yeast cells; the EIS registration started instantly after the addition of vitamins (redox mediators pair) into the PBS solution.

(ii) the 'System 2': 12.5 μM Vit-K_1 and 12.5 μM Vit-K_3 was added onto immobilized anddried yeast cells drop, when a PBS solution was added. The EIS registration started only after the addition of the buffer solution to the Petri dish with immobilized before the yeast cells and pretreated with vitamins/ redox mediators.

All the EIS measurements in this part of experiments, were carried out at the ambient temperature, at the frequency range of AC between 1.5 Hz and 50 kHz. The EIS experiments were performed using platinum UME, RG=5 were performed at potential-1.2 V *vs* Ag|AgCl|$KCl_{(sat.)}$ selected from CV. However the EIS spectra of graphite electrode (diameter 3mm) were recorded at -0.84 V *vs* Ag|AgCl|$KCl_{(sat.)}$ considering to the CV results. For the EIS, the AC-perturbation amplitude of 10-15 mV was applied, in order to avoid non-linearity of the response signal. As usual, the EIS spectra were evaluated using "ZView" program. The fit results were presented in graphs using OriginPro 9.0.

2.5.5. Statistical analysis and calculations of hmMSC measurements results

The steady-state diffusion-controlled current was used to normalize the experimentally observed tip (UME) current. It was related to the initial concentration of the redox active species, when the UME is far from the hmMSC cell's surface, by formula (3) [152]:

$$i_{T\infty} = 4\, n_e\, F\, D\, C\, a; \tag{3}$$

where n_e is a number of electrons involved in a reaction on the UME, F – Faraday's constant, D – diffusion coefficient, C – concentration of MD and a – radius of the UME.

A Hill's equation with some modifications, was used to calculate a cooperativity of MD with the hmMSC [149].

$$\mathrm{i}_T = i_{max} \cdot [MD]^n / (k^n + [MD]^n) \tag{4}$$

i_T – UME tip current, n – Hill number, k – kinetic constant, showing the concentration of MD at which half of the maximal current was registered.

The ***k*** is often used in basic enzymatic catalysis described by Michaelis-Menten kinetics. The statistical analysis was performed from three independent measurements. For the each type of cells it was done measurements of a single cell and the results of three cells of each type for every measurement was done. All data of measurements were summarized and the statistical analysis was done using Excel programme at 5% significance level. All data are presented in tables (6 and 7) as means ± standard error (Mean ± SEM).

2.5.6 On detecting appropriate parameters for hmMSC experiments

The potential set for all type of experiments was found from CV as in a previous studies. Conventional EIS measurements near the hmMSC surface, as a system testing step, were performed using potentiostat/galvanostat FRA by registering an EIS in the frequency range of 50 kHz – 1.5 Hz, the collection of EIS spectra lasted for 8 min (not shown here). The most convenient SECM parameters for the hmMSC investigation, were chosen from CV. The CV cycles were done with adition of different concentration of MD from 1 to 200 µM, which was added in to the hmMSC cell growth media, but without the cells. The sample of differences of CV are represented in (Fig. 5). The CV in cell growth media with MD showed the most stable current at potential range are between -200 mV and -400 mV for

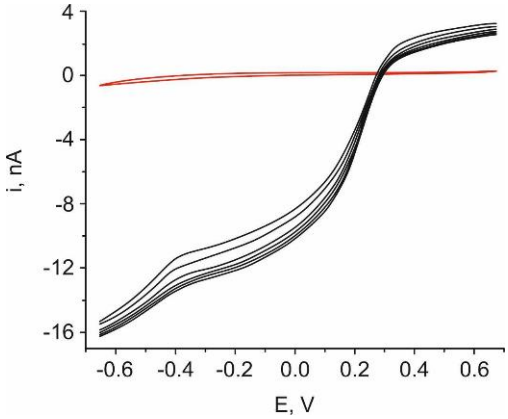

Fig. 5. Determination of CV in cell's growth media without the cells. Red line - CV in full composition cell's growth media. Black line - 10 µM of MD was added to the cell's growth media. Scan speed was 0.01 V/s, potential range was from 0.65 V to -0.65 V, step of potential 0.005 V. The positive and negative potentials for further experiments were chosen based on this CV curves.

non-Faradaic measurements. The other selected potential, -500 mV, was within the Faradaic current range. It has been used for the further measurements at a negative potential. In the sigmoidal CV curve shape, at positive potential range, mostly stable was at potential between +300 mV and +400 mV. So, The +400 mV potential was chosen in order to prevent any Faraday process in solution and to record current changes occurring only due to the products released by the hmMSC.

The immobilized cell suitability for experiment and the location on a surface for all experiments, was determined by a light microscope with digital camera (Fig. 6 B). After this procedure, additionaly adjusted location of the cell was identified by the SECM horizontal scanning at a negative FB- mode. The horizontal scan was performed at the distance about 15 µm or 3d/a from expected distance from the cell surface. A first the search of the cell was performed with addition 0.02µmol/L of $K_3Fe(CN)_6$ and after without additional electrolytes, and was chossen because the cell growth medium contains some electrolytes, sufficient amount to perform electrochemical search of cell location [45]. The lowest current point (Figure 6a) shows the cell location. The decrease of current value from 1.5 nA to 0.5 nA was reliable to confirm the location of the cell. The point marked by an arrow (Figure 5a) was chosen for the further vertical scans of cell by the SECM. To find out when the cell is damaged, it was performed experiment with pressing UME to a surface of the glass plate (Fig. 5C).

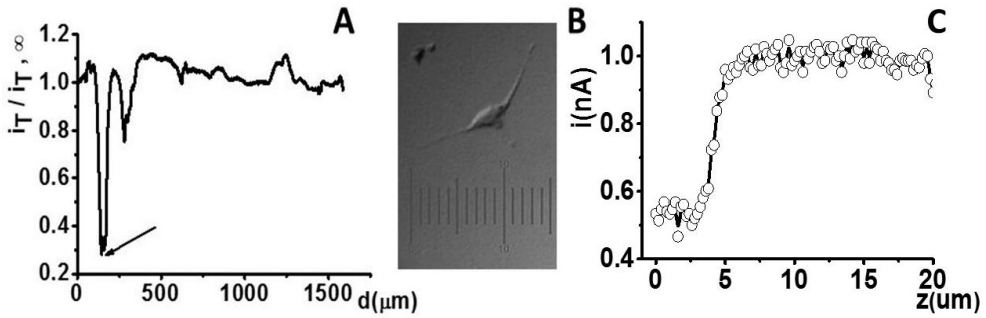

Fig. 6. Determination of the hmMSC position on surface. (A) Horizontal linear scan, FB-mode, UME- Pt 10µm *vs* Ag/AgCl, UME potential of +400 mV. Step 0.5 µm, scan rate 10 µm/s. Black arrow shows a point selected for aproach by the SECM. (B) The cell optical image before the SECM measurement made by light microscope with side light (C) Aproach curve to the hmMSC with damaging it. UME- Pt10 *vs* Ag/AgCl; +400 mV. Step 0.5 µm, speed of approaching 1 µm/s

The reliable distance from UME, or the "zero distance" from the cell surface was found in a few steps. At First, the aproach curves were made in the area of a sample, where was no immobilized cells. The UME was retreated 15 µm (3d/a)

and horizontal line scan was done. When location of cell was found, the next aproach curve was done by pressing the cell to the bottom of the Petri dich to investigate the change in current when a cells is damaged. Based on this measurement it was selected current value when to stop the UME's aproach to cell surface. Before the completely damage and UME's touch to plastics Petri dish it was registered a little current growth (Fig.6 C). A point then UME was stoped before damaging cell was named the "zero distance". The position of UME coordinates were set for all followed experiments near this one cell.

In the SECM measurements for the redox conversion investigation in the hmMSC cell, the current changes was registered by the UME in culture medium containing MD at varying distances from the immobilized cells (Fig. 7). It is known, the MD can diffuse through the cell membrane and is reduced by an intracellular nicotinamide adenine dinucleotide phosphate (NAD(P) NAD(P)H)-depending enzymes, which is transfering two electrons and two protons to MD [46–49]. The reduced form of MD or menadiol (MH_2) can diffuse from the intracellular part of the cell to the extracellular solution around the cell. In the SECM measurement, RC-SECM mode, the UME is registering the current, which is directly proportional to the initial amount of MD in solution (Fig.7 A). The dependencies of current *vs* distance were registered in the RC-SECM mode by vertical or **z**-direction, approaching to the cell's surface to "zero" distance. The GC-mode SECM measurements were performed at a positive potential with retracting the UME from the cell surface in order to evaluate the presence of MDH_2.

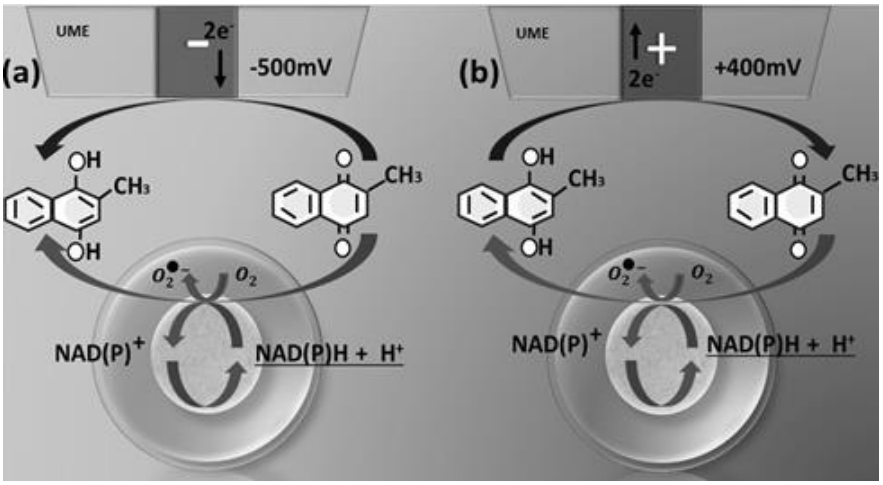

Fig. 7. SECM-based investigations of redox-conversion of MD to MDH_2 in both types of human heart hmMSC. (A) RC-SECM mode, (B) Using GC-SECM mode.

The current change was registered near the single cell's surface, which can be described by the equations presented of other authors [149]. All the measurements in this study were done over three steps. First, an approaching curve was registered at a negative -500 mV potential, measurement was done in the absence of redox mediator in the solution. A second step, the mediator MD was added into the solution and finally – the retracting curve was registered at a positive was selected +400 mV potential. The increase of current in the system is due to removal of the menadiol from the single hmMSC. The last step was a aproach measurement at -500 mV potential, to collect information about menadiol leavings in liquid.

3. RESULTS AND DISCUSION

3.1 Hybrid system based on Fast Fourier transform electrochemical impedance spectroscopy combined with scanning electrochemical microscopy

The gold (Au) UME was positioned at several different distances from conductive (carbon) and non-conductive (teflon) surfaces, with the expectation that registered EIS will show the same positive/negative- FB behavior, which is the specific for amperometric mode of SECM. Not only a FB behavior was determined. Also some additional information about processes occurring at a different distances from the surfaces using Au UME was observed. In amperometric SECM mode, a positive-FB can be observed while approaching a conducting surfaces, as it expected. A negative-FB is mostly obtained when UME is approaching non-conducting surfaces [8, 191] The involvement of the conducting surface in the electrochemical process is the main reason of current increase, when UME is approaching a conductive surface. The positive FB can be obtained when UME is approaching an unbiased substrate, even so, the current is lower than approaching a biased substrate [192]. As it is known, at a negative FB mode, the diffusion of electrolyte to UME is blocked by the non-conducting surface, because of UME‘s glass shell diameter. of both positive and negative-FB behaviors, by SECM theory, are mostly observed at distances which are equal to several UME radiuses from the investigated surface. FFT-EIS results (Fig. 9) is showing a charge transfer resistance (Rct) dependencies on a distance, when UME is approaching the graphite unbiased surface: far from the surface R_{ct} is a slightly higher, and it is decreasing when the UME is approaching the conducting surface, for example the graphite (Fig. 9A). The contanct quality of graphite and conductive part of the UME, or the „zero“ distance, is the main factor of the efficiency of positive-FB behavior on UME. Therefore, the direct contact or the „zero“ distance of the graphite sample and UME was achieved when amperometrically was registered a positive FB by approaching SECM curve. So, during the next step of experiment, the distance between UME and graphite was set a 2d/a, and FFT-EIS spectra were registered. The same procedure was performed at other represented in figure 7, all distances while approaching the graphite surface, definitively. When the UME was approaching a non-conductive, a PTFE surface, a negative-FB behavior in system was observed (Fig. 10). According to the SECM theory, a negative-FB in this case, is a limiting factor for the diffusion of the redox mediator hexacyanoferrate ions. Due to the hindered diffusion of the hexacyanoferrate ions, higher R_{ct} was registered at the ‘zero’ distance, in comparing to a registered at distances up to 1d/a. At 2d/a distance between the UME and graphite surface, a Nyquist plot shows that it is only a

charge transfer as limiting factor, The diffusion part in equivalent circuit is not observed (Fig. 9) for UME with this geometry. If an amperometric measurements are performed faster, an electrochemical reactions kinetics on the surface can be calculated. The EIS measured at the different distances from the surface can provide much more information about all processes which are occurring in the electrochemical cell. Using this experimental setup, the combined FFT-EIS/SECM is exploitable, because the measurement are as fast enough. As it is noticed in the literature, that a hindered diffusion has a notable influence on amperometrically results, measured near the conducting or non-conducting surface by UME. But an electrochemical impedance measurements show that with approaching the conducting surface, the limiting factor is a charge transfer, in an opposite to the non-conducting surface, which depends only on diffusion rate of redox mediator molecules. The localized EIS was investigated in the different distances from the conducting platinum surface in previous research by other authors [193]. Impedance at a different distances was evaluated in some previous studies too [194-196]. During our first attempt to combine the FFT-EIS and SECM techniques of positive- and negative-FB modes of SECM were examined at the different distances, and a notable influence of the diffusion of the redox species towards UME was observed. According to the SECM theory, in the negative-FB the significant diffusion-limited current can be observed at the distance which is equal from one to two conductive part of UME radiuses. In the positive-FB, the diffusion-limited current can be recorded at a distances shorter than one of UME‘s radius [87, 197]. In our research, all measurements were performed at a several selected distances recalculated in radiuses of the UME, or normalized distances: a ‘zero’ distance or 0 μm, 0.2 d/a or 1 μm, 0.4 d/a or 2 μm, 1d/a or 5 μm , and 2d/a or 10 μm distance from UME (RG=10) to surface. One of the limitations of the EIS measurements is that the influence of electrochemical/electric noise and various distortions are very critical, but the applied FFT-EIS device has the possibility to test the quality of the measurement. In order to ensure the quality of registered EIS spectra, the reliability of measured impedance data was tested during each FFT-EIS measurement by checking how the registered responses correspond to the applied perturbations. In order to facilitate the scanning process it is reasonable to perform the evaluation of the surface as quickly as it possible, but due to limited equilibration time some fluctuations of an ion concentrations in close the proximity to UME still remain and they reduce the quality of the FFT-EIS signal, especially if it is registered at lower frequencies. Practically, some distortions in the FFT-EIS signal could be observed when the UME is moved to a new measurement position and for this reason in order to compromise SECM scanning rate *vs* quality of the FFT-EIS signal it is reasonable to apply the frequencies higher than 1.5 Hz.

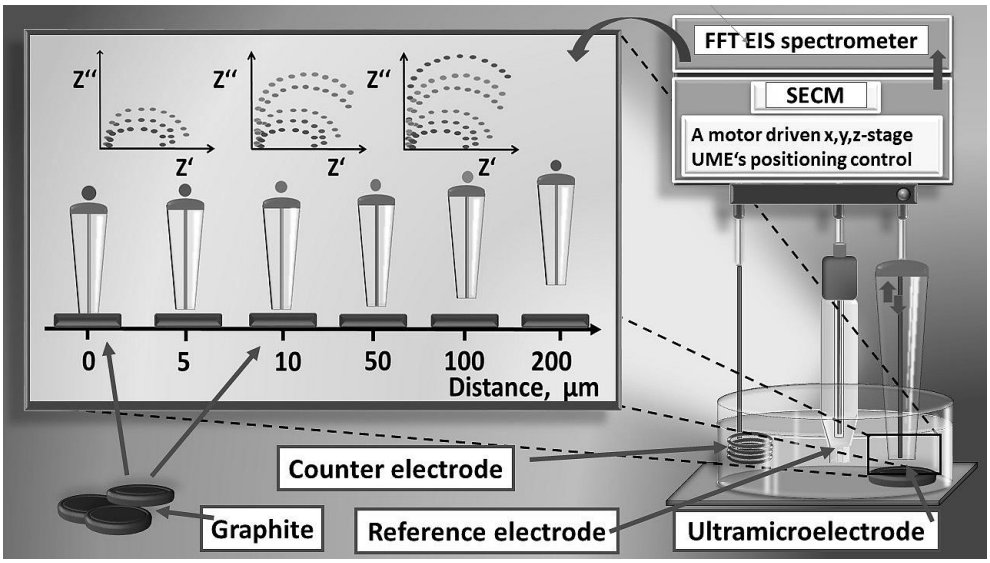

Fig. 8. The conceptual visual scheme of the experiment of EIS measurement with SECM combined FFT-EIS.

On Fig. 8 is shown a graphical image explaining how EIS results depends on distance UME from graphite sample. Experiment was performed in ambient temperature in Faraday cage. All steps of experiment were controlled manualy.

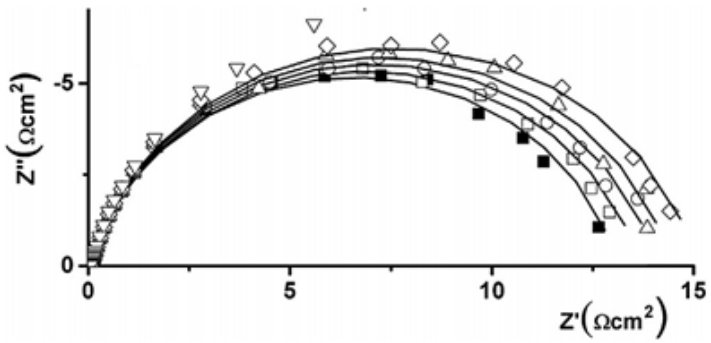

Fig. 9. FFT-EIS spectra obtained in PBS pH 6.8 solution with 0.02 mol/L of a ferricyanide/ferrocyanide as a redox couple, using UME positioned at different distances (d, μm or d/a) from the graphite surface: ■-0 μm, d/a, □-0.2 d/a or 1 μm, ○-0.4 d/a or 2 μm, ◁-1d/a or 5 μm, ◇-2d/a or 10 μm,

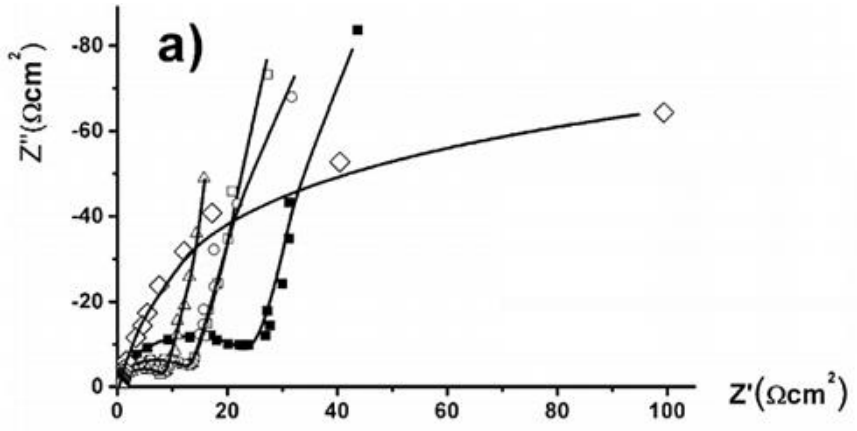

Fig. 10. FFT-EIS spectra obtained in PBS pH 6.8 solution with 0.02 mol/L of $K_3Fe(CN)_6$/ $K_4Fe(CN)_6$ as a redox couple, using UME positioned at different distances (d, μm) from the polytetrafluoroethylene surface. ■-0 μm, d/a, □-0.2 d/a or 1 μm, ○-0.4 d/a or 2 μm, ◁-1d/a or 5 μm, ◇-2d/a or 10 μm;

The electrolyte solution resistance (R_S) was calculated by fitting an equivalent circuit. It is varying only at a distance is more than 5 μ or more than 1 d/a (distance d *vs* UME radius a), where Warburg element is absent in equivalent circuit.

CPE in equivalent circuit represents a non-ideal capacitor based on heterogenity of the interface. The Warburg element (W) was expected to register and it represents the impedance of diffusion [27]. The diffusion based resistance (W_R) should be hidden in our system, it was calculated 448 to 490 Ω cm^2 with exponential number was calculated 0,86 wich can be of electric capacitance related expected nature of W_R depending on UME inperfect geometry.

As it was menthioned, the combined FFT-EIS and SECM technique opens a new way in fast localized EIS measurements. The combination of this two techniques provides a new and effective way to measure the local variations of FFT-EIS at different surfaces, in which the processes are evolving much faster than could be registered by the traditional devices for EIS, which are collecting whole the EIS spectra at points frequency by frequency. To evaluate the reliability of this combined technique, the FFT-EIS spectra registration was performed in positive and negative-FB SECM modes. The FFT-EIS measurements at a different distances from surface showed: during the approach the UME to the conducting and non-conducting surfaces the variation of R_{ct} *vs* distance of UME above the surface of interest are similar to the variation of amperometric signal registered at FB mode SECM. In summary: A) when UME is approaching the insulating surface, then the R_{ct} becomes higher due to hindered diffusion; B) when UME is approaching the conducting unbiased surface, the R_{ct} resistance becomes lower due to the reversible reaction in the space between the UME and the surface.

3.2. Redox-probe-free scanning electrochemical microscopy combined with fast Fourier transform electrochemical impedance spectroscopy

The SECM combined with FFT -based electrochemical impedance spectroscopy (FFT-EIS) is presented to be an effective variation of SEIM, the advantage of this techniques FFT-SEIM and can be used for the sensitive investigation at the single living cell. In a most EIS-based experiments, harmful enough the redox mediators are applied, which can affect the functioning of a living cells and distort the cell response data. The development of a redox-probe-free FFT-SEIM is important challenge in the electrochemistry. In this research we have demonstrated by EIS measurements of a redox-probe-free evaluation of conducting and non-conducting surfaces by combining SECM with FFT-EIS. The EIS spectra using this combined technique could be registered much faster compared to experiments performed using the conventional EIS equipment and can be a new point of view to theory of SECM. In these experiments the UME (RG 10) was used as a scanning electrode to ensure high spatial resolution. We have performed FFT-SEIM measurements in a redox-probe-free mode (without any additional redox probes) and have investigated several surfaces with different conductivities.

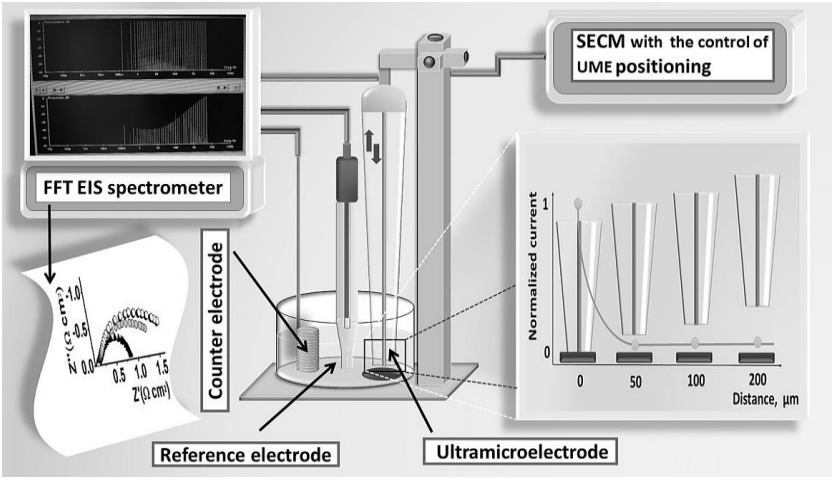

Fig. 11 The experimental set-up based on hybridized FFT-EIS and SECM systems.

The FFT-EIS equipment and the built-in software help to avoid the influence of possible formation of a hydrogen bubbles on the UME. This research opens up a new avenue for the application of FFT-SEIM in the investigation of the samples that are unstable and very sensitive to redox mediators. Visual representation of experment is in figure11. The electrodes by replacement were connected to FFTS or SECM during all measurements.

3.2.1. SECM amperometric measurements

A two samples of very different electrical conductivities were evaluated: one sample was a conducting non-polarized sample (graphite), the other one was non-conducting (polytetrafluoroethylene). The UME was positioned at various distances from the samples' surface. We expected that the impedance will depend on the distance (d) between the UME tip and the surface of the sample, whereby some parameters of its respective equivalent circuit will show dependence on the distance (d), which is similar to the positive–negative FB behavior and is a specific feature for SECM amperometric measurements. The amperometric measurements for surface search were performed at −0.5 V vs. Ag|AgCl|$KCl_{sat.}$ (Fig. 12) in the negative FB mode.

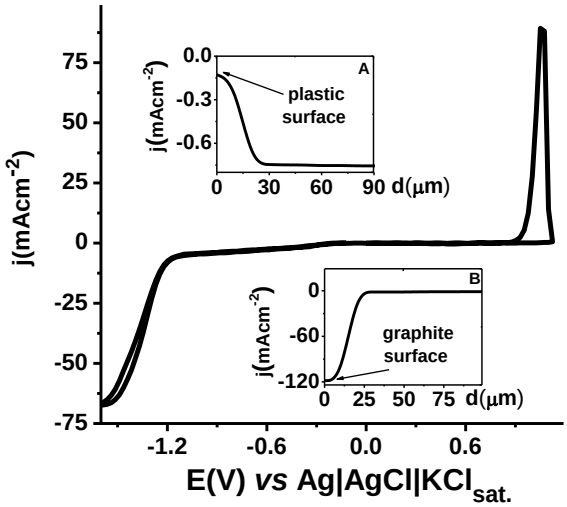

Fig. 12. CV in PBS, pH 6.8, performed by Au UME with diameter of 10 μm (RG=10), scan rate 0.2 V s^{-1}. Insets – approaching curves registered with SECM tip above (A) polytetrafluoroethylene and (B) non-polarized graphite surfaces, at applied potential of -0.5 V *vs* Ag|AgCl|$KCl_{sat.}$. The UME approach step 1 μm/s.

The diffusion of ions to UME was blocked by the non-conducting surface, and the current close to the surface becomes very low (Fig. 12 A). However, in the positive the FB mode, the current registered when the UME is in very close proximity to the conducting surface, which becomes polarized due to potential applied to UME, and the surface area (on which redox processes are occurring) increases significantly. Therefore, a significant increase in the UME current is observed (Fig. 12B). Positive FB can be observed when the UME is approaching conducting surfaces, while negative FB is mostly observed when the UME is approaching the non-conducting surfaces [96, 164].

3.2.2. SECM-FFT-EIS measurements

The application of FFT-SEIM, where the FFT-EIS is combined with the SECM, has some advantages over the use of the well-known frequency response analyzer-based EIS technique (FRA-EIS). First, the duration of a EIS measurement is significantly reduced due to the fact that a multi-sine signal, being a sum of up to all set single sine signals, serves as a perturbation of the working electrode and the FFTS is used to reveal their respective responses. Second, the registered EIS can be checked for validity very easily and reliably [198]. The errors might be related to (i) the UME initiated turbulence of a solution during the movement and the time left for the equilibration of the ion concentration near the UME, and (ii) the sufficient small area of the UME, leading to the small currents and the necessity of using very high gain amplifiers for the efficient registration of the EIS spectra of sufficient quality. The above all the mentioned problems were addressed by awaiting the steady-state conditions at any new location prior to EIS measurement and by setting the DC potential in the faradaic current zone. The electrochemical impedance spectroscopy measurements were performed in the PBS (pH 6.8) after the UME was positioned at a various distances from the non-polarized graphite or polytetrafluoroethylene surfaces. For these measurements, a potential of −1.2 V vs. Ag|AgCl|$KCl_{sat.}$ was selected from the range where the faradaic current was already observed very clearly (Fig. 12). In the potential region more positive than −1.2 V and 0.9 V vs. Ag|AgCl|$KCl_{sat.}$, the faradaic processes were not observed. Therefore, the EIS spectra were almost independent of the distance between UME and the surface of investigation (Fig. 13).

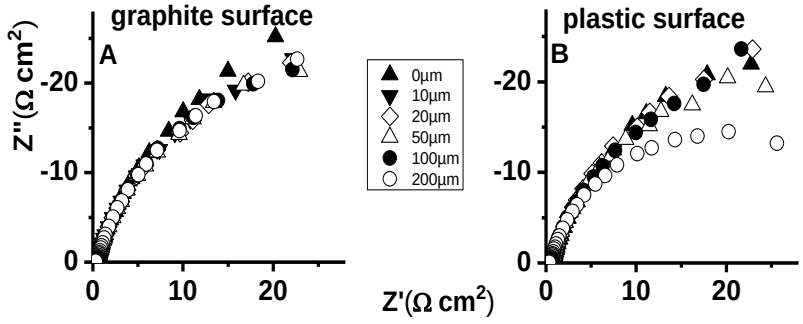

Figure 13. The FFT-EIS Nyquist plot spectra registered at -1.0 V *vs* Ag|AgCl|$KCl_{sat.}$, in PBS pH 6.8, using UME positioned at different distances: A – approaching towards the non-polarized graphite sample; B – approaching towards the polytetrafluoroethylene surface.

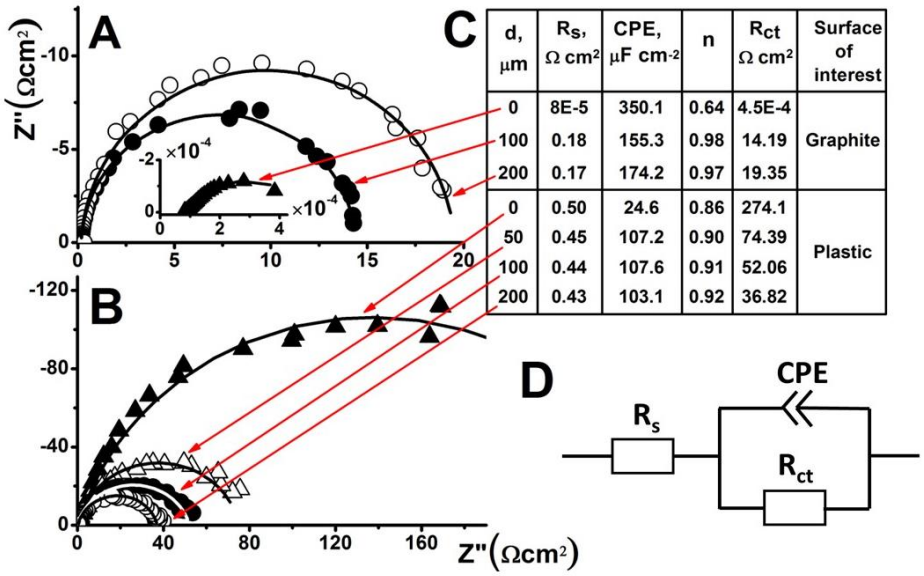

d, μm	R_S, Ω cm²	CPE, μF cm⁻²	n	R_{ct} Ω cm²	Surface of interest
0	8E-5	350.1	0.64	4.5E-4	Graphite
100	0.18	155.3	0.98	14.19	
200	0.17	174.2	0.97	19.35	
0	0.50	24.6	0.86	274.1	Plastic
50	0.45	107.2	0.90	74.39	
100	0.44	107.6	0.91	52.06	
200	0.43	103.1	0.92	36.82	

Figure 14. FFT-SEIM Nyquist plot spectra registered at -1.2 V *vs* Ag|AgCl|$KCl_{sat.}$, in PBS, pH 6.8, using UME positioned at different distances (d, μm): A – approaching towards non-polarized graphite; B – approaching towards polytetrafluoroethylene surface. Table C represents distances between the UME tip and surfaces of interest and calculated parameters of the equivalent circuit (D), where R_s - electrolyte resistance, R_{ct} - charge transfer resistance, CPE - constant phase element.

The FFT-EIS spectra registered at a potential of −1.2 V *vs* Ag|AgCl|$KCl_{sat.}$, i.e. in the presence of the faradaic currents, are presented in Fig. 14 part A and B. At this conditions, the influence of a hydrogen bubbles on the surface of UME of EIS spectra should be avoided. Therefore, in this research, a several strategies were applied to avoid the formation of hydrogen bubbles and this interfering effect to get the EIS spectra of a good quality. In this research, the advantage of FTT spectrometer to register very fast the EIS spectra before the formation of any hydrogen bubbles on UME allowed to perform experiments under selected conditions. Therefore, a significant advantage of FFT-EIS is the capability to register all spectra within a few seconds for this and similar systems. Due to the very small UME surface area compared to conventional in electrochemistry and the very initial phase of the water electrolysis as is seen from the CV (Fig. 12), the intensity of the formation of an atomic and a molecular hydrogen is too less to form a hydrogen bubbles in sufficient volume during the few seconds of our measurement. The quality of EIS spectra was checked by an advanced FFT-EIS a control software and the EIS data acquisition system of this device. It is very important, that during the FFT-EIS experiments, the measured response data could be observed/controlled. If necessary, the 'mismatching' points or even

whole the EIS spectra, which not related to the process of interest, were excluded. This procedure is possible because the used configuration of FFT-EIS spectrometer allows to determine how the EIS response corresponds to the applied perturbation and to evaluate the quality of the registered EIS spectra. It is seen from the Nyquist plot, that the radius of the semicircles strongly depends on the distance between the UME and the non-polarized graphite or the polytetrafluoroethylene surface. One of the main challenges of these experiments was to ensure a stationarity of the measurement conditions by avoiding the effect of possible formation of hydrogen bubbles on the UME surface during the FFT-EIS measurements. The intensity of the hydrogen gas bubble formation depends on the solution/electrolyte composition, the electrode material and even a high quality surface area of the electrode. Fortunately, in our case and with the short measurement time of the FFT-EIS, the chosen gold UME potential of −1.2 V *vs* $Ag|AgCl|KCl_{sat.}$ resulted in sufficient current response but had a negligible effect on the hydrogen generation. Thus, the measurements could be completed before the formation of any the hydrogen bubbles. The impedance data validity was checked for each EIS measurement. Experimental EIS data were fitted to an equivalent circuit model presented in fig. 14D, consisting a solution resistance R_s; constant phase element (CPE) [96, 163, 198], which represents the capacitance of the electric double layer that was forming at the interface between UME and the buffer solution; and a charge transfer resistance (R_{ct}), which represents the charge transfer at the interface between the UME and the PBS. An electrochemical parameters under the selected equivalent circuit model were calculated and are presented in the table in Fig. 14 C. The values of charge transfer resistance R_{ct} strongly depend on whether the gold UME is almost touching the graphite surface ('zero distance') or is positioned at a distance 20d/a or 40 d/a from the investigated surface (Fig. 14A). The R_{ct} becomes very small (4.5×10^{-4} Ω cm^2) when the UME approaches the conductive (graphite) surface (Fig. 14A), marked by filled triangles. This result is related to the SECM measurements performed in the amperometric mode, because the measured current became a very high when the UME approached and touches the conductive surface (Fig. 12B). This phenomenon as was mentioned already is called as positive FB, and it is clearly represented by the registered FFT-EIS spectra (Fig. 14A). When gold the UME was located relatively far from the graphite surface (Fig. 14), marked in figure as an opened and filled circles, the R_{ct} became a relatively high: 14.19 Ω cm^2 and 19.35 Ω cm^2 at a 20d/a and 40 d/a distance. The FFT-SEIM measurements, performed an approach towards the polytetrafluoroethylene surface (Fig. 14B) shows the negative FB phenomena, which means that when the UME is located close to the surface of substrate then the current becomes very low due to the hindered diffusion of the redox-active species in PBS. Therefore,

the highest value of R_{ct} was registered at 'zero distance' (274.1 Ω cm^2), when the UME was almost touching the surface of the polytetrafluoroethylene (Fig. 14B , filled triangles), and the resistance became significantly lower when the UME was positioned at a higher distances from the insulating surface: 74.39 Ω cm^2, 52.06 Ω cm^2 and 36.82 Ω cm^2 at the 10 d/a, 20 d/a and 40 d/a, respectively. In this case, the diffusion of the compounds (primarily dissolved oxygen) to the UME is hindered by the insulating glass shield of the electrode. So, the retraction of the gold UME from the insulating soft polytetrafluoroethulene surface forms a 'free space' and made available diffusion.

3.3. Evaluation of electrochemical properties of immobilized active and inactivated yeast cells

Before the starting SECM EIS and SEIM measurements, which were performed to investigate an electrochemical properties of an immobilized active and inactivated yeast cells, some preliminary experiments were carried out. At first, the cyclic votammogram of mechanically and electrochemically cleaned UME was registered in the buffer solution, pH 6.75, containing 12.5 μM of Vit-K_1 and 12.5 μM of Vit-K_3, which were acting as redox mediators according to the scheme presented in figure 15.

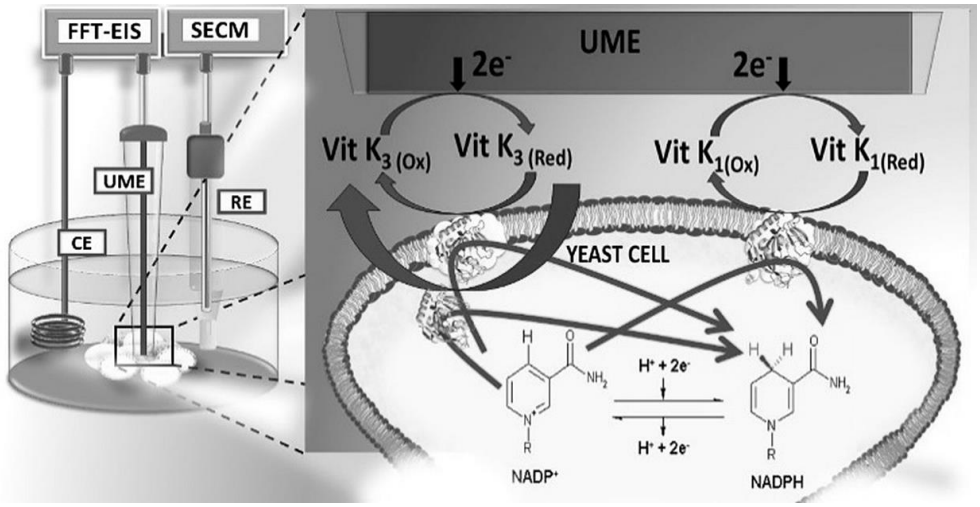

Fig. 15. Visual representation of experiment. Interaction of vitamins K_1 and K_3 with yeast cell and platinum UME.

As it is shown in the figure 15, the Vitamin K_1 is able to transfer an electrical charge from a redox enzymes and other the redox-able species, which are

localized in the membrane of the cell, while the Vitamin K_3 is able to penetrate the yeast cell membrane and to transfer the charge from the redox enzymes and other redox-able species which are localized inside of the yeast cell. The oxidation reduction processes of these enzymes are presented in the figure 1, which illustrates that significant part of the related redox processes are based on a $NADP^+$/NADPH- based enzymes. The CV (Fig. 16 A) was used for the determination of suitable electrode potential for experiment, which is required for the correct registration of EIS spectra at the potentiostatic conditions. For here proposed research, it was important to select appropriate the UME potential at which the Faradaic current is generated on the UME, because it was expected that no a significant changes in the EIS spectra can be obtained while performing the EIS measurements at the potentials where an 'ideal polarization' of the electrode can be observed, at such conditions when is no oxidation and/or reduction processes on the electrode. Therefore, we have selected - 1.2 V potential *vs* $Ag|AgCl|KCl_{(sat.)}$ for EIS measurements, because at this chosen potential a significant variation of the current density was observed during the registration of CV (Fig. 16A) in PBS. Before the EIS measurements, the working UME was used for the registration of approach curves by SECM above the plastics Petri dish surface modified by an active and inactivated yeast cells in order to investigate the process of charge transfer at the interface between UME and the electrolyte, when UME is approaching the surface of yeast cells with different viability. The registered approach curves are presented in figure 16 B, where presented current is normalized by dividing measured current values by maximally registered one.

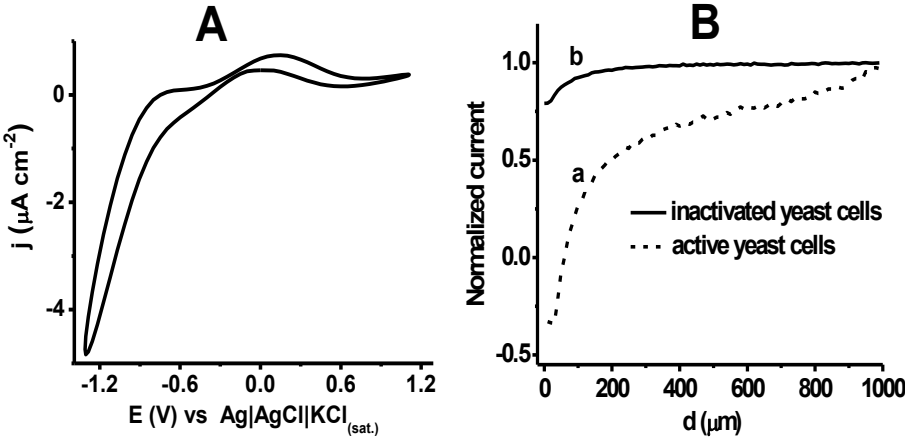

Fig. 16. A – CV of UME in PBS, pH 6.75, containing 12.5 μM of Vitamin K_1 and 12.5 μM of Vitamin -K_3. Potential sweep rate – 0.2 V/s. **B** – approach curves registered when UME was approaching towards the surface modified with active (a) and inactivated (b) yeast cells. Approaching was performed at 10 μm/ s in PBS, pH 6.75, at -0.5 V potential *vs* $Ag|AgCl|KCl_{(sat.)}$.

The potential of -0.5 V for aproach curves was chosen, based on the current density registered in CV, in mediator-free PBS pH 6.75. From the obtained current-distance approach curves (Fig. 16 B) it is seen that the normalized current values decrease significantly when the UME approaches the surface of the active or alive yeast cells (Fig. 16 B, curve A). This result indicates that electrochemical processes at the UME are blocked while approaching the surface modified by the yeast cells, which is specific indication of a negative- FB behaviour, that is usually registered when the UME is approaching non-conducting surfaces [28]. A significant decrease of the UME current density has been observed when the distance between the UME and the active yeast cells is below 40 d/a. On the one hand, such a significant change in the current density can be explained by the reduction of dissolved oxygen, which produces a current flow at UME, when the electrode is retracted from the yeast cell-modified Petri plastics dish surface at the distance, which exceeds 40 d/a. But if the UME is approaching closer to the surface of interest, the concentration of the oxygen becomes lower due to the consumption of the oxygen by metabolic processes, which are taking a part in active yeast cells, what is causing a significant decrease of UME current in comparing with deactivated one.

When UME is approaching the surface modified by inactivated or the dead yeast cells, only a negligible decrease in current density was observed (Fig. 16 B, curve b), because inactivated yeast cells are not consuming the oxygen and only hindered diffusion can be observed. This means if the UME is positioned above the inactivated yeast cells, it is only blocked by diffusion limitations for the dissolved oxygen in PBS, when the UME is approaching closer than 10 d/a towards the surface modified by inactivated yeast cells. When the distance between the electrode and the surface modified by inactivated yeast cells reaches 60 d/a, then the electrode current starts to decrease until it becomes very low (below 0.01 nA) at the point when the UME is reaching ‘zero distance’, which was initially determined by SECM approaching the cell-modified surface and AFM measurement. In comparing currents, which were registered during the approaching of the UME to the active yeast cell modified surface (Fig. 16 B, curve A), with that registered when the UME approached the surface modified by inactivated yeast cell (Fig. 16 B, curve b), it was determined that active yeast cells shows much higher oxygen consumption rate comparing to that of inactivated yeast cells, as expected. The registered approach curves (Fig. 16 B) allow us to gain information about the current flow, when the electrode is positioned at ‘zero distance’ from the yeast cell modified surface. When UME approaches ‘zero distance’ above either active or inactivated yeast cells, the registered current values do not decrease down to ‘zero level’. It means that at ‘zero distance’ from the yeast cell modified surface the delivery of oxygen towards UME is still

blocked only partially, therefore, charge transfer proceeds at the interface between UME and the electrolyte, which still contains some amount of oxygen, because there is no ideal contact between UME and surface.

It should be noted that during the registration of the approach curves there is a risk to contaminate the conducting part of UME by direct touching the surface of yeast cells. Hence, the UME should be cleaned thoroughly after the registration of each approach curve. Therefore, in this work UME was cleaned in 0.5 mol/L H_2SO_4 solution by potential cycling as specified by the manufacturer, until the shape of CV become constant, sigmoidal in PBS and only then the UME was used for this EIS measurements.

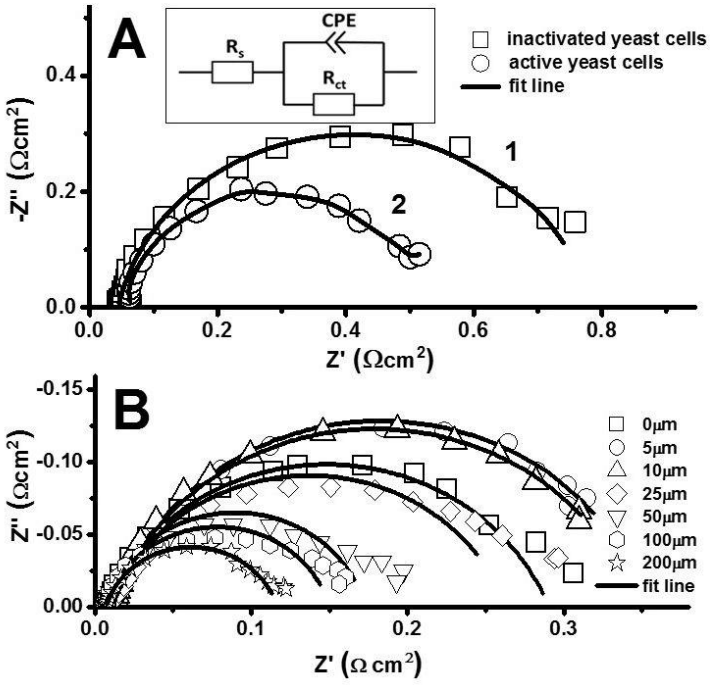

Fig. 17. A - EIS registered in PBS, pH 6.75, at -1.2 V *vs* Ag|AgCl|$KCl_{(sat.)}$ by using UME positioned at 'zero distance' from the active (curve 2) and inactivated (curve 1) yeast cells surface. Inset - equivalent circuit model used for fitting of EIS data: R_s – electrolyte solution resistance; *CPE* – constant phase element; R_{ct} – charge-transfer resistance. **B** - electrochemical impedance spectra registered in FFT-SEIM mode, in PBS, pH 6.75, at -1.2 V *vs* Ag|AgCl|$KCl_{(sat.)}$ when UME was positioned at different distances (not normalized for UME RG=5) from the petri dish surface, which was modified by active yeast cells.

The registration of a significant currents during whole approaching cycle revealed that for both active and inactivated yeast cell modified petri dish surfaces it is possible to perform the measurements of electrochemical impedance spectroscopy and to determine electrochemical characteristics. At first step, electrochemical impedance spectra were recorded in the buffer solution at -1.2 V potential *vs* Ag|AgCl|$KCl_{(sat.)}$ using UME positioned at 'zero distance' from the active and inactivated yeast cells surface. The obtained EIS data are displayed as Nyquist plots in figure 13A.

Table 1. The values of equivalent circuit elements (Fig. 17, inset) calculated by analysing EIS data registered by using UME positioned at 'zero distance' from petri dish surface modified by active and inactivated yeast cells (Fig. 17A).

Electrode positioning	R_s, mΩ cm^2	*CPE*, mF cm^{-2}	*n*	R_{ct}, mΩ cm^2
Above active yeast cells	57.90	30.46	0.90	0.47
Above inactivated yeast cells	44.42	32.22	0.88	0.74

Table 2. The values of equivalent circuit (Fig. 3A, inset) obtained by analysing EIS data registered in FFT-SEIM-mode when UME was positioned at different distances from the petri dish surface modified by active yeast cells (Fig. 17 B).

d, μm	d/a	R_s, mΩ cm^2	*CPE*, mF cm^{-2}	*n*	R_{ct}, mΩ cm^2
0	0	10.96	35.47	0.91	0.27
5	1	11.98	54.65	0.88	0.34
10	2	11.98	59.45	0.80	0.34
25	5	10.69	56.79	0.80	0.25
50	10	6.75	52.51	0.86	0.17
100	20	6.97	61.73	0.85	0.14
200	40	6.87	65.49	0.84	0.11

A typical equivalent circuit model (Fig. 17 A, inset) was chosen for the assessment of the EIS data using this work andit was taking into account the fact that in our system the Faraday process occurs under the applied potential of -1.2 V *vs* Ag|AgCl|$KCl_{(sat.)}$ (see Fig. 17 A). In this case, the equivalent circuit consists the solution resistance (R_s), constant phase element (*CPE*), which is representing a capacitance of the electric double layer, that forms at the interface between UME and PBS, and parallel resistance R_{ct}, which represents the charge transfer at the

interface between UME and the PBS. The fitting of the experimental EIS data (Fig. 17 B, different symbols) to the equivalent circuit model (Fig. 17 A, solid lines) was observed and following fitting parameters were calculated for both SEIM experiments: (i) when the electrode was positioned above active yeast cells then R_s=57.90 mΩ cm^2; *CPE*=30.46 mF cm^{-2} (with exponent n=0.90); R_{ct}=0.47 mΩ cm^2; (ii) when the electrode was positioned above inactivated yeast cells then R_s=44.42 mΩ cm^2; *CPE*=32.22 mF cm^{-2} (with exponent n=0.88); R_{ct}=0.74 mΩ cm^2 (Table 1). These values of equivalent circuit (Fig. 17 A, inset) were calculated by analysing EIS data registered by using UME positioned at 'zero distance' from the plastics Petri dish surface modified by active and inactivated yeast cells respectively (Fig. 17 A). FFT-EIS spectra registered when UME was approaching towards surface modified by inactivated cells are presented in figure 18.

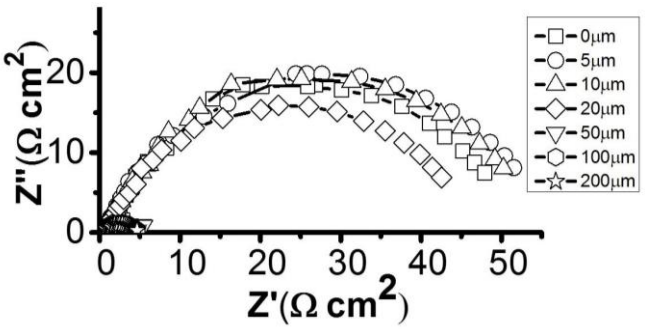

Fig. 18. FFT-EIS spectra registered, when UME was approaching towards surface modified by inactivated yeast cells.

The calculated EIS characteristics (Table 2) obviously indicate that charge transfer resistance R_{ct} above the surface modified by active yeast cells is by 0.27 Ωcm^2 lower than that above the surface modified by inactivated yeast cells. This effect can be explained by the formation of oxidized forms of some the charge-transfer-able materials as a result of a metabolic processes inside of active yeast cells. In opposite, the limited metabolism does not occur on the petri dish surface modified by inactivated yeast cells, thus around inactivated cells there is a lower concentration of oxidized forms of some charge-transfer-able materials close to the surface of cells and it is in agreement with the increase of R_{ct} value.

Further a series of EIS experiments were performed in FFT-SEIM configuration, in order to investigate the influence of the distance between UME and surface of active yeast cells on the registered electrochemical impedance spectra. FFT-EIS data registered by using the UME positioned at a different distances from the surface of plastics Petri Disch modified by immobilized yeast cells are presented as a Nyquist plots in figure 19 B. By fitting the experimental EIS data to the equivalent

circuit model (Fig. 16 A, inset), the electrochemical characteristics of selected equivalent circuit were calculated and are presented in Table 3.

As it can be expected, due to diffusion limitations, the values of charge transfer resistance (R_{ct}) increase slightly when the UME approaches down from 2 d/a until 1d/a the surface modified by an active yeast cells. However, when the UME is positioned at a higher distances from the surface of active yeast cells (i.e. at 25 µm) the R_{ct} is decreasing when the distance between UME and the surface of interest increases. Summarising it can be concluded, that performing an experiments in FFT-SEIM configuration: (i) electrochemical activity and oxygen consumption (breathing) of yeast can be electrochemically observed when the distance between UME and surface of yeast cells is from 0 d/a to 1 d/a; (ii) 2d/a is the maximum distance suitable for efficient investigation of the yeast cell activity.

Once the redox activity of the immobilized active and inactivated yeast cells was investigated by FFT-SEIM, the time based experiments were performed investigating a charge transfer between the active yeast cells and a lipophilic (Vitamin -K_3) and a hydrophilic (Vitamin -K_1) redox mediators. For this experiment we have applied the FFT-EIS, therefore, we were able to monitor the EIS almost in real time of registration, and to determine how fast the equilibrium of concentrations of added vitamins (Vitamin t-K_1 and Vitamin -K_3) between the solution and immobilized yeast cells is achieved. The FFT-EIS spectra were registered at the FFT-SEIM mode in PBS at the -1.2 V potential *vs* Ag|AgCl|$KCl_{(sat.)}$, when the UME was positioned more than 0.2 d/a away from the plastics Petri dish surface, which was modified by the yeast cells (Fig. 19). All the FFT-SEIM experiments were carried out with two differently prepared yeast samples in which the same concentration (12.5 µM/L) of each redox mediator (Vitamin -K_1 and Vitamin -K_3) was formed in the electrochemical system by two different ways: They were named (i) in 'System 1', where the Petri dish, contained the immobilized yeast cells, was filled with 5 ml of PBS solution containing 12.5 µM/L concentration of each Vitamin -K_1 and Vitamin -K_3 and then FFT-EIS spectra were recorded at a different time intervals (Fig. 19 A); (ii) in 'System 2', 0.5 ml of solution containing 12.5 µMol/L concentration of each Vitamin -K_1 and Vitamin -K_3 was added into the plastics Petri dish with the immobilized yeast cells, incubated at 4°C for a 24 h, during which solvent has evaporated and then the plastics Petri dish was filled with a 5 ml of PBS solution (final concentration of Vitamin -K_1 and Vitamin -K_3 was expected to be the same as it was in the 'System 1'), incubated for 1 h, gently mixed and then FFT-EIS spectra were recorded at a different time intervals (Fig. 19 B). Registered EIS spectra were fitted according to equivalent circuit (Fig. 16 A, inset) and calculated fit results are presented in Table 3.

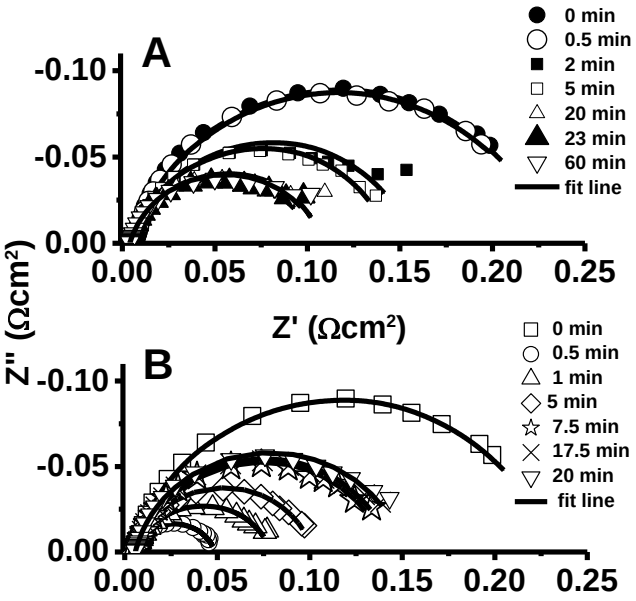

Fig. 19. Time-dependent FFT-EIS spectra registered in FFT-SEIM mode in PBS, pH 6.75, at -1.2 V *vs* Ag|AgCl|$KCl_{(sat.)}$ when UME was positioned above petri dish surface modified by active yeast cells. **A** – 'System 1', the redox mediators (12.5 μM of Vitamin -K_1 and Vitamin -K_3) were added into the buffer solution in the petri dish where active yeast cells were immobilized onto petri dish surface before the addition of Vit-K_1 and Vit-K_3, **B** – 'System 2', the same amount of Vitamin -K_1 and Vitamin -K_3 was added onto immobilized yeast cells to dry and then the petri dish was filled with the buffer solution.

Table 3. Electrochemical characteristics obtained by fitting FFT-EIS data (Fig. 19) to that calculated by using equivalent circuit model, which is presented in figure 17A inset.

'System 1' Vit-K_1 and Vit-K_3 added to the buffer solution				
t, min	R_s, mΩ cm^2	*CPE*, mF cm^{-2}	*n*	R_{ct}, Ω cm^2
0	5.5	41.42	0.86	0.22
0.5	6.2	49.92	0.86	0.22
2	5.8	58.12	0.85	0.15
5	5.8	52.89	0.86	0.14
20	5.0	58.89	0.85	0.10
23	3.9	98.88	0.84	0.09
60	4.0	95.05	0.84	0.10

'System 2' Vit-K_1 and Vit-K_3 added onto dry yeast cells				
t, min	R_s, mΩ m^2	*CPE*, mF cm^{-2}	*n*	R_{ct}, Ω cm^2
0	5.48	41.42	0.86	0.22
0.5	5.1	76.76	0.83	0.04
1	5.96	80.26	0.82	0.07
5	5.68	61.22	0.85	0.10
7.5	6.42	59.99	0.84	0.14
17.5	5.62	55.21	0.86	0.14
20	5.69	54.14	0.86	0.15

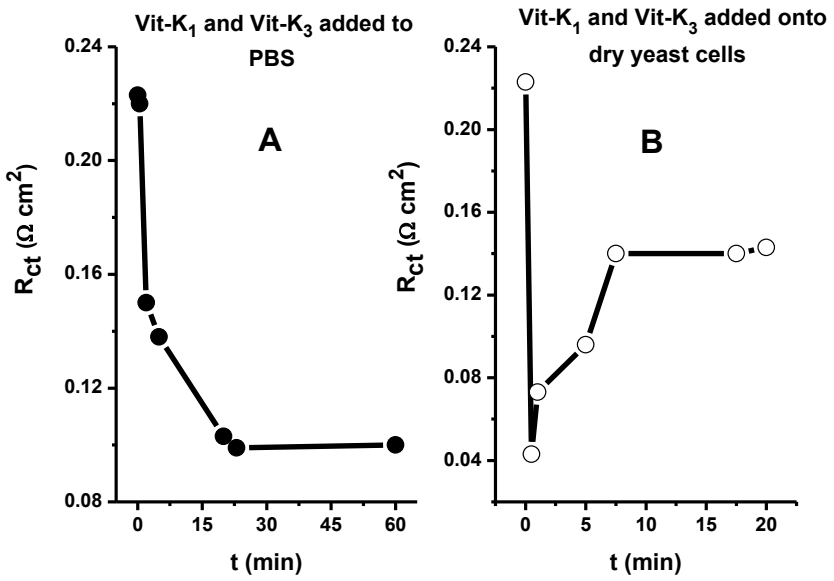

Fig. 20. Evolution of charge transfer resistance (R_{ct}), calculated by fitting the FFT-EIS data presented in figure 19, in time: **A** – 'System 1', Vitamin -K_1 and Vitamin -K_3 are added into the PBS into a Petri dish with immobilized yeast cells; **B** – 'System 2', immobilized yeast cells are modified by Vitamin -K_1 and Vitamin -K_3 before adding the PBS.

In order to investigate a kinetics of interactions between the active yeast cells and lipophilic (Vitamin -K_3) and hydrophilic (Vitamin -K_1) redox mediators, the values of a charge transfer resistance are the most important and, therefore, they were analysed very thoroughly and represented in figure 20. It was found, that R_{ct} values become constant: (i) within 20 min for 'System 1' (Vitamin -K_1 and Vitamin -K_3 are added to the buffer solution) (Fig. 20 A), and within 7.5 min for

'System 2' (Vitamin -K_1 and Vitamin -K_3 are added onto dry immobilized yeast cells) (Fig. 20 B). These results show that in the case of 'System 2' the equilibrium of Vitamin -K_1 and Vitamin -K_3 concentrations between solution and the yeast cells is reached faster. The difference in the duration of reaching steady-state conditions is related to the fact that during the investigation of 'System 1' Vitamin -K_1, which is lipophilic, should diffuse into yeast cell membrane, where it serves as a redox mediator between inside redox enzymes and hydrophilic Vitamin -K_3, while in the case of 'System 2' the immobilized yeast cells are pretreated by solution containing Vitamin -K_1on the petri dish and with modified in that way the yeast cells an electrochemical cell was filled with the PBS. Therefore, in the case of 'System 2' reaching steady-state conditions takes longer, which is reflected by time required for reaching steady-state R_{ct} value.

To investigate the influence of redox mediators pair Vitamin -K_1 and Vitamin -K_3, on electrochemical activity of an active yeast cells, the yeast cells sample was immobilized on the surface of graphite electrode (geometric surface area 0.071 cm^2), and then the FFT-EIS spectra were recorded (Fig. 21) at -0.84 V potential *vs* Ag|AgCl|$KCl_{(sat.)}$ at which a Faradaic current was observed according to CV data (Fig. 21, inset).

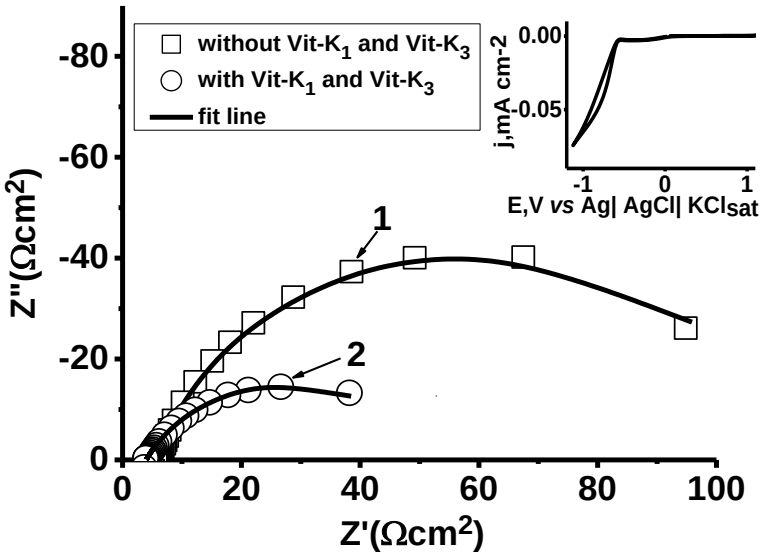

Fig. 21. FFT-EIS spectra of graphite electrode modified by immobilized active yeast cells in PBS, pH 6.75, at -0.84 V *vs* Ag|AgCl|$KCl_{(sat.)}$ without any redox mediators (curve 1) and with 12.5 μM of lipophilic (Vitamin -K_3) and 12.5 μM of hydrophilic (Vitamin -K_1) redox mediators (curve 2). The inset represents CV of UME electrode in PBS, pH 6.75. Potential sweep rate 50 mVs^{-1}.

The electrochemical characteristics obtained by fitting the FFT-EIS data (Fig. 21) to equivalent circuit model presented in figure 17 A inset, were the following: (i) the experiment was performed in the presence of Vitamin -K_1 and Vitamin -K_3, which were serving as redox mediators then R_s=3.95 mΩ cm^2; *CPE*=2.09 mF cm^{-2} (with exponent number n=0.71); R_{ct}=47.79 mΩ cm^2; (ii) when the experiment was performed in the absence of vitamins as redox mediators then R_s=5.77 mΩ cm^2; *CPE*=0.49 mF cm^{-2} (with exponent number n=0.83); R_{ct}=107.3 mΩ cm^2 (Table 4).

Comparing FFT-EIS data obtained during the investigation of a similar graphite electrode modified by immobilized yeast cells in the absence of redox mediators (Fig. 6, curve 1) and in the presence of lipophilic (Vitamin -K_3) and hydrophilic (Vitamin -K_1) redox mediators (Fig. 21, curve 2), it is obvious that charge transfer resistance, R_{ct}, (Table 4) decreases more than twice (from 107.3 Ωcm^2 down to 47.8 Ωcm^2) in presence of Vitamin -K_1 and Vitamin -K_3.

Table 4. Electrochemical characteristics of an equivalent circuit obtained by fitting FFT-EIS data (Fig. 21) to the equivalent circuit model, which is presented in figure 17 inset.

Yeast cells	R_s, Ω cm^2	*CPE*, mF cm^{-2}	n	R_{ct}, Ω cm^2
With redox mediators	3.95	2.09	0.71	47.79
Without redox mediators	5.77	0.49	0.83	107.3

3.4. Evaluation of redox activity of human myocardium-derived mesenchymal stem cells by scanning electrochemical microscopy

3.4.1 Investigation of human heart hmMSC by the RC-SECM mode.

First of all, the hmMSC cell surface was found in a negative FB mode using a potential of -500 mV chosen from CV.-The potential was further changed to +400 mV and after addition of redox mediator MD, the electrode was withdrawn from the hmMSC cell in a GC-mode, identifying a reduced MD. At the distance of 100μm or 20 d/a, the potential has been changed again to -500 mV and the platinum UME was moved toward the cell in order to ensure that the cell was not pierced or moved, i.e. whether the distance from the electrode to the cell has not been changed or the electrode was not blocked by adsorption. In addition, a change of potential allowed to perform the tests without a significant blocking the electrode: the current at the negative potential reduced oxidized forms of some redox/able compounds and repelled negatively charged ions away from the electrode.

So, the dependencies of current *vs* distance in the healthy hmMSC were registered by the RC-SECM mode, approaching the UME to the hmMSC (Fig. 22 a). The approaching curve at the beginning was done without redox mediators couple, where the only breathing products and some amount of electrolytes as a "base line" near the cell surface can be detected. The current as expected in negative FB behavior, was decreasing due to hindered diffusion when UME was close to the cell's surface. At the MD concentration range from 4 µM/L up to 10 µM/L, the current generated by the reduction of MD became significantly higher than the diffusion-limited current. The increase of current measured by the RC-SECM mode showed the highest MD concentration close to the cell's surface.

In order to evaluate the rate of MD uptake by healthy hmMSC, the experimental data were plotted as dependence of current *vs* concentration (Fig. 22 b). The MD consumption phenomenon is seen at 0 d/a and 0.2 d/a distances. At 0 d/a distance the current is decreasing up to concentracion till 2 µM/L of MD. At higher than 2 µM/L concentrations of MD, the current was increasing along with the MD concentration, showing that the measured current was no longer related to the consumption of MD by the cells. When the concentration of MD has reached 4 µM/L, the increase of the current was no longer dependent on the concentration of MD. The similar experiment has been performed with the pathological hmMSC. The uptake of MD by the pathological hmMSC has been registered first of all without MD and then with the 1 µM/L of MD (Fig. 22 c). The significant increase of current was observed already at 2 µM/L of MD compared to the 4 µM/L for the healthy cells. It shows that the pathological cells are less able to reduce MD. When the concentration of MD reached 5 µM/L, the current became constant independently of the increasing concentration of MD. So, the best uptake of MD by the pathological cells was observed at MD concentration lower than 5 µM/L (Fig. 22 d).

The fitting of data obtained by the RC-SECM (dependence of the current *vs* MD concentration) by a Hill's function, showed a positive cooperative binding $n > 1$ for both the healthy and pathological hmMSC, which means that the affinity of MD for the both type of the hmMSC is increasing with the increase of MD concentration (Table 5). The Hill's coefficients n for the healthy hmMSC were two folds higher than that for the pathological hmMSC ($n = 6$ for healthy; $n = 3$ for pathological) revealing that pathological hmMSC can faster take up the MD and faster start to release the menadiol. It might be also related to the increased permeability of a membrane of the pathological hmMSC. Comparing the MD concentrations, at which half of the reaction rate was achieved, we can conclude, that healthy hmMSC cells slower reacted to the MD than the pathological hmMSC: for healthy hmMSC $k = 2.65 - 1.7$; for pathological cells $k = 1.7 - 1.6$, given in the table below.

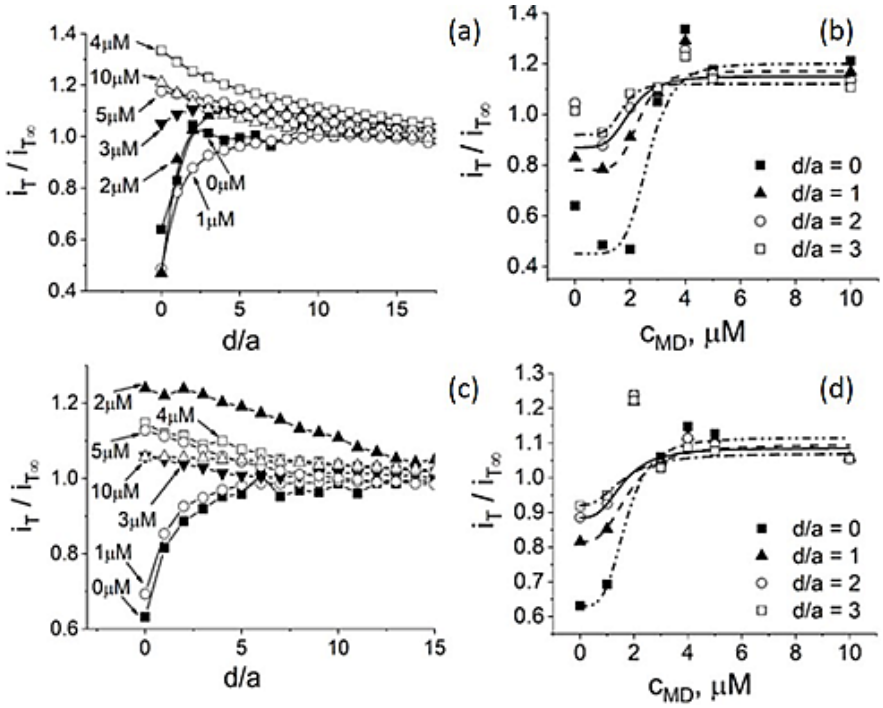

Fig. 22. The investigation of healthy and pathological hmMSC by RC-SECM mode. (a) The dependence of normalized current on the distance between the UME and healthy hmMSC at different concentrations of MD at -500 mV *vs* Ag/AgCl potential. (b) The dependence of current on MD concentration in healthy hmMSC; fitting by Hill's function has been applied. (c) The dependence of normalized current on normalized distance between the UME and pathological hmMSC and exposed to the different concentrations of MD in culture medium. -500 mV *vs* Ag/AgCl potential was applied. (d) The dependence of current on MD concentration in pathological hmMSC; fitting by Hill's function has been applied.

Table 5. Fitting parameters of the Hill's function for healthy and pathological hmMSC determined by RC-SECM mode.

Healthy hmMSC			**Pathological** hmMSC		
d/a	**k**	**n**	**d/a**	**k***	**n***
0	2.65±0.08	6±0.6	0	1.7±0.08	3.8±0.07
1	2.3±0,07	6±0.6	1	1.8±0.08	3±0,05
2	2±0,06	4.5±0.5	2	1.6±0.06	3±0.08
3	1.7±0,06	6±0.6	3	1.6±0.06	2.5±0.07

***** data are significant at $p \leq 0.05$ comparing healthy and pathological hmMSC.

3.4.2 Investigation of hmMSC by GC-SECM mode.

Both types of the cells were evaluated by the GC-SECM mode at +400mV *vs* Ag/AgCl potential (Fig. 23), which determines the reduced form of MD. It was determined that the healthy heart-derived hmMSC start to reduce MD immediately after its addition to the solution (Fig. 23 a). The significant increase of UME current in the healthy MSC cells after the addition of 1 µM/L MD can be explained by a very fast reaction of MD with NAD(P)H. At 5-10 µM/L of MD, the MD-related current is not decreasing any longer because healthy hmMSC reaches the threshold of MD reduction. The fitting Hills' equation to the dependence of current *vs* concentration did not show a sudden increase of the current at 1µM/L MD concentration (Figure 23 b).

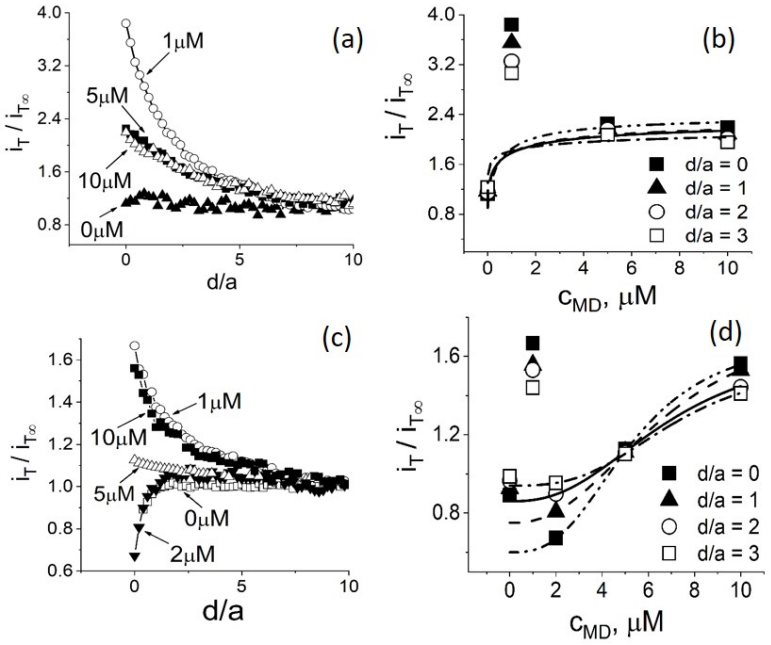

Fig. 23. The investigation of healthy and pathological human myocardium-derived hmMSC by GC-SECM mode. (a) The dependence of normalized current on the distance between UME and healthy hmMSC. The healthy hmMSC were grown at standard conditions and exposed to different concentrations of MD. +400 mV *vs* Ag/AgCl potential was applied. (b) The dependence of current on MD concentration. Fitting by Hill's function has been applied. (c) The dependence of normalized current on normalized distance between UME and pathological hmMSC and exposed to different concentrations of MD, +400 mV *vs* Ag/AgCl potential was applied. (d) The dependence of current of pathological hmMSC on MD concentration; Hill's function was applied for the fitting.

The reaction of 1 µM/L MD with NAD(P)H in pathological hmMSC was less intensive than in healthy hmMSC but also very quick (Figure 19c). It shows that redox capacity of pathological cells is lower compared to the healthy cells. However, at 2 µM/L of MD the dependence of current *vs* distance in pathological hmMSC showed 'negative feedback' (Figure 23 d). This effect can be related to the uptake of 2 µM/L of MD by the pathological hmMSC. Higher than 2 µM/L of MD concentrations (5-10 µM/L) did not show the increase of the UME current. The fitting of the dependence of current *vs* MD concentration showed that 1 µM/L of MD is too low to generate registerable redox current in pathological hmMSC (Figure 23 d).

Hill's coefficient n for the pathological human heart-derived hmMSC was higher than 1 ($n > 1$) showing the positive cooperative binding between MD and the pathological hmMSC (Table 6). It shows that increasing MD concentration increases the affinity between MD and the pathological hmMSC, i.e. MD better penetrated to the pathological compared to the healthy hmMSC. This phenomenon could be explained by possible damage of pathological MSC cell membrane (Table 6). The Hill's coefficient n for the healthy hmMSC cells was lower than 1 ($n < 1$), which means a negative cooperative binding between MD and healthy hmMSC, i.e. the affinity of MD to the healthy hmMSC decreases with the increase of MD concentration. Altogether, the lower MD affinity to the healthy compared to the pathological hmMSC can be related not only to the better redox capacities of healthy hmMSC but also to the more intact membrane of healthy hmMSC.
The data, presented in the table 6 show that measurement of healthy and pathological hmMSC by GC-SECM mode allow to distinguish them by two main indications: (i) different cooperative binding, which is negative for the healthy and positive for the pathological hmMSC; (ii) significant difference between reaction rate (the Michaelis constant *k* for the pathological cells was from 10.6 to 14.4 folds higher than for the healthy hmMSC).

Table 6. Fitting parameters of the Hill's function for healthy and pathological hmMSC determined by GC-SECM mode.

Healthy hmMSC			**Pathological hmMSC**		
d/a	**k**	**n**	**d/a**	**k***	**n***
0	0.5±0.06	0.8±0.06	0	5.3±1.3	2.8±0.07
1	0.5±0.08	0.55±0.08	1	6.7±1.2	2.4±0.07
2	0.5±0.05	0.52±0.02	2	6.9±1.5	2.5±0.06
3	0.5±0.05	0.27±0.015	3	7.2±1.5	3±0.07

It can be concluded, that the SECM is suitable for the identification of the membrane integrity and the intracellular redox activities of healthy and pathological human heart myocardium-derived MSC and can be used for the selection and/or modification of stem cells for their further regeneration purposes.

Generalized dissusions

In this research, we have combined two devices, the SECM with the FFT electrochemical impedance spectrometer and developed the FFT-SEIM system capable of performing very fast EIS measurements. We have demonstrated that, due to the fast FFT-EIS measurements and the easy data evaluation/validation, it is possible to the significantly advance the SECM capabilities in EIS measurements and to apply it for the investigation of the fast electrochemical processes. The measurement of the FFT-EIS spectra in the absence of a redox mediator increases the capability of the FFT-EIS and SECM technique for the investigation of the samples sensitive to the redox probe. The ability to perform FFT-EIS experiments without the redox probe is important for the SECM-based evaluation of the living cells or other fast localized EIS. The combination of this two state-of-the-art techniques, FFTS and SECM, provides a new and effective way to measure a local variations of FFT-EIS at a various surfaces, in which the processes are evolving much faster than could be registered by the traditional EIS equipment, which collect the EIS spectra frequency by frequency in all range of spectrum. The measurements FFT-EIS combined with the SECM at a different distances are compared to the approaching curves of UME by SECM in FB-mode, then it is aproaching to the conducting and non-conducting surfaces. The variation of R_{ct} *vs* distance of the UME above the surface of interest is the similar to the variation of amperometric signal registered at feedback mode (FB- SECM mode): a) when the UME is approaching the insulating surface, then the R_{ct} becomes higher due to hindered diffusion; b) when the UME is approaching the conducting surface, then the R_{ct} resistance becomes lower due to reversible reaction in the space between UME and the surface of investigation. As expected, a significant difference of the charge transfer resistance through the electrode-solution interphase was registered when a gold UME was approaching a petri dish surface modified by an active and inactivated yeast cells at potential -1.2 V *vs* $Ag|AgCl|KCl_{(sat.)}$ in the PBS solution (pH 6.75). The charge transfer resistance was 0.74 Ωcm^2 of active and 0.47 Ωcm^2 for the inactivated yeast cells. While performing experiments in FFT-SEIM configuration by combined SECM with FFTS, electrochemical activity and oxygen consumption (breathing) by the yeast cells, can be electrochemically observed when the distance between UME and surface of yeast cells is from a „zero“ distance to 2d/a, the maximum distance, which is still suitable for an efficient investigation of the yeast cell activity by FFT-SEIM. The yeast quality examination is an easiest method may be the way

of this sort of measurements. Since the yeast cells wall is also used as a separated product, this FFT-SEIM method can also be used to examine the quality of the other yeast products, not only for a viability of them.

The group of vitamin K is a well known and in detail examined materials by many other researchers, is playing important role in a single cell and whole organisms processes. So, the menadione and menadiol as a redox mediator couple, with their well studied properties, can be succesfully used in a human cell pathologicity investigations by SECM.

The SECM aproach curves method can be successfully used to identify the changed the redox capacity of the healthy and pathological hmMSC. Investigation of hmMSC by two different SECM modes (RC-SECM and GC-SECM) shows two main processes that occur in the hmMSC in the presence of MD: (i) uptake of MD by the cells; (ii) reduction of MD inside the cells. The investigation of MD uptake by RC-SECM mode additionally shows the integrity of the membrane. The membranes of healthy hmMSC were more undamaged, in comparing to the pathological hmMSC, therefore, the pathological hmMSC consumed the MD faster. The data of measurement by RC-SECM show that healthy and pathological human myocardium-derived MSC can be characterized by the Hill's equation coefficient n, which shows the affinity between MD and hmMSC and it was two folds higher for healthy hmMSC than for the pathological hmMSC cells according to our calculation. The reduction of MD, which has been identified by the GC-SECM mode, can be used for the investigation of intracellular redox changes when are attempting to recognize the healthy or pathological are hmMSC. The GC-SECM measurement results, processed by calculations using Hill's equation of dependence of measured current *vs* concentration of menadione, provides Michaelis constant (k) differences, which can be a main feature to recognize hmMSC cells pathologicity. Healthy hmMSC detected by GC-SECM mode had a negative binding, whereas pathological MSC cells –a positive. However, apparent Michaelis constant for the reduction of menadione in pathological MSC cells was 10.6 - 14.4 times higher, compared to calculated for the healthy hmMSC. It shows that the penetration of MD in the pathological cell is going faster, whereas its reduction is slower due to the reduced redox status of pathological hmMSC. RC-SECM and GC-SECM are a promising tool for the identification of membrane integrity and reduction potential of healthy and pathological human left ventricle myocardium-derived MSC. The apparent catalytic constant and cooperative binding were calculated from the data registered at different distances from the cells surface and can be used to evaluate stability or whole complex intracellular processes.

CONCLUSIONS

1. SEIM measurements performed with sinchronized FFT and SECM instruments, allows the possibility quantitatively and quick record of EIS by SECM when the object is sensitive to redox mediators, the system is unstable, processes are performing a few seconds or in case of instability and it is possible to register the changes of oxygen concentrations.
2. The system sensitive to the redox mediators may be tested by the SEIM method performed by FFTS-SECM as advantage of SECM.
3. The FFT-SEIM method can be used for investigation of yeast cells electrochemical activity and breathing process by using redox mediator vitamin K group compounds.
4. SECM aproach curves, with vitamin K as redox mediator pair, can be an appropriate method for investigation of differences electrochemical activity between pathological and healthy human myocardium mesenchymal stem cells

Acknowledgements

The research was supported by the Lithuanian Research council, project No. S-MIP-17-13; project No. SEN-21/2015; „Development of Cometences of Scientists, other Researchers and Students through Practical Research Activities“ under Measure project No. 09.3.3-LMT-K-712; project No. 09.3.3-LMT-K-712-02-0137. ‘Research Projects Implemented by World-class Researcher Groups’ under Measure No. 01.2.2-LMT-K-7; ‘Research Projects Implemented by World-class Researcher Groups’ under Measure No. 01.2.2-LMT-K-718 grant No 09.3.3-LMT-K-718-01-0063, “Smart membranes for electrochemical devices”

Authors thanks for AFM imaging performed by Asoc. Prof. Dr. Inga Morkvenaite-Vilkonciene and Prof. Assist. Dr. Lina Mikoliunaite.

Special acknowledgements for Prof. H.Cesiulis and Prof. (HP) A.Ramanavičius for consultations and lectures, Senior Researcher Dr. Daiva Bironaitė from Inovative Medical Center, Department of Regenerative Medicine for cell samples.

REFERENCES

1. Aoki, K., Akimoto, K., Tokuda, K., Matsuda, H., & Osteryoung, J., *Linear sweep voltammetry at very small stationary disk electrodes.* Journal of electroanalytical chemistry and interfacial electrochemistry, 1984. **171**(1-2): p. 219-230.
2. Heinze, J., *Ultramicroelectrodes in electrochemistry.* Angewandte Chemie International Edition in English, 1993. **32**(9): p. 1268-1288.
3. Amatore, C., *Electrochemistry at ultramicroelectrodes.* Physical Electrochemistry: Principles, Methods and Applications, 1995. **4**: p. 131-208.
4. Davies, P.W. and F. Brink Jr, *Microelectrodes for measuring local oxygen tension in animal tissues.* Review of Scientific Instruments, 1942. **13**(12): p. 524-533.
5. Kissinger, P.T. and W.R. Heineman, *Cyclic voltammetry.* Journal of Chemical Education, 1983. **60**(9): p. 702.
6. Penner, R.M. and C.R. Martin, *Preparation and electrochemical characterization of ultramicroelectrode ensembles.* Analytical Chemistry, 1987. **59**(21): p. 2625-2630.
7. Bard, A.J., Denuault, G., Friesner, R. A., Dornblaser, B. C., Tuckerman, L. S., *Scanning electrochemical microscopy: theory and application of the transient (chronoamperometric) SECM response.* Analytical chemistry, 1991. **63**(13): p. 1282-1288.
8. Kwak, J., A.J. Bard, *Scanning electrochemical microscopy. Theory of the feedback mode.* Analytical Chemistry, 1989. **61**(11): p. 1221-1227.
9. Bard, A.J., Mirkin, M. V., Unwin, P. R., & Wipf, D. O., *Scanning electrochemical microscopy. 12. Theory and experiment of the feedback mode with finite heterogeneous electron-transfer kinetics and arbitrary substrate size.* The Journal of Physical Chemistry, 1992. **96**(4): p. 1861-1868.
10. Casillas, N., Mirkin, M. V., Unwin, P. R., & Wipf, D. O., *Pitting corrosion of titanium.* Journal of the Electrochemical Society, 1994. **141**(3): p. 636-642.
11. Wipf, D. O., *Initiation and study of localized corrosion by scanning electrochemical microscopy.* Colloids and Surfaces A: Physicochemical and Engineering Aspects, 1994. **93**: p. 251-261.
12. Kaya, T., Torisawa, Y. S., Oyamatsu, D., Nishizawa, M., Matsue, T., *Monitoring the cellular activity of a cultured single cell by scanning electrochemical microscopy (SECM). A comparison with fluorescence viability monitoring.* Biosensors and Bioelectronics, 2003. **18**(11): p. 1379-1383.
13. Kranz, C., Kueng, A., Lugstein, A., Bertagnolli, E., & Mizaikoff, B., *Mapping of enzyme activity by detection of enzymatic products during AFM imaging with integrated SECM–AFM probes.* Ultramicroscopy, 2004. **100**(3-4): p. 127-134.

14. Zheng, X. T. and C. M. Li, *Single cell analysis at the nanoscale.* Chemical society reviews, 2012. **41**(6): p. 2061-2071.
15. Isaacs, H., *The measurement of the galvanic corrosion of soldered copper using the scanning vibrating electrode technique.* Corrosion science, 1988. **28**(6): p. 547-558.
16. Cui, N., Ma, H. Y., Luo, J. L., & Chiovelli, S., *Use of scanning reference electrode technique for characterizing pitting and general corrosion of carbon steel in neutral media.* Electrochemistry communications, 2001. **3**(12): p. 716-721.
17. Annergren, I., F. Zou, and D. Thierry, *Application of localised electrochemical techniques to study kinetics of initiation and propagation during pit growth.* Electrochimica Acta, 1999. **44**(24): p. 4383-4393.
18. Salomo, M., Pust, S. E., Wittstock, G., & Oesterschulze, E., *Integrated cantilever probes for SECM/AFM characterization of surfaces.* Microelectronic Engineering, 2010. **87**(5-8): p. 1537-1539.
19. Fasching, R., Y. Tao, and F. Prinz, *Cantilever tip probe arrays for simultaneous SECM and AFM analysis.* Sensors and actuators B: Chemical, 2005. **108**(1-2): p. 964-972.
20. Xin, Y., Gao, Y., Guo, J., Chen, Q., Xiang, J., & Zhou, F., *Real-time detection of Cu2+ sequestration and release by immobilized apo-metallothioneins using SECM combined with SPR.* Biosensors and Bioelectronics, 2008. **24**(3): p. 369-375.
21. Smith, D.E., *Data Processing in Electrochemistry.* Analytical Chemistry, 1976. **48**(2): p. 221A-240A.
22. Popkirov, G. and R. Schindler, *A new approach to the problem of "good" and "bad" impedance data in electrochemical impedance spectroscopy.* Electrochimica acta, 1994. **39**(13): p. 2025-2030.
23. Popkirov, G. and R. Schindler, *A new impedance spectrometer for the investigation of electrochemical systems.* Review of scientific instruments, 1992. **63**(11): p. 5366-5372.
24. Baltrunas, G., G. Popkirov, and R. Schindler, *Time evolution of the active silver electrode area after immersion in cyanide containing solutions.* Journal of Electroanalytical Chemistry, 1997. **435**(1-2): p. 95-101.
25. Baltrūnas, G., *The mechanism of electrode process in the system silver/silver cyanide complexes.* Electrochimica Acta, 2003. **48**(24): p. 3659-3664.
26. Baltrūnas, G., Valiūnienė, A., Margarian, Ž., Viselgienė, G., & Popkirov, G, *The electroreduction kinetics of silver sulfite complexes.* Electrochimica Acta, 2008. **53**(22): p. 6513-6520.
27. Valiūnienė, A., Rekertaitė, A. I., Ramanavičienė, A., Mikoliūnaitė, L., Ramanavičius, A.., *Fast Fourier transformation electrochemical impedance spectroscopy for the investigation of inactivation of glucose biosensor based on graphite electrode modified by Prussian blue,*

polypyrrole and glucose oxidase. Colloids and Surfaces A: Physicochemical and Engineering Aspects, 2017. **532**: p. 165-171.
28. Morkvenaite-Vilkonciene, I., Valiūnienė, A., Petroniene, J., Ramanavicius, A., *Hybrid system based on fast Fourier transform electrochemical impedance spectroscopy combined with scanning electrochemical microscopy*. Electrochemistry Communications, 2017. **83**: p. 110-112.
29. Biesheuvel, P. J. Dykstra, *The difference between Faradaic and Nonfaradaic processes in Electrochemistry*. arXiv preprint arXiv:1809.02930, 2018.
30. Bard, A.J., Faulkner, L. R., Leddy, J., & Zoski, C. G,, *Electrochemical methods: fundamentals and applications*. Vol. 2. 1980: wiley New York.
31. Erdey-Gruz, T. and T. Grúz, *Kinetics of electrode processes*. 1972: Wiley-Interscience Budapest.
32. Ching, S., R. Dudek, and E. Tabet, *Cyclic voltammetry with ultramicroelectrodes.* Journal of chemical education, 1994. **71**(7): p. 602.
33. Mohilner, D., *The electrical double layer*, in *Electroanalytical chemistry*. 1966, Marcel Dekker New York. p. 331.
34. Richards, F.M., Eisenberg, D. S., Kim, P. S., & Di Cera, E., *Linkage thermodynamics of macromolecular interactions*. Vol. 51. 1998: Academic Press.
35. Myland, J.C. and K.B. Oldham, *Uncompensated resistance. 1. The effect of cell geometry*. Analytical chemistry, 2000. **72**(17): p. 3972-3980.
36. Nanis, L. and W. Kesselman, *Engineering applications of current and potential distributions in disk electrode systems*. Journal of The Electrochemical Society, 1971. **118**(3): p. 454-461.
37. Winkler, J., Hendriksen, P. V., Bonanos N., Mogensen. M.,, *Geometric requirements of solid electrolyte cells with a reference electrode.* Journal of The Electrochemical Society, 1998. **145**(4): p. 1184-1192.
38. Svensson, A.M., K. Nis, *Interpretation of measured polarization resistance at a solid electrode/electrolyte interface.* Journal of The Electrochemical Society, 1999. **146**(5): p. 1840-1846.
39. Macdonald, J.R., *Impedance spectroscopy*. Vol. 41. 1987: Wiley New York etc.
40. Kissinger, P., W.R. Heineman, *Laboratory Techniques in Electroanalytical Chemistry, revised and expanded*. 1996: CRC press.
41. Zoski, C.G., *advances in scanning electrochemical microscopy (SECM).* Journal of The Electrochemical Society, 2016. **163**(4): p. H3088-H3100.
42. Wightman, R. M. D. O. Wipf, *Voltammetry at ultramicroelectrodes.* Electroanalytical chemistry, 1989. **15**: p. 267-353.

43. Zoski, C.G., J.C. Aguilar, A.J. Bard, *Scanning electrochemical microscopy. 46. Shielding effects on reversible and quasireversible reactions.* Analytical chemistry, 2003. **75**(13): p. 2959-2966.
44. Huigen, E., A. Peper, C. Grimbergen, *Investigation into the origin of the noise of surface electrodes.* Medical and biological engineering and computing, 2002. **40**(3): p. 332-338.
45. Amemiya, S., Bard, A. J., Fan, F. R. F., Mirkin, M. V., Unwin, P. R.,, *Scanning electrochemical microscopy.* Annu. Rev. Anal. Chem., 2008. **1**: p. 95-131.
46. Wightman, R. D. Wipf, *Electroanalytical chemistry.* ed. AJ Bard, 1989. **15**: p. 267-353.
47. Bard, A., *J.; Faulkner, L., R.* Electrochemical methods Fundamentals and Applications, 2001.
48. Mirkin, M.V., L.O. Bulhoes, A.J. Bard, *Determination of the kinetic parameters for the electroreduction of fullerene C60 by scanning electrochemical microscopy and fast scan cyclic voltammetry.* Journal of the American Chemical Society, 1993. **115**(1): p. 201-204.
49. Horrocks, B.R., M.V. Mirkin, A.J. Bard, *Scanning electrochemical microscopy. 25. Application to investigation of the kinetics of heterogeneous electron transfer at semiconductor (WSe2 and Si) electrodes.* The Journal of Physical Chemistry, 1994. **98**(37): p. 9106-9114.
50. Bertoncello, P., *Advances on scanning electrochemical microscopy (SECM) for energy.* Energy & Environmental Science, 2010. **3**(11): p. 1620-1633.
51. Nagamine, K., Takahashi, Y., Ino, K., Shiku, H., & Matsue, T,, *Influence of tip size on single yeast cell imaging using scanning electrochemical microscopy.* Electroanalysis, 2011. **23**(5): p. 1168-1174.
52. Aoki, K., *Theory of ultramicroelectrodes.* Electroanalysis, 1993. **5**(8): p. 627-639.
53. Zoski, C.G., *Ultramicroelectrodes: design, fabrication, and characterization.* Electroanalysis: An International Journal Devoted to Fundamental and Practical Aspects of Electroanalysis, 2002. **14**(15-16): p. 1041-1051.
54. Astrauskas, R., Ivanauskas, F., Morkvenaite-Vilkonciene, I. Ramanavicius, A.,, *Mathematical Modelling of the Influence of Ultra-micro Electrode Geometry on Approach Curves Registered by Scanning Electrochemical Microscopy.* Electroanalysis, 2019. **31**(11): p. 2214-2223.
55. Lee, Y., S. Amemiya, A.J. Bard, *Scanning electrochemical microscopy. 41. Theory and characterization of ring electrodes.* Analytical chemistry, 2001. **73**(10): p. 2261-2267.
56. Wittstock, G., Burchardt, M., Pust, S. E., Shen, Y., & Zhao, C.,, *Scanning electrochemical microscopy for direct imaging of reaction*

rates. Angewandte Chemie International Edition, 2007. **46**(10): p. 1584-1617.
57. Pandolfo, A. A. Hollenkamp, *Carbon properties and their role in supercapacitors.* Journal of power sources, 2006. **157**(1): p. 11-27.
58. McCreery, R.L., *Carbon electrodes: structural effects on electron transfer kinetics.* Electroanalytical chemistry, 1991. **17**: p. 221-374.
59. Randin, J.-P. E. Yeager, *Differential capacitance study on the basal plane of stress-annealed pyrolytic graphite.* Journal of Electroanalytical Chemistry and Interfacial Electrochemistry, 1972. **36**(2): p. 257-276.
60. Amemiya, S., Chen, R., Nioradze, N. Kim, J., *Scanning electrochemical microscopy of carbon nanomaterials and graphite.* Accounts of chemical research, 2016. **49**(9): p. 2007-2014.
61. Bates, T. W. Stockmayer, *Conformational energies of perfluoroalkanes. III. Properties of polytetrafluoroethylene.* Macromolecules, 1968. **1**(1): p. 17-24.
62. Chessick, J., F. Healey, A. Zettlemoyer, *Adsorption and heat of wetting studies of teflon.* The Journal of Physical Chemistry, 1956. **60**(10): p. 1345-1347.
63. Hanford, W. R. Joyce, *Polytetrafluoroethylene.* Journal of the American Chemical Society, 1946. **68**(10): p. 2082-2085.
64. Gerhard-Multhaupt, R., Kunstler, W., Gome, T., Pucher, A., Weinhold, T., Seiß, M., Xia, Z., Wedel, A. and Danz, R.,, *Porous PTFE space-charge electrets for piezoelectric applications.* IEEE Transactions on Dielectrics and Electrical Insulation, 2000. **7**(4): p. 480-488.
65. Sun, P., F.O. Laforge, and M.V. Mirkin, *Scanning electrochemical microscopy in the 21st century.* Physical Chemistry Chemical Physics, 2007. **9**(7): p. 802-823.
66. Mirkin, M.V., Sun, P., F.O. Laforge, ., *Scanning electrochemical microscopy in the 21st century. Update 1: five years after.* Physical Chemistry Chemical Physics, 2011. **13**(48): p. 21196-21212.
67. Bard, A.J., Fan, F. R. F., Pierce, D. T., Unwin, P. R., Wipf, D. O., Zhou, F., *Chemical imaging of surfaces with the scanning electrochemical microscope.* Science, 1991. **254**(5028): p. 68-74.
68. Niu, L., Yin, Y., Guo, W., Lu, M., Qin, R., & Chen, S.,., *Application of scanning electrochemical microscope in the study of corrosion of metals.* Journal of Materials Science, 2009. **44**(17): p. 4511-4521.
69. Lu, X., Q. Wang, X. Liu, *Recent applications of scanning electrochemical microscopy to the study of charge transfer kinetics.* Analytica chimica acta, 2007. **601**(1): p. 10-25.
70. Edwards, M.A., Martin, S., Whitworth, A.L., Macpherson, J.V. and Unwin,, *Scanning electrochemical microscopy: principles and applications to biophysical systems.* Physiological measurement, 2006. **27**(12): p. R63.
71. Amemiya, S., Guo, J., Xiong, H., & Gross, D. A., *Biological applications of scanning electrochemical microscopy: chemical*

imaging of single living cells and beyond. Analytical and bioanalytical chemistry, 2006. **386**(3): p. 458-471.
72. Gyurcsányi, R.E., Jágerszki, G., Kiss, G., & Tóth, K, *Chemical imaging of biological systems with the scanning electrochemical microscope.* Bioelectrochemistry, 2004. **63**(1-2): p. 207-215.
73. Barker, A.L., Gonsalves, M., Macpherson, J. V., Slevin, C. J., Unwin, P. R.., *Scanning electrochemical microscopy: beyond the solid/liquid interface.* Analytica chimica acta, 1999. **385**(1-3): p. 223-240.
74. Unwin, P.R. A.J. Bard, *Scanning electrochemical microscopy. 14. Scanning electrochemical microscope induced desorption: a new technique for the measurement of adsorption/desorption kinetics and surface diffusion rates at the solid/liquid interface.* The Journal of Physical Chemistry, 1992. **96**(12): p. 5035-5045.
75. Engstrom, R.C., Weber, M., Wunder, D.J., Burgess, R. Winquist, S,, *Measurements within the diffusion layer using a microelectrode probe.* Analytical Chemistry, 1986. **58**(4): p. 844-848.
76. Bard, A.J. and M.V. Mirkin, *Scanning electrochemical microscopy*. 2012: CRC Press.
77. Bard, A.J., Fan, F. R. F., Kwak, J., Lev, O., *Scanning electrochemical microscopy. Introduction and principles.* Analytical Chemistry, 1989. **61**(2): p. 132-138.
78. Liljeroth, P., Vanmaekelbergh, D., Ruiz, V., Kontturi, K., Jiang, H., Kauppinen, E., & Quinn, B. M., *Electron transport in two-dimensional arrays of gold nanocrystals investigated by scanning electrochemical microscopy.* Journal of the American Chemical Society, 2004. **126**(22): p. 7126-7132.
79. Cornut, R. and C. Lefrou, *New analytical approximation of feedback approach curves with a microdisk SECM tip and irreversible kinetic reaction at the substrate.* Journal of Electroanalytical Chemistry, 2008. **621**(2): p. 178-184.
80. Cornut, R. and C. Lefrou, *New analytical approximations for negative feedback currents with a microdisk SECM tip.* Journal of Electroanalytical Chemistry, 2007. **604**(2): p. 91-100.
81. Eckhard, K., Chen, X., Turcu, F., & Schuhmann, W.,, *Redox competition mode of scanning electrochemical microscopy (RC-SECM) for visualisation of local catalytic activity.* physical chemistry chemical physics, 2006. **8**(45): p. 5359-5365.
82. Horrocks, B.R., M. Mirkin, *Scanning electrochemical microscopy. 19. Ion-selective potentiometric microscopy.* Analytical Chemistry, 1993. **65**(9): p. 1213-1224.
83. Horrocks, B. and M. Mirkin, *Evidence for a potential-dependent reversible inactivation of urease adsorbed on a gold electrode.* Journal of the Chemical Society, Faraday Transactions, 1998. **94**(8): p. 1115-1118.

84. Wittstock, G., T. Asmus, and T. Wilhelm, *Investigation of ion-bombarded conducting polymer films by scanning electrochemical microscopy (SECM).* Fresenius' journal of analytical chemistry, 2000. **367**(4): p. 346-351.
85. Nogala, W., Szot, K., Burchardt, M., Roelfs, F., Rogalski, J., Opallo, M. and Wittstock, G., *Feedback mode SECM study of laccase and bilirubin oxidase immobilised in a sol–gel processed silicate film.* Analyst, 2010. **135**(8): p. 2051-2058.
86. Szot, K., Nogala, W., Niedziolka-Jönsson, J., Jönsson-Niedziolka, M., Marken, F., Rogalski, J., Kirchner, C.N., Wittstock, G. and Opallo, M., *Hydrophilic carbon nanoparticle-laccase thin film electrode for mediatorless dioxygen reduction: SECM activity mapping and application in zinc-dioxygen battery*. Electrochimica Acta, 2009. **54**(20): p. 4620-4625.
87. Cornut, R., Bhasin, A., Lhenry, S., Etienne, M., & Lefrou, C.,., *Accurate and simplified consideration of the probe geometrical defaults in scanning electrochemical microscopy: theoretical and experimental investigations.* Analytical chemistry, 2011. **83**(24): p. 9669-9675.
88. Bauermann, L.P., W. Schuhmann, and A. Schulte, *An advanced biological scanning electrochemical microscope (Bio-SECM) for studying individual living cells.* Physical Chemistry Chemical Physics, 2004. **6**(15): p. 4003-4008.
89. Liu, B., S.A. Rotenberg, and M.V. Mirkin, *Scanning electrochemical microscopy of living cells: Different redox activities of nonmetastatic and metastatic human breast cells.* Proceedings of the National Academy of Sciences, 2000. **97**(18): p. 9855-9860.
90. Mauzeroll, J. and A.J. Bard, *Scanning electrochemical microscopy of menadione-glutathione conjugate export from yeast cells.* Proceedings of the National Academy of Sciences, 2004. **101**(21): p. 7862-7867.
91. Alonso, L., Palmero, S., Muñoz, E., Sanllorente, S. and García-García, M.A.., *Electrochemical behavior of menadione on glassy carbon rotating disk electrode (RDE).* Electroanalysis: An International Journal Devoted to Fundamental and Practical Aspects of Electroanalysis, 2000. **12**(10): p. 757-762.
92. Ramos-Peralta, L., Ramos-Peralta, L., López-López, L.I., Silva-Belmares, S.Y., Zugasti-Cruz, A., Rodríguez-Herrera, R. and Aguilar-González, C.N.,, *Naphthoquinone: Bioactivity and Green Synthesis.* The Battle Against Microbial Pathogens: Basic Science, Technological Advances and Educational Programs, 2015: p. 542-550.
93. Brittain, H.G., *Profiles of drug substances, excipients, and related methodology*. 2013: Academic Press.
94. Van Ballegooijen, A. and J. Beulens, *The role of vitamin K status in cardiovascular health: evidence from observational and clinical studies.* Current nutrition reports, 2017. **6**(3): p. 197-205.

95. Macdonald, D.D. and M. Urquidi-Macdonald, *Kramers-Kronig Transformation of Constant Phase Impedances.* Journal of The Electrochemical Society, 1990. **137**(2): p. 515-517.
96. Macdonald, J.R., *Impedence Spectroscopy--Emphasizing Solid Materials and Systems.* Wiley-Interscience, John Wiley and Sons, 1987: p. 1-346.
97. Macdonald, D.D., *Reflections on the history of electrochemical impedance spectroscopy.* Electrochimica Acta, 2006. **51**(8-9): p. 1376-1388.
98. Tiginyanu, I., P. Topala, V. Ursaki, *Nanostructures and thin films for multifunctional applications.* Editura Springer, 2016, 550 pg, 2016.
99. Creason, S.C., J.W. Hayes, D.E. Smith, *Fourier transform faradaic admittance measurements III. Comparison of measurement efficiency for various test signal waveforms.* Journal of Electroanalytical chemistry and interfacial electrochemistry, 1973. **47**(1): p. 9-46.
100. Popkirov, G. R. Schindler, *Optimization of the perturbation signal for electrochemical impedance spectroscopy in the time domain.* Review of scientific instruments, 1993. **64**(11): p. 3111-3115.
101. Alavi, S.M.M., Mahdi, A., Payne, S.J., Howey, D.A., *Identifiability of generalized randles circuit models.* IEEE Transactions on Control Systems Technology, 2016. **25**(6): p. 2112-2120.
102. Chang, B.-Y. , S.-M. Park, *Electrochemical impedance spectroscopy.* Annual Review of Analytical Chemistry, 2010. **3**: p. 207-229.
103. Morkvenaite-Vilkonciene, I., Genys, P., Ramanaviciene, A. , Ramanavicius, A.., *Scanning electrochemical impedance microscopy for investigation of glucose oxidase catalyzed reaction.* Colloids and Surfaces B: Biointerfaces, 2015. **126**: p. 598-602.
104. Bandarenka, A.S., Eckhard, K., Maljusch, A., Schuhmann, W., *Localized electrochemical impedance spectroscopy: Visualization of spatial distributions of the key parameters describing solid/liquid interfaces.* Analytical chemistry, 2013. **85**(4): p. 2443-2448.
105. Estrada-Vargas, A., Bandarenka, A., Kuznetsov, V. , Schuhmann, W, *In situ characterization of ultrathin films by scanning electrochemical impedance microscopy.* Analytical chemistry, 2016. **88**(6): p. 3354-3362.
106. Cesiulis, H., Tsyntsaru, N., Ramanavicius, A., & Ragoisha, G., *The study of thin films by electrochemical impedance spectroscopy*, in *Nanostructures and thin films for multifunctional applications*. 2016, Springer. p. 3-42.
107. Cesiulis, H., R. Levinas, , N. Ţînţaru. *Application of electrochemical impedance spectroscopy (EIS) for materials and processes characterization*. in *Materials Science and Condensed Matter Physics*. 2016.

108. Cesiulis, H. , N. Ţînţaru. *EIS–method for characterization of metal oxides: physical meaning of equivalent electric circuits*. in *Materials Science and Condensed Matter Physics*. 2018.
109. Koster, D., Du, G., Battistel, A., La Mantia, F, *Dynamic impedance spectroscopy using dynamic multi-frequency analysis: A theoretical and experimental investigation.* Electrochimica Acta, 2017. **246**: p. 553-563.
110. Battistel, A. , F. La Mantia, *On the physical definition of dynamic impedance: How to design an optimal strategy for data extraction.* Electrochimica Acta, 2019. **304**: p. 513-520.
111. Tanak, A.S., Jagannath, B., Tamrakar, Y., Muthukumar, S., Prasad, S, *Non-faradaic electrochemical impedimetric profiling of Procalcitonin and C-reactive protein as a dual marker biosensor for early sepsis detection.* Analytica Chimica Acta: X, 2019: p. 100029.
112. Guo, X., Kulkarni, A., Doepke, A., Halsall, H.B., Iyer, S., Heineman, W.R, *Carbohydrate-based label-free detection of Escherichia coli ORN 178 using electrochemical impedance spectroscopy.* Analytical chemistry, 2011. **84**(1): p. 241-246.
113. Jagannath, B., S. Muthukumar, S. Prasad, *Electrical double layer modulation of hybrid room temperature ionic liquid/aqueous buffer interface for enhanced sweat based biosensing.* Analytica chimica acta, 2018. **1016**: p. 29-39.
114. Daniels, J.S. N. Pourmand, *Label-free impedance biosensors: Opportunities and challenges.* Electroanalysis: An International Journal Devoted to Fundamental and Practical Aspects of Electroanalysis, 2007. **19**(12): p. 1239-1257.
115. Lin, K.-C., Jagannath, B., Muthukumar, S. Prasad, S., *Sub-picomolar label-free detection of thrombin using electrochemical impedance spectroscopy of aptamer-functionalized MoS 2*. Analyst, 2017. **142**(15): p. 2770-2780.
116. Jacobse, L., S.J. Raaijman, M.T. Koper, *The reactivity of platinum microelectrodes.* Physical Chemistry Chemical Physics, 2016. **18**(41): p. 28451-28457.
117. Katemann, B.B., Schulte, A., Calvo, E.J., Koudelka-Hep, M. Schuhmann., *Localised electrochemical impedance spectroscopy with high lateral resolution by means of alternating current scanning electrochemical microscopy.* Electrochemistry Communications, 2002. **4**(2): p. 134-138.
118. Gębala, M., W. Schuhmann, F. La Mantia, *A new ac-SECM mode: on the way to high-resolution local impedance measurements in SECM*. Electrochemistry Communications, 2011. **13**(7): p. 689-693.
119. Kuznetsov, V., Maljusch, A., Souto, R.M., Bandarenka, A.S. Schuhmann, W, *Characterisation of localised corrosion processes using scanning electrochemical impedance microscopy*. Electrochemistry Communications, 2014. **44**: p. 38-41.

120. Chen, X., Wang, Y., Zhou, J., Yan, W., Li, X. , Zhu, J.J, *Electrochemical impedance immunosensor based on three-dimensionally ordered macroporous gold film.* Analytical chemistry, 2008. **80**(6): p. 2133-2140.
121. Walters, M., Garland, J.E., Pettit, C.M., Zimmerman, D.S., Marr, D.R. , Roy, D., *Weak adsorption of anions on gold: measurement of partial charge transfer using Fast Fourier Transform electrochemical impedance spectroscopy.* Journal of Electroanalytical Chemistry, 2001. **499**(1): p. 48-60.
122. Park, J.-Y., Chang, B.Y., Nam, H. , Park, S.M., *Selective electrochemical sensing of glycated hemoglobin (HbA1c) on thiophene-3-boronic acid self-assembled monolayer covered gold electrodes.* Analytical chemistry, 2008. **80**(21): p. 8035-8044.
123. Yoo, J.-S., Song, I., Lee, J.H. ,Park, S.M., *Real-time impedance measurements during electrochemical experiments and their application to aniline oxidation.* Analytical chemistry, 2003. **75**(14): p. 3294-3300.
124. Valiūnienė, A., Baltrūnas, G., Valiūnas, R. , Popkirov, G., *Investigation of the electroreduction of silver sulfite complexes by means of electrochemical FFT impedance spectroscopy.* Journal of hazardous materials, 2010. **180**(1-3): p. 259-263.
125. Valiūnienė, A., Ž. Margarian, R. Valiūnas, *Electrooxidation of cyanide ion on a platinized Ti electrode.* Reaction Kinetics, Mechanisms and Catalysis, 2015. **115**(2): p. 449-461.
126. Barker, G., *Large signal aperiodic equivalent electrical circuits for diffusion and faradaic impedances.* Journal of Electroanalytical Chemistry and Interfacial Electrochemistry, 1975. **58**(1): p. 5-18.
127. Instruments, G., *Basics of electrochemical impedance spectroscopy.* G. Instruments, Complex impedance in Corrosion, 2007: p. 1-30.
128. Orazem, M.E. and B. Tribollet, *Electrochemical impedance spectroscopy*. 2017: John Wiley & Sons.
129. Jorcin, J.-B., Orazem, M.E., Pébère, N. , Tribollet, B., *CPE analysis by local electrochemical impedance spectroscopy.* Electrochimica Acta, 2006. **51**(8-9): p. 1473-1479.
130. Honeychurch, K., *Printed thick-film biosensors*, in *Printed Films*. 2012, Elsevier. p. 366-409.
131. Baronian, K., Downard, A., Lowen, R. , Pasco, N., *Detection of two distinct substrate-dependent catabolic responses in yeast cells using a mediated electrochemical method.* Applied microbiology and biotechnology, 2002. **60**(1-2): p. 108-113.
132. Heiskanen, A., Yakovleva, J., Spégel, C., Taboryski, R., Koudelka-Hep, M., Emnéus, J.,Ruzgas T.J., *Amperometric monitoring of redox activity in living yeast cells: comparison of menadione and menadione sodium bisulfite as electron transfer mediators.* Electrochemistry communications, 2004. **6**(2): p. 219-224.

133. Heiskanen, A., Spegel, C., Kostesha, N., Lindahl, S., Ruzgas, T. and Emnéus, J, *Mediator-assisted simultaneous probing of cytosolic and mitochondrial redox activity in living cells.* Analytical biochemistry, 2009. **384**(1): p. 11-19.
134. Zhao, J., M Wang, Z Yang, Z Wang, H Wang, Z Yang,., *The different behaviors of three oxidative mediators in probing the redox activities of the yeast Saccharomyces cerevisiae.* Analytica chimica acta, 2007. **597**(1): p. 67-74.
135. Pänke, O., Balkenhohl, T., Kafka, J., Schäfer, D., Lisdat, F., *Impedance spectroscopy and biosensing*, in *Biosensing for the 21st Century*. 2007, Springer. p. 195-237.
136. Bao, N., J. Wang, and C. Lu, *Recent advances in electric analysis of cells in microfluidic systems.* Analytical and bioanalytical chemistry, 2008. **391**(3): p. 933-942.
137. Lisdat, F. and D. Schäfer, *The use of electrochemical impedance spectroscopy for biosensing.* Analytical and bioanalytical chemistry, 2008. **391**(5): p. 1555.
138. Lieberzeit, P.A. and F.L. Dickert, *Rapid bioanalysis with chemical sensors: novel strategies for devices and artificial recognition membranes.* Analytical and bioanalytical chemistry, 2008. **391**(5): p. 1629-1639.
139. Qavi, A.J., Washburn, A.L., Byeon, J.Y. and Bailey, R.C, *Label-free technologies for quantitative multiparameter biological analysis.* Analytical and bioanalytical chemistry, 2009. **394**(1): p. 121-135.
140. Morkvenaite-Vilkonciene, I., A. Ramanaviciene, and A. Ramanavicius, *9, 10-Phenanthrenequinone as a redox mediator for the imaging of yeast cells by scanning electrochemical microscopy.* Sensors and Actuators B: Chemical, 2016. **228**: p. 200-206.
141. Willaert, R.G., G.V. Baron, and L. De Backer, *Immobilised living cell systems.* 1996.
142. Wijffels, R., C. De Gooijer, and J. Tramper, *Gel immobilised living cell systems: Part 2*, in *Immobilised living cell systems: modelling and experimental methods*. 1996. p. 215-236.
143. Kosaric, N., *Ethanol–potential source of energy and chemical products.* Biotechnology: Products of Primary Metabolism, 1996: p. 121-203.
144. Chen, H., Heng, C.K., Puiu, P.D., Zhou, X.D., Lee, A.C., Lim, T.M. Tan, S.N.., *Detection of Saccharomyces cerevisiae immobilized on self-assembled monolayer (SAM) of alkanethiolate using electrochemical impedance spectroscopy.* Analytica chimica acta, 2005. **554**(1-2): p. 52-59.
145. Morkvenaite-Vilkonciene, I., Ramanaviciene, A., Genys, P. Ramanavicius, A., *Evaluation of Enzymatic Kinetics of GOx-based Electrodes by Scanning Electrochemical Microscopy at Redox Competition Mode.* Electroanalysis, 2017. **29**(6): p. 1532-1542.

146. Ostergaard, S., L. Olsson, and J. Nielsen, *Metabolic engineering of Saccharomyces cerevisiae.* Microbiol. Mol. Biol. Rev., 2000. **64**(1): p. 34-50.
147. Gunawardena, A., S. Fernando, and F. To, *Performance of a yeast-mediated biological fuel cell.* International journal of molecular sciences, 2008. **9**(10): p. 1893-1907.
148. Castro, F.A.V., Mariani, D., Panek, A.D., Eleutherio, E.C.A. Pereira, M.D.., *Cytotoxicity mechanism of two naphthoquinones (menadione and plumbagin) in Saccharomyces cerevisiae.* PloS one, 2008. **3**(12).
149. Ramanavicius, A., Morkvenaite-Vilkonciene, I., Kisieliute, A., Petroniene, J. and Ramanaviciene, A., *Scanning electrochemical microscopy based evaluation of influence of pH on bioelectrochemical activity of yeast cells− Saccharomyces cerevisiae.* Colloids and Surfaces B: Biointerfaces, 2017. **149**: p. 1-6.
150. Rodriguez, C.E., Shinyashiki, M., Froines, J., Yu, R.C., Fukuto, J.M. Cho, A.K., *An examination of quinone toxicity using the yeast Saccharomyces cerevisiae model system.* Toxicology, 2004. **201**(1-3): p. 185-196.
151. Shiku, H., Goto, S., Jung, S., Nagamine, K., Koide, M., Itayama, T., Yasukawa, T. and Matsue., *Electrochemical characterization of enzymatic activity of yeast cells entrapped in a poly (dimethylsiloxane) microwell on the basis of limited diffusion system.* Analyst, 2009. **134**(1): p. 182-187.
152. Tsionsky, M., Zhou, J., Amemiya, S., Fan, F.R.F., Bard, A.J. Dryfe, R.A, *Scanning electrochemical microscopy. 38. Application of SECM to the study of charge transfer through bilayer lipid membranes.* Analytical chemistry, 1999. **71**(19): p. 4300-4305.
153. Diakowski, P.M., Z. Ding, *Interrogation of living cells using alternating current scanning electrochemical microscopy (AC-SECM).* Physical Chemistry Chemical Physics, 2007. **9**(45): p. 5966-5974.
154. Huang, Y., Holzel, R., Pethig, R. ,Wang, X.B, *Differences in the AC electrodynamics of viable and non-viable yeast cells determined through combined dielectrophoresis and electrorotation studies.* Physics in Medicine & Biology, 1992. **37**(7): p. 1499.
155. Markx, G.H., M.S. Talary, and R. Pethig, *Separation of viable and non-viable yeast using dielectrophoresis.* Journal of biotechnology, 1994. **32**(1): p. 29-37.
156. Henry-Stanley, M.J., R.M. Garni, and C.L. Wells, *Adaptation of FUN-1 and Calcofluor white stains to assess the ability of viable and nonviable yeast to adhere to and be internalized by cultured mammalian cells.* Journal of microbiological methods, 2004. **59**(2): p. 289-292.
157. Brady, D., A. Stoll, J. Duncan, *Biosorptton of heavy metal cations by non-viable yeast biomass.* Environmental Technology, 1994. **15**(5): p. 429-438.

158. Egilmez, N.K., J.B. Chen, and S.M. Jazwinski, *Preparation and partial characterization of old yeast cells.* Journal of gerontology, 1990. **45**(1): p. B9-B17.
159. Tang, S.-Y., Zhang, W., Baratchi, S., Nasabi, M., Kalantar-zadeh, K. Khoshmanesh., *Modifying dielectrophoretic response of nonviable yeast cells by ionic surfactant treatment.* Analytical chemistry, 2013. **85**(13): p. 6364-6371.
160. Herker, E., Jungwirth, H., Lehmann, K.A., Maldener, C., Fröhlich, K.U., Wissing, S., Büttner, S., Fehr, M., Sigrist, S. and Madeo, F.,, *Chronological aging leads to apoptosis in yeast.* J Cell Biol, 2004. **164**(4): p. 501-507.
161. Váchová, L. and Z. Palková, *Physiological regulation of yeast cell death in multicellular colonies is triggered by ammonia.* The Journal of cell biology, 2005. **169**(5): p. 711-717.
162. Yamashoji, S., *Different characteristics between menadione and menadione sodium bisulfite as redox mediator in yeast cell suspension.* Biochemistry and biophysics reports, 2016. **6**: p. 88-93.
163. Sabirovas, T., A. Valiūnienė, and G. Valincius, *Mechanically polished titanium surface for immobilization of hybrid bilayer membrane.* Journal of The Electrochemical Society, 2018. **165**(10): p. G109-G115.
164. Lasia, A., *Electrochemical impedance spectroscopy and its applications*, in *Modern aspects of electrochemistry*. 2002, Springer. p. 143-248.
165. Diakowski, P.M. and Z. Ding, *Novel strategy for constant-distance imaging using alternating current scanning electrochemical microscopy.* Electrochemistry Communications, 2007. **9**(10): p. 2617-2621.
166. Baranski, A.S. and P.M. Diakowski, *Application of AC impedance techniques to Scanning Electrochemical Microscopy.* Journal of Solid State Electrochemistry, 2004. **8**(10): p. 683-692.
167. Gabrielli, C., Huet, F., Keddam, M., Rousseau, P., Vivier, V., *Scanning electrochemical microscopy imaging by means of high-frequency impedance measurements in feedback mode.* The Journal of Physical Chemistry B, 2004. **108**(31): p. 11620-11626.
168. Alpuche-Aviles, M.A. and D.O. Wipf, *Impedance feedback control for scanning electrochemical microscopy.* Analytical chemistry, 2001. **73**(20): p. 4873-4881.
169. Autio, K. and T. Mattila-Sandholm, *Detection of active yeast cells (Saccharomyces cerevisiae) in frozen dough sections.* Appl. Environ. Microbiol., 1992. **58**(7): p. 2153-2157.
170. Valiūnienė, A., Petroniene, J., Morkvenaite-Vilkonciene, I., Popkirov, G., Ramanaviciene, A. and Ramanavicius, A., *Redox-probe-free scanning electrochemical microscopy combined with fast Fourier transform electrochemical impedance spectroscopy.* Physical Chemistry Chemical Physics, 2019. **21**(19): p. 9831-9836.

171. Shiku, H., Shiraishi, T., Ohya, H., Matsue, T., Abe, H., Hoshi, H. Kobayashi, M., *Oxygen consumption of single bovine embryos probed by scanning electrochemical microscopy.* Analytical chemistry, 2001. **73**(15): p. 3751-3758.
172. Feng, W., S.A. Rotenberg, and M.V. Mirkin, *Scanning electrochemical microscopy of living cells. 5. Imaging of fields of normal and metastatic human breast cells.* Analytical chemistry, 2003. **75**(16): p. 4148-4154.
173. Hengstenberg, A., Blöchl, A., Dietzel, I.D., Schuhmann, W, *Spatially resolved detection of neurotransmitter secretion from individual cells by means of scanning electrochemical microscopy.* Angewandte Chemie International Edition, 2001. **40**(5): p. 905-908.
174. Liu, B., Cheng, W., Rotenberg, S.A., Mirkin, M.V., *Scanning electrochemical microscopy of living cells: Part 2. Imaging redox and acid/basic reactivities.* Journal of Electroanalytical Chemistry, 2001. **500**(1-2): p. 590-597.
175. Zhao, J., Zhang, N., Prestwich, G.D., Wen, X., *Recruitment of endogenous stem cells for tissue repair.* Macromolecular bioscience, 2008. **8**(9): p. 836-842.
176. Huh, D., G.A. Hamilton, and D.E. Ingber, *From 3D cell culture to organs-on-chips.* Trends in cell biology, 2011. **21**(12): p. 745-754.
177. Xie, Y., Ibrahim, A., Cheng, K., Wu, Z., Liang, W., Malliaras, K., Sun, B., Liu, W., Shen, D., Cheol Cho, H., Li, T., *Importance of cell-cell contact in the therapeutic benefits of cardiosphere-derived cells.* Stem Cells, 2014. **32**(9): p. 2397-2406.
178. Mauzeroll, J., Bard, A.J., Owhadian, O. and Monks, T.J., *Menadione metabolism to thiodione in hepatoblastoma by scanning electrochemical microscopy.* Proceedings of the National Academy of Sciences, 2004. **101**(51): p. 17582-17587.
179. Mirkin, M.V. and B.R. Horrocks, *Electroanalytical measurements using the scanning electrochemical microscope.* Analytica Chimica Acta, 2000. **406**(2): p. 119-146.
180. Bard, A.J., X. Li, and W. Zhan, *Chemically imaging living cells by scanning electrochemical microscopy.* Biosensors and Bioelectronics, 2006. **22**(4): p. 461-472.
181. McAmis, W.C., Schaeffer Jr, R.C., Baynes, J.W., Wolf, M.B., *Menadione causes endothelial barrier failure by a direct effect on intracellular thiols, independent of reactive oxidant production.* Biochimica et Biophysica Acta (BBA)-Molecular Cell Research, 2003. **1641**(1): p. 43-53.
182. Warren, M.C., Bump, E.A., Medeiros, D., Braunhut, S.J., *Oxidative stress–induced apoptosis of endothelial cells.* Free Radical Biology and Medicine, 2000. **29**(6): p. 537-547.
183. Criddle, D.N., Gillies, S., Baumgartner-Wilson, H.K., Jaffar, M., Chinje, E.C., Passmore, S., Chvanov, M., Barrow, S., Gerasimenko, O.V., Tepikin, A.V., Sutton, R.., *Menadione-induced reactive oxygen*

species generation via redox cycling promotes apoptosis of murine pancreatic acinar cells. Journal of Biological Chemistry, 2006. **281**(52): p. 40485-40492.
184. Giam, L.R., Massich, M.D., Hao, L., Wong, L.S., Mader, C.C. Mirkin, C.A, *Scanning probe-enabled nanocombinatorics define the relationship between fibronectin feature size and stem cell fate*. Proceedings of the National Academy of Sciences, 2012. **109**(12): p. 4377-4382.
185. Murata, T., Yasukawa, T., Shiku, H., Matsue, T., *Electrochemical single-cell gene-expression assay combining dielectrophoretic manipulation with secreted alkaline phosphatase reporter system.* Biosensors and Bioelectronics, 2009. **25**(4): p. 913-919.
186. Xiao, W., *Yeast protocols*. 2006: Springer.
187. Lewpiriyawong, N., Kandaswamy, K., Yang, C., Ivanov, V., Stocker, R., *Microfluidic characterization and continuous separation of cells and particles using conducting poly (dimethyl siloxane) electrode induced alternating current-dielectrophoresis.* Analytical chemistry, 2011. **83**(24): p. 9579-9585.
188. Davis, D.R., Zhang, Y., Smith, R.R., Cheng, K., Terrovitis, J., Malliaras, K., Li, T.S., White, A., Makkar, R., Marbán, E., *Validation of the cardiosphere method to culture cardiac progenitor cells from myocardial tissue.* PloS one, 2009. **4**(9): p. e7195.
189. Popkirov, G., R. Schindler, *Validation of experimental data in electrochemical impedance spectroscopy.* Electrochimica acta, 1993. **38**(7): p. 861-867.
190. Suchodolskis, A., Stirke, A., Timonina, A., Ramanaviciene, A., Ramanavicius, A, *Baker's yeast transformation studies by Atomic Force Microscopy.* Advanced Science Letters, 2011. **4**(1): p. 171-173.
191. Kwak, J., A.J. Bard, *Scanning electrochemical microscopy. Apparatus and two-dimensional scans of conductive and insulating substrates.* Analytical Chemistry, 1989. **61**(17): p. 1794-1799.
192. Xiong, H., J. Guo, and S. Amemiya, *Probing heterogeneous electron transfer at an unbiased conductor by scanning electrochemical microscopy in the feedback mode.* Analytical chemistry, 2007. **79**(7): p. 2735-2744.
193. Zou, F., D. Thierry, H. Isaacs, *A High-Resolution Probe for Localized Electrochemical Impedance Spectroscopy Measurements.* Journal of the Electrochemical Society, 1997. **144**(6): p. 1957-1965.
194. Trinh, D., Keddam, M., Novoa, X.R. and Vivier, V., *Alternating-Current Measurements in Scanning Electrochemical Microscopy, Part 1: Principle and Theory.* ChemPhysChem, 2011. **12**(11): p. 2169-2176.
195. Trinh, D., Keddam, M., Novoa, X.R., Vivier, V.., *Alternating current measurements in scanning electrochemical microscopy, part 2: detection of adsorbates.* ChemPhysChem, 2011. **12**(11): p. 2177-2183.

196. Trinh, D., Keddam, M., Nóvoa, X.R., Vivier, V., *Characterization of adsorbates by transient measurements in Scanning Electrochemical Microscopy*. Electrochimica Acta, 2014. **131**: p. 28-35.
197. Bard, A. and M. Mirkin, *Scanning Electrochemical Microscopy Marcel Dekker*. New York, 2001.
198. Brug, G., Van Den Eeden, A.L.G., Sluyters-Rehbach, M. and Sluyters, J.H.., *The analysis of electrode impedances complicated by the presence of a constant phase element.* Journal of electroanalytical chemistry and interfacial electrochemistry, 1984. **176**(1-2): p. 275-295.

SANTRAUKA

ĮVADAS

Vis dažniau elektrocheminio tyrimo objektu tampa gyva ląstelė. Žmogaus mezenchiminės ląstelės, t.y. pagrindinės kamieninės ląstelės, taip pat ne išimtis. Klinikiniai tyrimai iškelia tokių klausimų į kuriuos atsakyti galima tik aktyviai bendradarbiaujant su tokiomis mokslo sritimis kaip elektrochemija. Elektrocheminiai žmogaus širdies kairiojo skilvelio mezenchiminių kamieninių ląstelių tyrimai yra nuosekli tokių ląstelių tyrimo dalis ir gali padėti medicinos mokslo darbuotojams terapiniuose tyrimuose. Taigi elektrocheminiame procese dalyvaujančio paviršiaus detalesnis tyrimas yra natūralus šiuolaikinio mokslo interesų objektas, nes būtent paviršius atlieka vieną svarbiausių vaidmenų daugelyje elektrocheminių procesų. Elektrocheminiams tyrimams pasirinktą objektą, pvz. gyvą ląstelę, tenka vienaip ar kitaip imobilizuoti ant pasirinkto paviršiaus. Paviršiaus elektrinis laidumas yra viena svarbiausių savybių, nulemianti tos medžiagos pasirinkimą tiriamo objekto imobilizacijai. Tiriant lokalius, trumpai trunkančius procesus ant mažų objektų ar šalia jų, mikroelektrocheminiai metodai tampa patogia priemone leidžiančia naujai pažvelgti į gerai žinomus procesus ir jų vertinimus. Atsiradę nauji tyrimo objektai, tokie kaip poveikiui labai jautri gyva žmogaus mezenchiminė kamieninė ląstelė, iškelia poreikį tobulinti elektrocheminio tyrimo įrangą ir tyrimo metodus.

Ultramikroelektrodai (UME) jau nėra naujiena nuo praėjusio amžiaus vidurio. Jie dažniausiai naudojami skenuojančios elektrocheminės mikroskopijos (SECM) tyrimams, nes tokie elektrodai be pagrindinio privalumo- mažo darbinio/aktyviojo ploto, turi didelį difuzinį sluoksnį, leidžia greitai pasiekti pusiausvyros būsenas bei yra jautrūs menkiausiems aplinkos būklės pokyčiams. Jų dėka tiriamą procesą galima išmatuoti be didelių trikdžių, tačiau priartėjimo kreivių kaip pagrindinės SECM tyrimo rūšies duomenų iššifravimas vis dar turi neatsakytų klausimų, t.y. SECM teorija vis dar vystoma. Elektrocheminės pilnutinės varžos (impedanso) spektroskopija taip pat yra vienas efektyviausių tyrimo būdų elektrochemijoje. Elektrocheminio impedanso spektrai (EIS) gali būti užregistruoti įrenginiais veikiančiais skirtingais metodais bei gauti duomenys analizuojami įvairiomis automatizuotomis duomenų apdorojimo programomis, tačiau greitosios Furje transformacijos metodu signalus analizuojantis elektrocheminio impedanso spektrometras (FFTS) sinchroniškai veikiantis su skenuojančiu

elektrocheminiu mikroskopu (SECM) yra nauja šių prietaisų kombinacija, leidžianti sparčiau išmatuoti EIS, kontroliuojant darbinio elektrodo atstumą iki tiriamojo paviršiaus. Skirtingai nuo SECM tyrimo režimų ir metodų, EIS gali būti užregistruoti kai elektrocheminėje sistemoje nėra redokso tarpininkų, todėl FFTS ir SECM sinchronizuotais prietaisais užregistruoti EIS pageidaujamu atstumu iki laidaus ar nelaidaus paviršiaus leidžia naujai įvertinti tiriamų procesų visumą, vykstančią ultramikroelektrodui esant atstumais mažesniais nei 10 šio elektrodo spindulių iki substrato. Tai yra, galima stebėti ir greitai užregistruoti procesus kai prasideda UME pusiausferinės difuzijos apsunkinimas. Šiuo metodu gauti rezultatai gali papildyti SECM teoriją ir padėti geriau įvertinti vykstančius procesus kai elektrodas yra optimaliausiu tyrimams atstumu iki tiriamojo paviršiaus. Sinchronizavus šiuos du prietaisus galima atlikti matavimus tiksliai nustatant ultramikroelektrodo poziciją elektrocheminėje celėje substrato atžvilgiu ir registruoti EIS vos per kelias sekundes. Trumpiausiai trunkantis EIS registravimas šiuo būdu yra 1,3 sekundės. Tokia prietaisų sistemos galimybė leidžia tirti nestabilias sistemas arba gyvas ląsteles. Tai ypač aktualu tiriant trumpalaikius procesus ir vertinant UME signalus SECM teorijoje. Kai tyrimo objektas yra viena ląstelė užregistruojami itint maži srovės pokyčiai elektrocheminio tyrimo metu. Norint patikimai nustatyti tokio srovės pokyčio kilmę t.y. ar pokytį lemia procesai ląstelėje ar ant elektrodo paviršiaus, yra itint svarbu. Taigi parengiamieji darbai analizuojant procesus kai UME yra arti elektrai laidaus arba nelaidaus paviršiaus yra svarbūs, norint teisingai įvertinti ląstelių tyrimus.

DARBO TIKSLAS

Sinchronizuoti greitosios Furje transformacijos impedansometrą ir skenuojantį elektrocheminį mikroskopą matavimams, siekant sumažinti EIS matavimo laiką, tiksliai kontroliuojant ultramikroelektrodo buvimo poziciją substrato atžvilgiu. Šiuo metodu atlikti matavimus siekant pademonstruoti metodo patogumą tiriant elektrai laidžius ir nelaidžius paviršius, gyvas ląsteles ar kitas redoks mediatoriams jautrias bei nestabilias sistemas.

DARBO UŽDAVINIAI

1. Parodyti galimybę FFT-EIS pritaikymo skenuojančios elektrocheminės mikroskopijos lokalių procesų matavimams arti laidaus (grafito) ir nelaidaus (politetrafluoetileno) paviršių esant elektrolite redokso mediatorių porai $Fe(CN)_6^{3-}$/ $Fe(CN)_6^{4-}$ fosfatiniam pH6,8 buferyje.

2. Pademonstruoti galimybes FFT-EIS sinchroniškai veikiančio su SECM greitam lokalizuotų spektrų registravimui, keičiant atstumą nuo 0 iki 200 mikrometrų nuo laidaus arba nelaidaus paviršiaus, kai elektrolite nėra redox mediatorių poros. Šio metodo tikslas- pademonstruoti galimybę tirti tokius mėginius kurie yra jautrūs redokso junginiams, kai atstumas nuo ultramikroelektrodo iki tiriamo paviršiaus yra nuo 10 mikrometrų iki minimaliai įmanomo atstumo.
3. Sinchronizuotais FFT-EIS ir SECM prietaisais, skenuojančio elektrocheminio impedanso metodu užregistruoti aktyvių ir deaktyvuotų imobilizuotų mielių *Saccharomyces cerevisiae* ląstelių elektrocheminio aktyvumo skirtumus. Pademonstruoti galimybę tokia įranginių kombinacija vertinti mielių ląstelių gyvybingumą.
4. Skenuojančios elektrocheminės mikroskopijos metodais užregistruoti žmogaus širdies miokardo mezenchiminių kamieninių ląstelių galimus elektrocheminių matavimų skirtumus taikant menadiono/menadiolo mediatorių porą pagal iš anksto žinomą ląstelių patologiškumo laipsnį. Pademonstruoti SECM galimybę taikyti ląstelių patologiškumo atpažinimui kai naudojama menadiono ir menadiolo redokso tarpininkų pora.

MOKSLINIS NAUJUMAS

1. EIS spektrai išmatuoti FFTS, esant potencialų reikšmėms kai keičiasi ciklinės voltamperometrijos kreivių dinamika iš faradėjinio į nefaradėjinį procesą, taikant FFT-SEIM metodą, kontroliuojant atstumą iki substrato SECM-u.
2. Sinchronizuotais FFT ir SECM prietaisiais išmatuota EIS nesant redokso mediatorių elektrolite, atstumais iki substrato mažesniais nei 10 UME elektrodo spindulio reikšmių, kai EIS užregistravimas trunka nuo 1,3 iki 13 sekundžių.
3. Sinchronizuotais FFT ir SECM prietaisiais išmatuota EIS kontroliuojamu atstumu virš imobilizuotų aktyvių ir deaktyvuotų *Saccharomyces cerevisiae* mielių ląstelių gauti rezultatų skirtumai, kuriais remiantis galima atpažinti gyvų ląstelių išskiriamų produktų sukeltus EIS pokyčius.
4. SECM grįžtamojo ryšio ir redokso/konkurencijos metodais atlikti matavimai nustatytais atstumais iki žmogaus širdies miokardo mezenchiminių kamieninių ląstelių, taikant menadioną/menadiolą kaip redokso tarpininkų porą, užregistruoti priartėjimo kreivių skirtumai priklausomai nuo ląstelių patologiškumo.

Ginamieji teiginiai

1. Įrenginių FFTS ir SECM derinys sudaro sąlygas EIS išmatuoti kontroliuojamu atstumu iki tiriamo paviršiaus be redokso tarpininkų arba naudojant redokso tarpininkų porą elektrocheminėje celėje vykstant Faradėjiniams procesams.
2. Tinkamiausias atstumas laidininkų ir izoliatorių paviršių tyrimui taikant SECM sinchronizuotą kartu su FFTS yra ne didesnis nei 2d/a tarp tiriamo paviršiaus ir ultramikroelektrodo.
3. EIS, atliekamas FFTS derinyje su SECM gali būti taikomas mielių *Saccharomyces cerevisiae* gyvybingumo skirtumams užregistruoti tirpale esant redokso tarpininkų menadiono ir menadiolo porai. Mielių elektrocheminiam aktyvumui nustatyti tinkamiausias atstumas tarp UME ir tiriamų ląstelių yra ne daugiau kaip 2d/a.
4. SECM priartėjimo kreivių matavimo metodas, atliktas naudojant redokso tarpininkų medaniono ir menadiolo porą, taikomas sveikoms ir patologinėms žmogaus širdies mezenchiminėms kamieninėms ląstelėms, skirtas elektrocheminio aktyvumo skirtumams matuoti, gali būti naudojamas ląstelių patologiškumo nustatymui, kai atstumas tarp UME ir ląstelės yra ne daugiau kaip 3d/a, kai d- atstumas tarp UME ir tiriamo paviršiaus, a- elektrodo laidžiosios dalies spindulys.

EKSPERIMENTŲ METODIKA

Skenuojantis elektrocheminis mikroskopas (SECM) savo valdymo programoje dažniausiai turi elektrocheminio impedanso matavimo funkciją, tačiau šiuo būdu užregistruoti elektrocheminio impedanso spektrą (EIS) užtrunka net keletą minučių. Greitosios Furje transformacijos elektrocheminio impedanso spektrometras (FFTS) analogišką spektrą užregistruoti užtrunka vos 1 sekundę, arba priklausomai nuo pasirinktų parametrų esant sudėtingesnei sistemai- iki vienos minutės. EIS matavimai buvo atlikti sinchronizavus veikimą EIS-128/16 įrenginį sukurtą Kylio Universitete ir turintį FFT EIS registravimo funkciją su Sensolytics SECM (04-01003) įrenginiu, valdomu potenciostatu AUTOLAB PGSTAT 30, bei taikant du atskirus kompiuterius su atitinkama programine įranga prietaisams valdyti.
Tyrimai atlikti standartinėje plastikinėje Petri lėkštelėje pritaikytoje elektrocheminiams tyrimams, pagal FFT spektrometro reikalavimus- keturių elektrodų elektrocheminėje celėje. Matavimai atlikti 10 μm skersmens aukso ultramikroelektrodu (UME). Skenuojančio elektrocheminio impedanso (SEIM) be redokso mediatorių tyrimams atlikti buvo pasirinktas fosfatinis

buferinis pH 6.8 tirpalas, naudojant elektrai laidų pavyzdį- grafitą ir elektrai nelaidžią medžiagą- tefloną (politetrafluoretileną). Priartėjimo kreivėse stebimas aiškus elektrodo blokavimas (neigiamas grįžtamasis ryšys) priartinus prie nelaidaus paviršiaus ir ryškus teigiamojo grįžtamojo ryšio signalas priartinus UME prie grafito, t.y. srovė padidėja daugiau nei šimtą kartų UME priartinus maksimaliai įmanomu atstumu iki laidaus paviršiaus. EIS matavimams pasirinktas potencialas -1,2V*vs* Ag/AgCl| KCl_{sat} pagal prieš pagrindinį eksperimentą išmatuotą ciklinę voltamperinę (CV) kreivę. Šis pasirinktas potencialas yra tokiame CV taške kai Farajėjinis procesas pereina į nefaradėjinį. CV kreivės skleidimo greitis- 0.2 V s^{-1}, žingsnis 0,02V. EIS užregistruoti dažnių ruože nuo 1,5 Hz iki 50kHz, naudojant trijų pasikartojančių matavimų vidurkį kaip galutinį rezultatą. Pasirinkta kintamos srovės sužadinimo amplitudė 10-15 mV. Atstumas iki tiriamojo paviršiaus buvo nustatomas SECM-u matuojant priartėjimo kreives 1µ/s greičiu.

EIS matavimams fosfatiniame buferiniame pH6.8 tirpale su redokso mediatorių pora $Fe(CN)_6^{3-}$/ $Fe(CN)_6^{4-}$ pasirinktas potencialas iš CV duomenų,+0.2V*vs* Ag/AgCl| KCl_{sat}. Dažnių ruožas- atitinkamai nuo 1,5 Hz iki 50kHz, duomenys buvo pateikti gavus trijų pasikartojančių matavimų vidurkį kaip galutinį rezultatą. EIS užregistruoti kontroliuojant SECM-u atstumą iki laidaus arba nelaidaus paviršiaus 1 1µ/s žingsniu. EIS spektruose taip pat kaip ir SECM priartėjimo kreivėse yra matoma tendencija, kuomet elektrodui esant mažesniu atstumu nei du UME spinduliai, EIS spektrai įgyja kitokią formą ir jiems pritaikoma ekvivalentinė grandinė turinti Varburgo impedanso elementą. Šie matavimo duomenys pilnai atitinka SECM teoriją.

Taip pat atlikti EIS matavimai su gyvomis ląstelėmis. Matavimams gyvos *Saccharomyces cerevisiae* mielių ląstelės buvo imobilizuotos ant plastiko Petri paviršiaus lėkštelės su glutaro aldehidu laikant lėkštelę virš jo garų 15 minučių prieš imobilizavimą ir 15 minučių imobilizavus ir išdžiovinus mielių lašą. Susidariusio mielių lašo kokybė ir susidariusios dangos storis buvo įvertinta atominių jėgų mikroskopu (Bioscope II)/Catalyst from Veeco (Santa Barbara, USA), bei optiniu mikroskopu (CETI Medline Scientific, (Oxford, United Kingdom). Nusatyta, kad susidaręs mielių sluoksnis buvo 1.5-2 mikrometrai. Imobilizuotos aktyvios ir deaktyvuotos mielės prieš elektrocheminio impedanso matavimus buvo veikiamos dviejų mediatorių Vit-K_1ir Vit –K_3 mišiniu. Vienu atveju mediatorių mišinys buvo pilamas į buferinį tirpalą ir juo užpilamas imobilizuotų mielių pavyzdys. Kitų atveju ištirpintų mediatorių mišinys buvo užpilamas tiesiai ant aktyvių arba deaktyvių mielių ir tik išsausėjus bandiniui buvo užpilamas buferinis tirpalas ir atliekami EIS matavimai. Eksperimentai buvo atliekami nustačius potencialą pasirinktą iš CV kreivių priklausomai nuo eksperimentui pasirinkto elektrodo. Potencialas pasirinktas -1,2V*vs* Ag/AgCl|

KCl_{sat}, kai matavimai atlikti platinos 10 mikrometrų skersmens UME elektrodu ir -0.84V*vs* Ag/AgCl| KCl_{sat} kai elektrodas- 3mm grafito diskas. FFTS įrenginyje EIS matavimams parinkta kintamos srovės amplitudė 10-15 mV. Visų tyrimų metu užregistruoti spektrai buvo analizuojami „ZView“ analizės programa, duomenys pateikti paveiksluose atliktuose OriginPro9.0 programa.

Žmogaus širdies miokardo mezenchiminių kamieninių ląstelių (hmMSC) tyrimai atlikti matuojant SECM priartėjimo kreives. Tyrimai atlikti siekant išsiaškinti tokio metodo galimybes taikyti atpažinimui patologinėms ir sveikoms ląstelėms. Ląstelės į tiriamąją laboratoriją buvo atvežamos imobilizuotos ant pasirinkto paviršiaus, patalpintos mitybinėje terpėje. Pervežimo metu ir iki eksperimentų ląstelės buvo saugomos 37° C temperatūroje. Ląstelės buvo atgabenamos į elektrochemijos laboratoriją pilnai paruoštos SECM tyrimui, mitybinėje terpėje su atitinkančiais gyvybės palaikymui priedais ir elektrolitais. Po tyrimų likusi biologinė medžiaga buvo grąžinama tyrimo centrui utilizuoti. Kadangi ne linijose auginamos, t.y. gautos iš realių pacientų, hmMSC ląstelės pasižymi didele formos įvairove vertinant vizualiai optiniu mikroskopu. Šis faktas yra nurodomas ir literatūroje. Matavimams buvo pasirenktamos tos ląstelės kurios vizualiai buvo verpstės formos. Būtent dėl šios hmMSC savybės buvo pasirinktas gerai ištirtas redokso tarpininkas menadionas. Kaip nurodoma literatūroje, menadionasdifuziniu keliu gali difunduoti į ląstelę ir būti pašalintas elektrochemiškai aktyvaus junginio (menadiolo) pavidale, kurio atsiradimas siejamas su srovės padidėjimu arti ląstelės paviršiaus. Elektrocheminių matavimų metu hmMSC turi gebėjimą pasitraukti iš elektros lauko veikimo zonos, taip pat yra lengvai pažeidžiamos mechaniškai, eksperimentų rezultatuose „nulinis“ atstumas nėra tikslus, jis buvo apskaičiuotas atlikus preliminarius matavimus kai elektrodas buvo artinamas iki ląstelės ją sutraiškant ir iš gautų duomenų bei iš duomenų kuriuos buvo pateikusi ląsteles auginanti laboratorija, buvo priimta prielaida kokiu atstumu UME gali būti saugiai artinamas iki tiriamos ląstelės. Taip pat buvo pasirinkta matuoti SECM priartėjimo kreives ir iš srovės pokyčių arti ląstelės paviršiaus palyginimo esant skirtingoms menadiono koncentracijoms daryti prielaidas apie ląstelių membranos pralaidumą. Potencialas tinkamiausias tokiam tyrimui pasirinktas remiantis CV kreive, tai yra +0.4V *vs* Ag/AgCl| KCl_{sat} taikant generavimo/ surinkimo GC-SECM režimą ir -0.5V *vs* Ag/AgCl| KCl_{sat}, taikant redokso konkurencijos RC-SECM režimą kai tas pats procesas vyksta ant elektrodo ir ląstelės viduje. Buvo tiriamos sveikos ir patologiją turinčios ląstelės SECM priartėjimo kreivių metodu, bei lyginami gauti rezultatai atsižvelgiant į ląstelių patologiškumą.

Hibridinė sistema: FFT impedanso spektroskopija kombinuota su skenuojančia elektrochemine mikroskopija

UME poziciją substrato atžvilgiu kontroliuojant SECM-u buvo išmatuoti EIS, tai- skenuojanti elektrocheminio impedanso mikroskopija (SEIM). Teigiamas grįžtamasis ryšys registruojamas kai UME priartinamas prie laidaus, į elektrinę grandinę neprijunto grafito ir neigiams grįžtamasis ryšys- kai UME yra blokuojamas artinant prie nelaidaus substrato, teflono. FFT EIS, SEIM išmatuoti duomenys rodo esant tiesioginę priklausomybę krūvio pernašos varžos nuo atstumo iki laidaus paviršiaus. Vadinamas „nulinis“ atstumas nuo UME iki substrato labai priklauso nuo tiriamo paviršiaus bei laidžiosios UME dalies pasvirimo viena kitos atžvilgiu. Šių dviejų paviršių nelygiagretumas yra SECM matavimų problema, kuri dažniausiai išsprendžiama taikant matematinio duomenų apdorojimo programas. Paviršių nelygiagretumas yra sunkiai sukontroliuojamas, bet darbinio elektrodo kontaktas su laidžiu substratu yra įmanomas. Užregistruotas teigiamas grįžtamasis ryšys matuojant priartėjimo kreivę buvo pagrindinis kriterijus nustatant „nulinį“ atstumą, t.y. tiesioginį elektrai laidaus substrato ir UME kontaktą. Nustačius šį atstumą, elektrodas buvo atitraukiamas keliais kitais atstumais ir užregistruojami EIS. Atlikti matavimai rodo, kad artėjant prie laidaus paviršiaus, srovę ribojantis faktorius tėra krūvio pernaša, priklausanti nuo redokso jonų difuzijos greičio.

EIS spektrai buvo išmatuoti UME artinant iki nelaidaus paviršiaus. Remiantis neigiamo grįžtamojo ryšio teorija, ribojantis proceso greitį faktorius yra redokso mediatoriaus heksacianoferato jono difuzija, kai UME kontaktuoja su nelaidžiu paviršiumi arba yra tam tikru atstumu iki joDėl apribotos heksacianoferato jonų difuzijos, didžiausios krūvio pernašos varžos buvo užregistruota „nuliniu“ atstumu. Didesniu nei 10 μm atstumu tarp UME ir nelaidaus substrato difuziją atitinkančios Nyquist‘o spektro dalies neberegistruojame, difuziją atitinkančios dalies ekvivalentinėje grandinėje nebelieka. Kadangi matavimai yra greitesni nei standartiniai, tikėtina kad tokio pobūdžio matavimus galima pritaikyti elektrocheinių reakcijų kinetikai apskaičiuoti. EIS matavimai tiksliu atstumu iki paviršiaus trunkantys vieną sekundę gali suteiki daugiau informacijos apie procesus vykstančius elektrocheminėje celėje.

Skenuojančios elektrocheminė impedanso mikroskopijos kombinuotos su greitosios Furje transformacijos elektrocheminio impedanso mikroskopija taikymas sistemoms be redokso mediatorių.

EIS matavimai tiksliu atstumu iki paviršiaus buvo užregistruoti esant potencialui -1.0 V *vs* Ag|AgCl|KClsat., kai sistemoje nestebima faradėjinių procesų. Gauti spektrai nuo „nulinio“ iki 200µm nuo paviršiaus. Kai UME yra arti laidaus bet į elektros grandinę neprijungto grafito paviršiaus EIS spektrai kinta nežymiai ir nedideli reikšmių skirtumai išmatuojami tik žemų dažnių srityje. Tačiau analogiški matavimai prie nelaidaus paviršiaus jau šiek tiek skiriasi ir viršijus 100µm atstumą, izoliuojančio paviršiaus įtakos krūvio pernešimui jau nebestebime. Analogiški tyrimai esant potencialui -1.2 V *vs* Ag|AgCl|KClsat, kai sistemoje remiantis cikline voltamperine kreive aiškiai registruojami Faradėjiniai procesai stebima priklausomybė nuo atstumo EIS spektruose. Krūvio pernašos varža didėja tolstant nuo laidaus paviršiaus ir mažėja kai tolstama nuo nelaidaus teflono paviršiaus. Itint greitas FFT-EIS spektrų registravimas padeda išvengti dujų burbuliukų formavimosi įtakos tokiems rezultatams, nes vandens hidrolizės procesas per tokį laiko tarpą neduoda pakankamo kiekio vandenilio atomų vandenilio molekulėms susiformuoti ant mažo UME elektrodo ploto. Kadangi FFT impedansometro programinė įranga leidžia kontroliuoti paduodamo į sistemą ir ateinačio iš jos signalo kokybę bei atmesti netinkamus signalus bei triukšmus, galima elektrocheminėje celėje sukurti sąlygas kokybiškų EIS užregistravimui. Gautiems EIS pritaikytas ekvivalentinės grandinės modelis sudarytas iš tirpalo varžos, pastoviosios fazės elemento kuris atitinka dvigubo elektrinio lauko talpą susiformuojančio tarp UME ir buferinio tirpalo ir krūvio pernašos varžos kuri atirinka krūvio pernašą tarp UME ir elektrolito tirpalo. Gauti EIS rezultatai neprieštarauja priarėjimo kreivėje matomiems srovės pokyčiams ir gali papildyti SECM teorijos matematinius modelius.

Imobilizuotų aktyvių ir deaktyvuotų mielių elektrocheminių savybių tyrimas SECM ir SEIM metodais

Kadangi vitaminų K grupės medžiagos yra svarbios daugeliui gyvybinių procesų, o maistinių mielių ląstelės yra patogios tokiems tyrimams atlikti, buvo pasirinkta šiuo metodu ištirti dviejų vitaminų K mišinio poveikį mielių ląstelėms. Pirmiausia aiškūs skirtumai lyginant aktyvias ir deaktyvuotas mieles buvo pastebėti SECM priartėjimo kreivėse, kai srovių pokyčių reikšmės artinant UME prie imobilizuoto mielių pavyzdžio skyrėsi daugiau nei penkis kartus. Potencialai šiam tyrimui buvo pasirinkti iš CV kreivės

buferiname tirpale be mediatorių, sigmoidinėje kreivėje esančiose nusistovėjusios srovės ruožuose. Kadangi deaktyvuotos mielės nevartoja deguonies, pastebėtas UME blokavimas prasideda mažesniu nei 120µm atstumu iki mielių paviršiaus ir pasiekus 50µm atstumą iki tiriamojo pavyzdžio, registruojama tik elektrolito difuzijos apribojimai. UME kontaktas su mielėmis yra nepageidautinas, todėl „nulinė“ atstumo reikšmė ir registruojama srovė nėra lygi nuliui. Tarp UME ir elektrolito vis dar tebevyksta krūvio mainai dėl tirpale esančio deguonies, todėl kad elektrodas nėra pilnai blokuotas netolygaus mielių pavyzdžio paviršiaus ir tirpale esantis deguonis vis dar gali pasiekti UME laidžiosios dalies paviršių. Toks srovių priartėjimo kreivėse užregistravimas tiek arti aktyvių tiek deaktyvuotų mielių sudaro galimybę išmatuoti EIS ir nustatyti elektrocheminius parametrus įvairiais atstumais iki tiriamo objekto. EIS spektruose užregistruotiuose prie -1.2 V *vs* Ag|AgCl|$KCl_{(sat.}$ potencialo buferiniame pH 6.75 tirpale prie aktyvių mielių, įvairiais atstumais nuo 0 iki 200µm atstumu matoma EIS parametrų priklausomybė nuo atstumo iki aktyviomis mielėmis modifikuoto paviršiaus. Analogiški matavimai arti deaktyvuotų (negyvų) mielių tokio nuoseklumo neduoda ir rodo tik difuzijos apribojimą kai EIS parametrai šuoliškai pakinta viršijus UME ir modifikuoto paviršiaus atstumą daugiau nei 20 µm atstumu. Tyrimams taikyti du mielių veikimo mediatoriais metodai, kai mielės buvo tiesiogiai veikiamos vitaminų K mišiniu, pilant ant sauso pavyzdžio ir kai tas pats mediatorių mišinys buvo įpilamas į buferinį tirpalą esantį virš imobilizuotų mielių. Užregistruoti EIS spektrai stebint jų kpokyčius laike. Pastebėta skirtingas EIS parametrų kitimas priklausomai nuo poveikio mediatoriais mielėms metodo. Veikiant sausas mieles mediatoriais gauti R_{ct} reikšmių kitimai greičiausiai atspindi mielių žūties metu išskiriamas medžiagas. Esant -1.2 V *vs* Ag|AgCl|$KCl_{(sat.)}$ potencialui UME atžvilgiu, krūvio pernašos varža užregistruota 0.74 Ωcm^2 ir 0.47 Ωcm^2 aktyvioms ir deakyvuotoms mielėms atitinkamai. Taigi, mielių deguonies suvartojimas gali būti nustatytas elektrochemiškai tiriant imobilizuotų mielių elektrolite sistemą atstumu mažesniu nei 25 µm nenaudojant papildomo redokso mediatoriaus. Aktyvioms mielėms pastebėti EIS spektrų skirtumai atitinka literatūroje rastą teiginį, kad vitamino K grupės medžiagos difuziniu keliu patenka į ląsteles. Šie duomenys iliustruoja galimybę SEIM metodu taikant hibridinę FFT ir SECM prietaisų kombinaciją naudoti deguonies apykaitos arti ląstelių paviršiaus matavimams.

Žmogaus miokardo mezenchiminių kamieninių ląstelių redokso aktyvumo vertinimas SECM metodu

hmMSC ląstelės buvo tiriamos taikant SECM priartėjimo kreives. Priartėjimo kreivės išmatuotos artinant UME link vienos sveikos ląstelės buvo lyginamos su analogiškomis priartėjimo kreivėmis užregistruotomis UME artinant prie patologinės ląstelės. Kadangi menadionas difunduoja į ląstelę difuziniu keliu ir yra iš ląstelės pašalinama menadiolo pavidale, užregistruotas srovės padidėjimas arti ląstelės paviršiaus yra proporcingas susidariusio menadiolo kiekiui. Šiuo tirpalo elektrinio laidumo lyginimo metodu nustatyta, kad priklausomai nuo ląstelių patologiškumo srovės pokytis užregistruojamas esant tirpale tarp 1 ir 5 µM įlašinto menadiono koncentracijoms. Taigi SECM gali būti taikomas tokio tipo ląstelių patologiškumui atpažinti kai duomenys yra lyginami su analogiškais sveikų ląstelių matavimo duomenimis.

IŠVADOS

1. Atlikti matavimai SEIM sinchronizuotais FFT ir SECM prietaisais papildo galimybę kokybiškai ir greitai užregistruoti elektrocheminio impedanso spektrus skenuojančioje elektrocheminėje mikroskopijoje kai tyrimo objektas yra jautrus redokso mediatoriams, kai būtina sistemą ištirti nestabilioje būsenoje, arba procesai trunka vos kelias sekundes, o taip pat kai vyksta medžiagų išskyrimas iš gyvų ląstelių esant nepastoviam deguonies kiekiui tirpale. Galimybė kontroliuoti UME poziciją elektrocheminėje celėje ir spartus EIS spektrų registravimas nesant sistemoje redokso mediatoriams yra galimybė registruoti deguonies kaip mediatoriaus pokyčius tiriamoje sistemoje.
2. Redokso mediatoriams jautrios sistemos esant poreikiui gali būti tiriamos SEIM metodu ir gali papildyti SECM tyrimo metodus.
3. FFT-SEIM metodu galima užregistruoti mielių elektrocheminį aktyvumą ir deguonies suvartojimą mielių ląstelėmis taikant tyrimams redokso tarpininkas vitamino K grupės junginius.
4. SECM priartėjimo kreivėmis galima išmatuoti patologinių ir sveikų žmogaus širdies raumens nespecializuotų kamieninių (mezenchiminių) ląstelių elektrocheminius skirtumus naudojant redokso mediatorių porą-menadioną/menadiolą siekiant šį įrenginį pritaikyti ląstelių patologiškumo nustatymui ar regeneraciniams tikslams.

PADĖKA

Tyrimai buvo remiami: projekta Nr. S-MIP-17-13; projektas Nr. SEN-21/2015; projektas Nr. 09.3.3-LMT-K-712; projektas Nr. 09.3.3-LMT-K-712-02-0137. ‘Research Projects Implemented by World-class Researcher Groups’ under Measure Nr. 01.2.2-LMT-K-7; ‘Research Projects Implemented by World-class Researcher Groups’ under Measure No. 01.2.2-LMT-K-718 grant No 09.3.3-LMT-K-718-01-0063, “Smart membranes for electrochemical devices”. Šie tyrimai buvo remiami Inovatyvios medicinos centro Regeneracinės medicinos skyriaus, Kamieninių ląstelių bei jų terapinio panaudojimo tyrimų laboratorijos. Dėkoju visiems patikėjusiems, kad galiu parašyti disertaciją. Ypatingai dėkinga profesoriui A. Ramanavičiui kantriai vadovavusiam mano tyrimams, profesorei A. Valiūnienei išmokiusiai visko ko reikia teisingai atlikti tyrimus ir susisteminti duomenis, docentei I. Morkvėnaitei-Vilkončienei išmokiusiai dirbti skenuojančiu elektrocheminiu mikroskopu, ypatinga padėka profesoriui H. Cesiuliui už elektrocheminio impedanso paskaitas ir konsultacijas, dr. D. Bironaitei suteikusiai daug žinių ir išmokiusiai dirbti su žmogaus kamieninėmis ląstelėmis, taip pat visiems darbuotojams ir doktorantams, ypatingai Aurai Kisieliūtei ir kitiems padėjusiems sunkesnėmis akimirkomis, taip pat šeimai kuri kantriai laukė kada sugrįšiu namo.

CURRICULUM VITAE

AFFILIATION

Department of Physical Chemistry, Institute of Chemistry, Faculty of Chemistry and Geosciences, Vilnius University, Naugarduko str. 24, Vilnius, Lithuania. Tel. +370 5 219 3105, e-mail: info@chgf.vu.lt

ACADEMIC EDUCATION

1. 2015-2019 Vilnius University, Faculty of Chemistry and Geoscience, doctoral studies in Chemistry, Supervisor prof. Dr. A.Ramanavičius
2. 1980-1985 Vilnius University, Faculty of Chemistry, 5 year studies with Master degree, Chemist, lecturer, Supervisor Assoc. Prof. T. Jankauskas

WORK EXPERIENCE:

1. 2018-2020 Vilnius University, Faculty of Chemistry and Geoscience, Department of Physical Chemistry, laboratory technician
2. Project: „Investigation of regenerative potential and mechanoptosis of Human heart muscles primary cardiospheres*“ („Žmogaus širdies raumens pirminių kardiosferų regeneracinio potencialo ir mechanoptozės tyimai“)* REsearch institute of Innovative Medicine Center K. 302877556:(Valstybinis Mokslinių tyrimų institutas Inovatyvios medicinos centras, įm. K. -302877556) junior researcher, 2017-2020m. Determination of parameters of electrical stimulation for culturing of cardiospheric cultures, (*Stimuliavimo elektriniais dirgikliais, reikalingais kardiosferų kultūrų kultivavimui parinkimas*).
3. Project: Vilnius University, Faculty of Medicine, Institute of Biomedical Science, Department of Pathology, Biochemistry and Farmacology, „Developement and Implementation of Non-formal Education Program For Qualification Developement of Pharmacy Assistants (Pharmacists) in Vilnius University“ (*"Neformaliojo švietimo programos, skirtos vaistininko padėjėjų (farmakotechnikų) kvalifikacijos tobulinimui farmacijos srityje, parengimas ir įgyvendinimas Vilniaus universitete")* (2013 m. 04 25 d. financing and Administration Agreement Nr. VP1-2.2-ŠMM-04-V-06-017/LSS-15000-874) senior specialist in research auxiliary, basic extra hour work.

4. 1989-2018 Vilnius University, Faculty of Chemistry and Geoscience, Department of Physical Chemistry, senior specialist
5. 1985-1989 Scientific Production Association“Venta“ a senior engineer for Chemistry in Chief technologist department.

PROFESIONAL TRAINING

1. Erasmus Practice: Institute of Physical Chemistry Polish Academy of Sciences, Department of Electrode Processes Nanoelectrochemistry group, Kasprzaka 44/52, PL-01 Warsaw, http://ichf.edu.pl Wojtech Nogala, group leader +4822343375. 2019-06 iki 2019-08
2. Online Linguistic support/ Erasmus+, English online, 2019-06-08
3. Training for students “Atviros prieigos kompetencijų tobulinimas, taikant žaidimo metodą” (0,5 ECTS kredito)
4. International Summer school Advanced Materials and Technologies 2017 KTU, Palanga, Lithuania.
5. InternationalSummer school. Advanced Materials and technologies 2018. International conference - school, 27-31 August 2018, Palanga, Lithuania
6. InternationalSummer school/ conference. Advanced Materials and technologies 2019. - school, August 2019, Palanga, Lithuania.
7. Specialist developement courses in 1986-1989 Scientific Production Association“Venta“ and Vilnius University Faculty of Physics

CONFERENCES

1. J. Petroniene. I. Morkvenaite-Vilkonciene, A. Ramanavičius, 18th International Conference School “Advanced Materials and Technologies Poster: Scanning Electrochemical Microscopy for the Determination of 2-Methyl-1,4-Naphthoquinone Toxicity to Bone Marrow Stem Cells, 27-31 August 2016, Palanga Lithuania ISSN:1822-7759
2. J. Petroniene, I. Morkvenaite-Vilkonciene, A. Ramanavičius, 60 conference Open Readings Scanning Electrochemical Microscopy Combined with Fast Fourier Transform Impedance Spectrometer for Local Electrochemical Impedance Measurements. 2017, March,14-17, Vilnius, Lithuania.ISSN:2029-4425,
3. Petroniene, J. Kisieliūtė, A., Morkvėnaitė-Vilkončienė, I., Ramanavičius, A., Advanced Materials and Technologies. p.28; Evaluation of quinone toxicity for yeast *Saccharomyces cerevisiae* by Scanning Electrochemical Microscopy. 2017 Palanga, Lithuania; ISSM:1822-7759

4. J. Petroniene, D. Bironaitė;R. Mikšiūnas; L. Mikoliūnaitė; A. Ramanavičius; Open readings 2018: 61st international conference for students of physics and natural sciences, p. 269.Scanning electrochemical microscopy for the investigation of muscle-derived mesenchymal stem cells. March 20-23, 2018, Vilnius, Lithuania 2018,
5. J. Petroniene, D. Bironaitė; R. Mikšiūnas; A. Ramanavičienė; L. Mikoliūnaitė; A.Ramanavičius; ElecNano8: Electrochemistry for nano & nano for electrochemistry, Nancy. LCPME, 2018. abstract no. P56. p. 123. Poster: Scanning electrochemical microscopy for the investigation of human myocardium-derived mesenchymal stem cells. May 29-31, 2018, Nancy, France.
6. J. Petronienė, I. Morkvėnaitė-Vilkončienė, A. Ramanavičienė, L. Mikoliūnaitė, R. Mikšiūnas, D. Bironaitė, K. Ručinskas, V. Janušauskas, A. Ramanavičius, Advanced Materials and technologies 2018. International conference - school, The Investigation of Endomyocardium-Derived Mesenchymal Cells by Scanning Electrochemical Microscopy Advanced materials and technologies: book of abstracts of 20th international conference - school, 27-31 August 2018, Palanga, Lithuania.
7. Petroniene, Jūratė; Morkvėnaitė-Vilkončienė, Inga; Rožėnė, Justė; Ramanavičius, Arūnas; Electrochemical impedance spectroscopy as a tool for the investigation of redox activity of living cells. Open readings 2019: 62nd international conference for students of physics and natural sciences, March 19-22, 2019, Vilnius, Lithuania, Vilnius University, 2019. P1-42, p. 120 ISBN: 9786090701379.
8. J. Petroniene, D. Bironaitė, R. Miksiunas, K. Rucinskas, V. Janusauskas, A. Ramanavicius, „Advances Materials and Technologies 2019“ 21st International Conference-School August 19-23, 2019, KTU, Palanga, Lithuania Scanning Electrochemical Impedance Microscopy for the Comparison of Healthy and Pathological Human Myocardium-Derived Mesenchymal Stem Cell. ISSN:1822-7759
9. J. Petroniene, D. Bironaite, R. Miksiunas, A. Ramanaviciene, K. Rucinskas, V. Janusauskas, A. Ramanavicius, 10th Workshop on Scanning Electrochemical Microscopy. Paris, Fontainebleau. 2019.09.28-30. Comparison of Healthy and Pathological Munam Myocardium-Derived Stem Cells by SECM, Abstract book p.p. 161.

1. Article title: Hybrid system based on Fast Fourier transform electrochemical impedance spectroscopy combined with scanning electrochemical microscopy. Authors: Inga Morkvenaite-Vilkonciene, Aušra Valiūnienė, Jurate Petroniene, Arunas Ramanavicius. *Electrochemistry Communications*, **2017**, Volume 83, 110-112 https://doi.org/10.1016/j.elecom.2017.08.020 ISSN: 1388-2481
2. Article title: Redox-probe-free scanning electrochemical microscopy combined with fast Fourier transform electrochemical impedance spectroscopy Valiūnienė, Aušra; Petroniene, Jurate; Morkvenaite-Vilkonciene, Inga; Popkirov, Georgi; Ramanavičienė, Almira; Ramanavičius, Arūnas. *Physical Chemistry Chemical Physics*, Cambridge : Royal Society of Chemistry. **2019**, vol. 21, p. 9831-9836. ISSN-number: 1463-9076 ; eISSN: 1463-9084 ; DOI: 10.1039/c9cp00187e;
3. Authors: Aušra Valiūnienė, Jūratė Petronienė, Mindaugas Dulkys, Arūnas Ramanavičius. Investigation of Active and Inactivated Yeast Cells by Scanning Electrochemical Impedance Microscopy, *Electroanalysis* **2020**, 32, 367–374,ISSN-number: 1040-0397, DOI: 10.1002/elan.201900414,
4. Authors: Jurate Petroniene, Inga Morkvenaite-Vilkonciene, Rokas Miksiunas, Daiva Bironaite, Almira Ramanaviciene, Lina Mikoliunaite, Aura Kisieliute, Kestutis Rucinskas, Vilius Janusauskas, Ieva Plikusiene, Siegfried Labeit, Arunas Ramanavicius, Evaluation of Redox Activity of Human MyocardiumDerived Mesenchymal Stem Cells by Scanning Electrochemical Microscopy, *Electroanalysis*, **2020**, volume 32, issue 6, pages 1337-13451-10, DOI: 10.1002/elan.201900723

ARTICLE 1

Article title: Hybrid system based on Fast Fourier transform electrochemical impedance spectroscopy combined with scanning electrochemical microscopy

Authors: Inga Morkvenaite-Vilkonciene, Aušra Valiūnienė, Jurate Petroniene, Arunas Ramanavicius

Journal title, edition and volume:
Electrochemistry Communications, 2017, Volume 83, 110-112
https://doi.org/10.1016/j.elecom.2017.08.020
ISSN: 1388-2481

Electrochemistry Communications 83 (2017) 110–112

Contents lists available at ScienceDirect

Electrochemistry Communications

journal homepage: www.elsevier.com/locate/elecom

Hybrid system based on fast Fourier transform electrochemical impedance spectroscopy combined with scanning electrochemical microscopy

Inga Morkvenaite-Vilkonciene[a,b,c], Aušra Valiūnienė[b], Jurate Petroniene[b], Arunas Ramanavicius[b,c,*]

[a] Vilnius Gediminas Technical University, Department of Mechatronics and Robotics, Vilnius, Lithuania
[b] Vilnius University, Faculty of Chemistry and Geosciences, Institute of Chemistry, Vilnius, Lithuania
[c] State Research Institute Centre for Physical Sciences and Technology, Vilnius, Lithuania

ARTICLE INFO

Keywords:
Fast Fourier transform
Electrochemical impedance spectroscopy
Scanning electrochemical microscopy
Redox probe

ABSTRACT

Fast Fourier transform electrochemical impedance spectroscopy (FFT-EIS) is a technique that simultaneously applies 30–50 frequencies and simultaneously all data of EIS spectra at these frequencies are registered. Therefore EIS spectra can be acquired many times faster compared to experiments performed by conventional EIS equipment. Scanning electrochemical microscopy (SECM) allows localized electrochemical measurements to be performed by ultramicroelectrode (UME). In this research a hybrid system based on combined SECM and FFT-EIS techniques (FFT-EIS/SECM) was developed and it was applied to register impedance spectra at different distances from surfaces of interest. The applicability of the FFT-EIS/SECM-based system for the investigation of electrochemical processes on conducting and non-conducting surfaces was demonstrated. The results show negative- and positive-feedback behavior, which are specific for amperometric measurements by SECM, when electrochemical signals are registered by UME, while approaching insulating and conducting surfaces, respectively.

1. Introduction

Electrochemical impedance spectroscopy (EIS) is an informative, non-destructive method, which enables physical modelling of the electrochemical interface and fitting supposed models to experimental spectra in order to extract relevant physico-chemical parameters, which are determining the properties of the electrode/electrolyte boundary [1,2]. However, conventional EIS-based techniques represent only an averaged response of the entire electrochemical system. In order to get more advanced mapping of the electrochemical system, scanning electrochemical microscopy (SECM) has been merged with EIS, and such a combined technique is named scanning electrochemical impedance microscopy (SEIM), which can be applied in EIS-based mapping and other investigations of surfaces [3–5]. In the SEIM-based technique localized impedance measurements can be performed in the range of frequencies when the surface of interest is scanned by ultramicroelectrode (UME) and therefore detailed electrochemical information can be extracted at each measurement point [1]. Therefore, the SEIM becomes an important new electrochemical technique, which provides a lot of information about electrochemically and/or redox active surfaces. However, measurements based on this SEIM technique performed by conventional EIS-spectrometers take a very long-time due to point-by-point collection of data for each EIS spectra [5,6]. Time, which is required for the registration of EIS spectra by conventional EIS-spectrometers, is the main limiting factor in the application of SEIM for the evaluation of fast processes. The problem related to the slow collection of EIS spectra could be solved by the fast Fourier transform based EIS technique (FFT-EIS) [7,8], which was developed and advanced by Popkirov and Schindler [9,10], because FFT-EIS allows the measurement of EIS spectra simultaneously at 30–50 different frequencies. Hence, the FFT-EIS electrochemical system is perturbed not by the consequently applied perturbations at different frequencies, but by the superposition of perturbations applied simultaneously at 30–50 frequencies. All frequencies are multiples of the lowest one, and they increase linearly in logarithmic scale. Such a method enables us to reduce the duration of impedance spectra registration by 5–20 times when compared with conventional EIS-equipment. Therefore, FFT-EIS can be applied in the study of very dynamic electrochemical systems [11].

The main aims of this research were: to demonstrate a possibility to apply FFT-EIS in SECM measurements and to apply such a hybrid system for fast/localized registration of EIS spectra at several distances

* Corresponding author at: Vilnius University, Faculty of Chemistry and Geosciences, Institute of Chemistry, Vilnius, Lithuania.
E-mail address: arunas.ramanavicius@chf.vu.lt (A. Ramanavicius).

http://dx.doi.org/10.1016/j.elecom.2017.08.020
Received 22 April 2017; Received in revised form 20 August 2017; Accepted 24 August 2017
Available online 01 September 2017

from conducting (graphite) and non-conducting (polytetrafluoroethylene (PTFE)) surfaces in the presence of $[Fe(CN)6]^{3-}$/$[Fe(CN)6]^{4-}$ (hexacyanoferrate) as a redox-couple.

2. Experimental

$K_3[Fe(CN)_6]$, $K_4[Fe(CN)_6]$, NaH_2PO_4, Na_2HPO_4 and KCl, were purchased from Sigma-Aldrich Chemie GmbH (Taufkirchen, Germany). Phosphate buffer solution (PBS), pH 6.8, was prepared in deionized water (with conductivity of 0.05 μS) 24 h before the experiment. Hexacyanoferrate-based redox couple was dissolved in PBS buffer, pH 6.8, 1 h before the experiment and stored in a dark room at ambient temperature. Disk-shaped gold ultramicroelectrode (UME) (diameter 10 μm, calculated area 7.85×10^{-7} cm^2) was purchased from Sensolytics (Bochum, Germany). The thickness of the UME glass shield was 50 μm. Before the experiment the UME consequently was polished with polishing paper with a grain size of 0.3 μm, washed in ethanol, cleaned in 0.5 M H_2SO_4 by cyclic voltammetry.

A three-electrode based electrochemical cell, where UME was connected as a working electrode, Ag|AgCl|KClsat. – as a reference electrode, and platinum wire – as a counter electrode, was applied for electrochemical measurements. Scanning electrochemical microscopy (from Sensolytics, Bochum, Germany) in combination with fast Fourier transform (FFT) impedance spectrometer EIS-128/16 (University of Kiel, Germany) [13] was applied for EIS measurements. SECM was used for the positioning of UME. The UME was positioned at several different distances from the graphite or PTFE surface and FFT-EIS spectra were registered. FFT-EIS experiments were performed in the presence of 0.02 M of hexacyanoferrate at + 0.2 mV *vs* Ag|AgCl|KCl_{sat} determined from cyclic voltammetry based experiments in the potential range at which Faradaic current is observed. The applied frequency range of alternating current was between 1.5 Hz and 50 kHz, ensuring the registration of the whole electrochemical impedance spectrum at 30 frequencies within 1.3 s.

3. Results and discussion

The UME was positioned at several different distances from surfaces of different conductivity with the expectation that registered impedance will show the same positive/negative-feedback behavior, which is specific for amperometric mode of SECM. We determined not only feedback behavior, but also gained some additional information about processes occurring at different distances from the surfaces. In amperometric mode, positive-feedback can be observed while approaching conducting surfaces, because negative-feedback is mostly obtained when approaching non-conducting surfaces [12,14]. At positive feedback mode, the current when approaching the conducting surface becomes higher due to the involvement of the conducting surface of interest in the electrochemical process. Positive feedback can be obtained even approaching an unbiased substrate, however, the current is lower than approaching a biased substrate [15]. At negative feedback mode, the diffusion to UME is blocked by the non-conducting surface, and the current close to the surface becomes very low. Both positive- and negative-feedback behaviors are mostly observed at distances which are equal to several UME radiuses from the surface of interest.

FFT-EIS results (Fig. 1) show charge transfer resistance (R_{ct}) dependencies on distance when approaching the graphite surface: far from the surface R_{ct} is a little bit higher, and it is decreasing when UME is approaching the conducting surface of graphite (Fig. 1A). At 'zero' distance the efficiency of positive-feedback behavior depends on UME and graphite contact quality. Therefore, the direct contact was achieved when UME was positioned at 'zero' distance from the graphite surface and amperometrically registered positive feedback was observed. Then during the next step UME was positioned at 10 μm distance from the graphite surface and FFT-EIS spectra were registered; the same was performed at other represented distances while approaching the graphite surface.

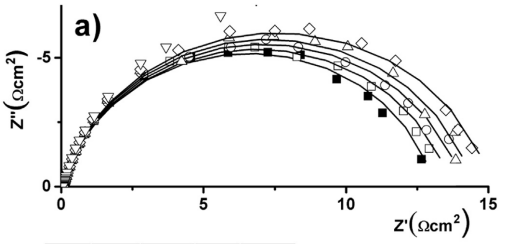

b)

d, μm	R_s Ωcm²	CPE, μFcm⁻²	n	R_{ct} Ωcm²
■ 0	0.06	898.8	0.85	13.05
□ 1	0.06	964.9	0.85	13.61
○ 2	0.06	945.3	0.85	14.03
△ 5	0.06	897.7	0.85	14.4
◇ 10	0.05	893.2	0.85	15.04

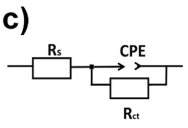

Fig. 1. FFT-EIS spectra obtained in buffer solution with 0.02 M of hexacyanoferrate as a redox couple, using UME positioned at different distances (d, μm) from the graphite surface: **a)** – Nyquist plot; **b)** – calculated characteristics of equivalent circuit (**c**)).

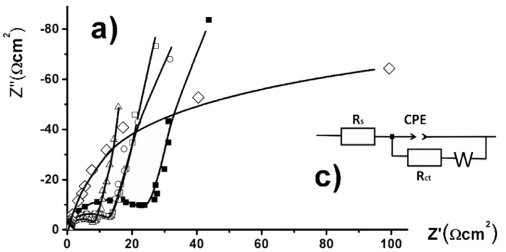

b)

d, μm	R_s Ωcm²	CPE μFcm⁻²	n(CPE)	R_{ct} Ωcm²	W-R Ωcm²	W-T Fcm⁻²	n(W)
■ 0	0.25	16.3	0.96	25.43	448.6	0.29	0.87
□ 1	0.25	16.5	0.96	13.82	467.4	0.3	0.86
○ 2	0.25	15.5	0.97	13.48	423.4	0.29	0.86
△ 5	0.25	16.2	0.96	8.839	490.1	0.29	0.88
◇ 10	0.33	665.2	0.89	155.8	-	-	-

Fig. 2. FFT-EIS spectra obtained in buffer solution with 0.02 M of hexacyanoferrate as a redox couple, using UME positioned at different distances (d, μm) from the polytetrafluoroethylene surface: **a)** – Nyquist plot; **b)** - calculated characteristics of equivalent circuit (**c**)).

When UME was approaching the non-conducting PTFE surface, negative-feedback behavior was observed (Fig. 2). According to negative-feedback theory in this case the limiting factor is the diffusion of hexacyanoferrate ions. Due to hindered diffusion of hexacyanoferrate ions, higher R_{ct} was registered at 'zero' distance compared to that registered at higher distances ranging up to 5 μm. At this 10 μm distance Nyquist plot shows that only charge transfer is a limiting factor, and therefore the diffusion part of equivalent circuit was not observed.

Thus, even if amperometric measurements are faster and electrochemical reactions' kinetics on the surface can be calculated, EIS measurements at different distances from the surface can provide more information about processes that are occurring in the electrochemical cell. Using in this research developed experimental setup the advantage of FFT-EIS/SECM can be exploited, because the measurement is as fast as an amperometric one. It is known that hindered diffusion has a significant influence on amperometrically obtained results and no matter what kind of surface – conducting or non-conducting – is

investigated. Differently from this, electrochemical impedance measurements show that while approaching the conducting surface, the limiting factor is charge transfer, contrary to the non-conducting surface, which depends on diffusion rate of redox molecules at different distances from the surface. Localized electrochemical impedance was investigated in detail at different distances from the conducting platinum surface in previous research [16]. Impedance at different distances was evaluated in some previous studies [17–19]. Therefore, during the first attempt to combine the FFT-EIS and SECM techniques, two main SECM modes (positive- and negative-feedback) were evaluated at the distances, where significant influence of diffusion of redox species towards UME has been observed. According to SECM theory, in negative-feedback the most significant diffusion-limited current can be observed at the distance which is equal to one – two UME radiuses, and in positive-feedback the diffusion-limited current can be registered at distances shorter than one UME radius [20,21]. In this research, measurements were performed at 'zero' distance (0 μm), 0.2 (1 μm), 0.4 (2 μm), 1 (5 μm), and 2 (10 μm) UME radiuses. One of the limitations of FFT-EIS measurements is that the influence of electrochemical/electric noise and various distortions are very critical, but the applied FFT-EIS device has the possibility to test the quality of measurement. In order to ensure the quality of registered EIS spectra, the reliability of measured impedance data was tested during each FFT-EIS measurement by checking how registered responses correspond to applied perturbations. In order to facilitate the scanning process it is reasonable to perform the evaluation of the surface as quickly as possible, but due to limited equilibration time some fluctuations of ion concentrations in close proximity to UME still remain and they reduce the quality of the FFT-EIS signal, especially if it is registered at lower frequencies. Therefore, some distortions in the FFT-EIS signal could be observed when the UME is moved to new measurement position and for this reason in order to compromise SECM scanning rate *vs* quality of FFT-EIS signal it is reasonable to apply frequencies higher than 1.5 Hz.

4. Conclusions

The combined FFT-EIS and SECM technique opens a new avenue in fast localized electrochemical impedance measurements. The combination of two state-of-the-art techniques provides a new and effective way to measure local variations of FFT-EIS at various surfaces, in which the processes are evolving much faster than could be registered by traditional EIS devices, which collect the EIS spectra frequency by frequency. To evaluate the reliability of the combined technique, FFT-EIS spectra registration was performed in two SECM modes (positive- and negative-feedback). The FFT-EIS measurements at different distances showed that during the approaching of the UME to the conducting and non-conducting surfaces the variation of R_{ct} *vs* distance of UME above the surface of interest is similar to the variation of amperometric signal registered at feedback mode SECM: i) when UME is approaching the insulating surface, then the R_{ct} becomes higher due to hindered diffusion; ii) when UME is approaching the conducting surface, then the R_{ct} resistance becomes lower due to reversible reaction in the space between UME and the surface.

Acknowledgement

Research granted by Research Council of Lithuania (Contract SEN-21/2015).

References

[1] I. Morkvenaite-Vilkonciene, P. Genys, A. Ramanaviciene, A. Ramanavicius, Scanning electrochemical impedance microscopy for investigation of glucose oxidase catalyzed reaction, Colloids Surf. B. Biointerfaces 126 (2015) 598–602.
[2] B.-Y. Chang, S.-M. Park, Electrochemical impedance spectroscopy, Annu. Rev. Anal. Chem. 3 (2010) 207–229.
[3] B.B. Katemann, A. Schulte, E.J. Calvo, M. Koudelka-Hep, W. Schuhmann, Localised electrochemical impedance spectroscopy with high lateral resolution by means of alternating current scanning electrochemical microscopy, Electrochem. Commun. 4 (2002) 134–138.
[4] M. Gębala, W. Schuhmann, F. La Mantia, A new AC-SECM mode: on the way to high-resolution local impedance measurements in SECM, Electrochem. Commun. 13 (2011) 689–693.
[5] V. Kuznetsov, A. Maljusch, R.M. Souto, A.S. Bandarenka, W. Schuhmann, Characterisation of localised corrosion processes using scanning electrochemical impedance microscopy, Electrochem. Commun. 44 (2014) 38–41.
[6] X. Chen, Y. Wang, J. Zhou, W. Yan, X. Li, J.-J. Zhu, Electrochemical impedance immunosensor based on three-dimensionally ordered macroporous gold film, Anal. Chem. 80 (2008) 2133–2140.
[7] J.-Y. Park, B.-Y. Chang, H. Nam, S.-M. Park, Selective electrochemical sensing of glycated hemoglobin (HbA1c) on thiophene-3-boronic acid self-assembled monolayer covered gold electrodes, Anal. Chem. 80 (2008) 8035–8044.
[8] J.-S. Yoo, I. Song, J.-H. Lee, S.-M. Park, Real-time impedance measurements during electrochemical experiments and their application to aniline oxidation, Anal. Chem. 75 (2003) 2962–2968.
[9] A. Valiūnienė, G. Baltrūnas, R. Valiūnas, G. Popkirov, Investigation of the electroreduction of silver sulfite complexes by means of electrochemical FFT impedance spectroscopy, J. Hazard. Mater. 180 (2010) 259–263.
[10] G. Popkirov, R. Schindler, A new impedance spectrometer for the investigation of electrochemical systems, Rew. Sci. Instrum. 63 (1992) 5366–5372.
[11] A. Valiūnienė, Ž. Margarian, R. Valiūnas, Electrooxidation of cyanide ion on a platinized Ti electrode, React. Kinet. Mech. Catal. 115 (2015) 449–461.
[12] A.J. Bard, J. Kwak, Scanning electrochemical microscopy. Apparatus and two-dimensional scans of conductive and insulating substrates, Anal. Chem. 61 (1989) 1794–1799.
[13] G. Popkirov, R. Schindler, Validation of experimental data in electrochemical impedance spectroscopy, Electrochim. Acta 38 (1993) 861–867.
[14] J. Kwak, A.J. Bard, Scanning electrochemical microscopy. Theory of the feedback mode, Anal. Chem. 61 (1989) 1221–1227.
[15] H. Xiong, J. Guo, S. Amemiya, Probing heterogeneous electron transfer at an unbiased conductor by scanning electrochemical microscopy in the feedback mode, Anal. Chem. 79 (2007) 2735–2744.
[16] F. Zou, D. Thierry, H. Isaacs, A high-resolution probe for localized electrochemical impedance spectroscopy measurements, J. Electrochem. Soc. 144 (1997) 1957–1965.
[17] D. Trinh, M. Keddam, X.R. Novoa, V. Vivier, Alternating-current measurements in scanning electrochemical microscopy, part 1: principle and theory, Chem. Phys. Chem. 12 (2011) 2169–2176.
[18] D. Trinh, M. Keddam, X.R. Novoa, V. Vivier, Alternating current measurements in scanning electrochemical microscopy, part 2: detection of adsorbates, Chem. Phys. Chem. 12 (2011) 2177–2183.
[19] D. Trinh, M. Keddam, X.R. Nóvoa, V. Vivier, Characterization of adsorbates by transient measurements in scanning electrochemical microscopy, Electrochim. Acta 131 (2014) 28–35.
[20] A.J. Bard, M.V. Mirkin, Scanning Electrochemical Microscopy, Marcel Dekker, NY, 2001.
[21] R. Cornut, A. Bhasin, S. Lhenry, M. Etienne, C. Lefrou, Accurate and simplified consideration of the probe geometrical defaults in scanning electrochemical microscopy: theoretical and experimental investigations, Amer, Chem. Soc. 83 (2011) 9669–9675.

ARTICLE 2

Article title: Redox-probe-free scanning electrochemical microscopy combined with fast Fourier transform electrochemical impedance spectroscopy

Valiūnienė, Aušra; Petroniene, Jurate; Morkvenaite-Vilkonciene, Inga; Popkirov, Georgi; Ramanavičienė, Almira; Ramanavičius, Arūnas

Journal title, edition and volume: Physical Chemistry Chemical Physics, Cambridge : *Royal Society of Chemistry*. 2019, vol. 21, p. 9831-9836.

ISSN-number: 1463-9076 ;
eISSN: 1463-9084 ;
DOI: 10.1039/c9cp00187e;

PCCP

PAPER

View Article Online
View Journal | View Issue

Cite this: *Phys. Chem. Chem. Phys.*, 2019, **21**, 9831

Redox-probe-free scanning electrochemical microscopy combined with fast Fourier transform electrochemical impedance spectroscopy

Aušra Valiūnienė,[a] Jurate Petroniene,[a] Inga Morkvenaite-Vilkonciene,[bd] Georgi Popkirov,[c] Almira Ramanaviciene[d] and Arunas Ramanavicius*[a]

Received 11th January 2019,
Accepted 4th April 2019

DOI: 10.1039/c9cp00187e

rsc.li/pccp

Scanning electrochemical microscopy (SECM) hybridized with fast Fourier transform-based electrochemical impedance spectroscopy (FFT-EIS) seems to be a powerful variation of scanning electrochemical impedance microscopy (SEIM), wherein both state-of-the-art techniques are combined (FFT-SEIM) and can be used for the investigation and treatment of tissues at single cell level. However, in most EIS-based experiments, harmful redox mediators are applied, which affect the functioning of living cells and tissues. Therefore, the development of a redox-probe-free FFT-SEIM is still a very important challenge in electrochemistry. For this reason, in this research, we have demonstrated a redox-probe-free evaluation of conducting and non-conducting surfaces by combining scanning electrochemical microscopy with FFT-EIS. It was demonstrated that using the fast Fourier transform-based FFT-EIS technique, EIS spectra could be registered much faster compared to experiments performed using the conventional EIS equipment. An ultramicroelectrode (UME) was used as a scanning electrode to ensure high spatial resolution. We have performed FFT-SEIM measurements in a redox-probe-free mode (without any additional redox probes) and have investigated several surfaces with different conductivities. The FFT-EIS equipment and the built-in software help to avoid the influence of possible formation of hydrogen bubbles on the UME. This research opens up a new avenue for the application of FFT-SEIM in the investigation of samples that are unstable and very sensitive towards redox mediators (*e.g.*, tissues and/or living cells).

Introduction

Scanning electrochemical impedance microscopy (SEIM), being a combination of SECM and EIS, is a powerful technique for the evaluation of local electrochemical changes on various surfaces.[1–4] Localized impedance measurements could be performed in a broad range of frequencies while the surface of interest is scanned by an ultramicroelectrode (UME). The small size of the electrode (<25 μm in diameter) allows the investigation of fast electrochemical reactions.[5] The measured signal is the response of a complex impedance and depends on the resistance of solution, double layer capacitances of both working and counter electrodes, and charge transfer resistance between these two electrodes.[6] Local electrochemical processes can be characterized using several parameters, which were registered after the fitting of the electrochemical spectra to appropriate models. Thus, SEIM-based techniques[3,7] yield maps of all calculated parameters, *e.g.* charge transfer resistance or double layer capacitance, as a function of 3D coordinates of the UME tip. Furthermore, the advantage of the SEIM technique is that the investigation can be performed without any redox mediators or redox probes.[7]

In our earlier researches, we showed the possibility of applying SEIM scanning at different distances from the surface under investigation.[1,2] However, the registration of a complete impedance spectrum at each UME position of interest was very time-consuming,[2] particularly, if the EIS was performed in a lower frequency range. A possible alternative was to use an alternating-current-based SECM (AC-SECM) instead of SEIM. The resolution of the registered (single frequency) impedance maps would, however, depend on the chosen frequency, whereby maps can be registered faster and with better resolution at higher frequencies compared with measurements at lower frequencies.[8–10] However, an optimal AC frequency has to

[a] *Department of Physical Chemistry, Faculty of Chemistry and Geosciences, Vilnius University, Naugarduko Str. 24, Vilnius, Lithuania. E-mail: arunas.ramanavicius@chf.vu.lt; Fax: +370 (5)233 09 87; Tel: +370 (5)2336310, +370 (5)2193115, +370 (5)2193185*
[b] *Department of Electrochemical Material Science, Center for Physical Sciences and Technology, Saulėtekio av. 3, Vilnius, Lithuania*
[c] *Bulgarian Academy of Sciences, Central laboratory of Solar Energy and New Energy, Sofia, Bulgaria*
[d] *NanoTechnas – Centre of Nanotechnology and Materials Science, Faculty of Chemistry and Geosciences, Vilnius University, Naugarduko 24, LT-03225 Vilnius, Lithuania*

be found for any specific case. Often SECM and SEIM are performed in feedback mode in the presence of redox mediators and/or redox probes in the electrolyte, yielding information for both topography and surface reactivity.[11] The response registered upon approaching the UME towards different and/or differently modified surfaces was investigated, *e.g.* (i) an insulator surface;[1,12] (ii) a conducting surface, which was not connected to an electric circuit;[1,12] (iii) conducting surface connected to an electric circuit and maintained at a constant potential;[12] and (iv) an enzyme-modified surface.[2] Commonly, amperometric experiments with SECM were performed using redox mediators.[13–16] However, certain biological systems, especially tissues and/or living cells, can be damaged by harmful redox mediators, which are used to ensure charge transfer at the electrodes, and/or redox probes that are used as oxidizable/reducible species.[17–20] Mathematical models[21–23] developed recently were created only for cases when redox mediators were applied in amperometric SECM. A model that describes a biological system evaluated by SECM without any redox mediator was introduced.[24] It suggests that avoiding the involvement of redox mediators in SEIM investigations will be beneficial because (i) redox mediators could negatively affect biological surfaces; (ii) some redox mediators can 'block' or modify the UME surface;[5] and (iii) biological surfaces could be investigated in their natural environment. In the case of impedance measurements, the correct choice of the working point, *i.e.* the applied direct current (DC) voltage, is of great concern. It determines which process, *i.e.* a faradaic or non-faradaic, controls the impedance response in the frequency range of the perturbation signal applied. It should be noted that (i) in the case of a faradaic process, charge is transferred through the interface, *i.e.* an oxidation/reduction process is taking place and redox mediators are mostly required in such cases;[1,25] (ii) in the case of non-faradaic processes, charge transfer *via* redox reactions is practically non-existent.[2,25] In any case, the time of EIS measurement at any location of the UME tip appears to be a limiting factor for the SEIM recording rate. The FFT-EIS technique[26,27] has proven to be a powerful tool for very fast EIS measurements.[28,29] Here, we demonstrate the advantage of using a FFT-EIS in combination with SECM measurements for the fast mapping of EIS spectra at varying distances from conducting (graphite) and non-conducting (polytetrafluoroethylene) surfaces in a redox-probe-free mode.

The main aim of this study is to demonstrate the possibility to apply FFT-EIS in SECM measurements (FFT-SEIM) for fast/localized registration of EIS spectra at several distances from conducting (graphite) and non-conducting (polytetrafluoroethylene) surfaces in a redox-probe-free mode (without any additional redox probes), which will open new applicability for this hybrid method in investigations of such samples that are sensitive to redox compounds (*e.g.* living tissues, cells and some other biological samples).

Experimental

Phosphate buffer solution (pH 6.8) was prepared 24 h before the experiment in deionized water (conductivity 0.05 μS). A disk-shaped gold-based ultramicroelectrode (UME) (diameter 10 μm, calculated area 7.85×10^{-7} cm^2) was purchased from Sensolytics (Bochum, Germany). Diameter of the glass shield of UME was 50 μm. Before the experiment, the UME was polished with polishing paper (grain size of 0.3 μm), washed in ethanol, and then UME was electrochemically cleaned in 0.5 M H_2SO_4 by 50 potential cycles in the potential range from −0.2 V to +1.0 V *vs.* Ag|AgCl|KCl$_{sat.}$ at the scan rate of 0.2 V s^{-1}. A three-electrode electrochemical cell, consisting of UME as a working electrode, Ag|AgCl|KCl$_{sat.}$ as a reference electrode and a platinum wire as a counter electrode, was assembled for the electrochemical measurements. In order to set an accurate potential for the UME, both the reference electrode and UME were placed as close as possible to each other using a Luggin capillary. Scanning electrochemical microscopy (Sensolytics, Germany) in combination with a fast Fourier transform (FFT) electrochemical impedance spectrometer EIS-128/16 (University of Kiel, Germany)[26] was applied for impedance measurements at different distances from the surface of interest (Fig. 1). SECM was used for the precise positioning of the UME. FFT-EIS spectra were potentiostatically registered after applying a potential of −1.2 V *vs.* Ag|AgCl|KCl$_{sat.}$, at which faradaic current was observed at the interface between the electrode and the electrolyte. Every EIS measurement was performed in the frequency range from 1.5 Hz to 50 kHz after applying 3 consecutive multi-sine signals at a perturbation of 1.3 s duration each. Thus, the evaluation of the EIS at any single UME position took approximately 3.9 s. The amplitude of the perturbation signal was chosen in such a way that the response voltage would not exceed 10–15 mV in order to avoid non-linearity in the response signal. The obtained impedance spectra were validated by comparing the power spectra of perturbation and response in the way described in the corresponding ref. 26. For the determination of electrochemical characteristics under a selected equivalent circuit model, gathered EIS spectra were evaluated using EIS data analysis software "ZView". The Nyquist plots of experimentally obtained EIS data and observed fitting results are presented in the corresponding figures.

Results and discussion

SECM amperometric measurements

Two samples of very different electrical conductivities were evaluated: one sample was conducting non-polarized sample (graphite), the other one was non-conducting (polytetrafluoroethylene). The UME was positioned at various distances from the samples' surface. We expected that the impedance will depend on the distance (d) between the UME tip and the surface of the sample, whereby some parameters of its respective equivalent circuit will show dependence on the distance (d), which is similar to the positive–negative feedback behavior and is a specific feature for SECM amperometric measurements. Amperometric measurements were performed at −0.5 V *vs.* Ag|AgCl|KCl$_{sat.}$ (Fig. 2). In the negative feedback mode, the diffusion to UME is blocked by the non-conducting

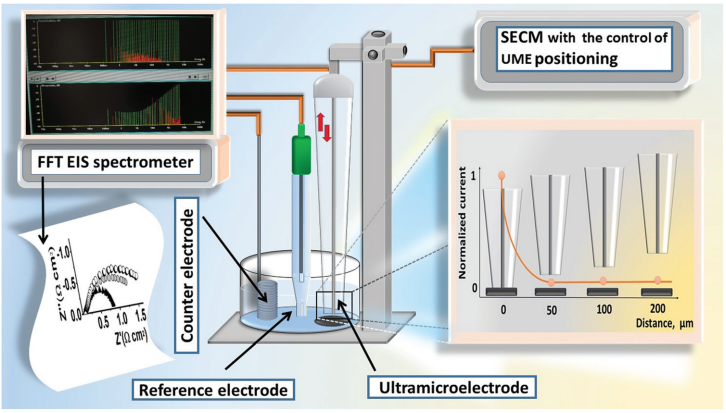

Fig. 1 Experimental set-up of FFT-SEIM system based on FFT-EIS and SECM.

surface, and the current close to the surface becomes very low (Fig. 2A). However, in the positive feedback mode, the current registered when the UME is in very close proximity to the conducting surface, which becomes polarized due to potential applied to UME, and the surface area (on which redox processes are occurring) increases significantly. Therefore, a significant increase in the UME current is observed (Fig. 2B). Positive feedback can be observed when the UME is approaching conducting surfaces, while negative feedback is mostly observed when the UME is approaching non-conducting surfaces.[30,31]

SECM-FFT-EIS measurements

The application of FFT-SEIM, where FFT-EIS is combined with the SECM, has two advantages over the use of the well-known frequency response analyzer-based EIS technique (FRA-EIS). First, the duration of measurement is significantly reduced due to the fact that a multi-sine signal, being a sum of up to 50 single sine signals, serves as a perturbation of working electrode and FFT is used to reveal their respective responses. Second, the registered impedance spectra can be checked for validity very easily and reliably.[30] Errors might be related to (i) the turbulence of solution during the movement of UME and the limited time left for the equilibration of ion concentration in the UME environment, and (ii) the extremely small area of the UME, leading to extremely small currents and the necessity of using very high gain amplifiers for the efficient registration of EIS spectra of sufficient quality. The abovementioned problems were addressed by awaiting the steady-state conditions at any new location prior to EIS measurement and by setting the DC potential in the faradaic current zone.

Impedance spectroscopy measurements were performed in phosphate buffer (pH 6.8) after the UME was positioned at various distances from the non-polarized graphite or polytetrafluoroethylene surfaces. For these measurements, a potential of −1.2 V *vs.* Ag|AgCl|$KCl_{sat.}$ was selected from the range where faradaic current was already observed very clearly (Fig. 2). In the potential region between −1.2 V and 0.9 V *vs.* Ag|AgCl|$KCl_{sat.}$, faradaic processes were not observed. Therefore, the EIS spectra were almost independent of the distance between UME and the surface of interest (Fig. 3).

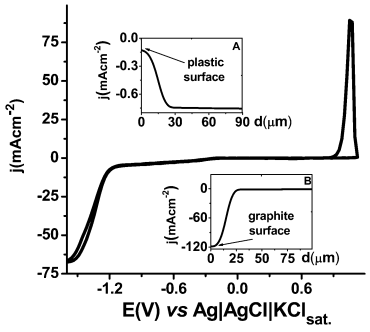

Fig. 2 Cyclic voltammogram in phosphate buffer (pH 6.8) obtained using gold UME with a diameter of 10 μm, scan rate 0.2 V s^{-1}. Inset: Approaching curves registered with an Au SECM tip above (A) polytetrafluoroethylene and (B) non-polarized graphite surfaces at an applied potential of −0.5 V *vs.* Ag|AgCl|$KCl_{sat.}$ the UME step at the *z* coordinate was 1 μm.

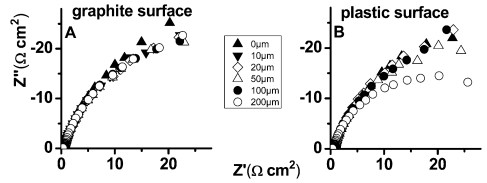

Fig. 3 FFT-EIS Nyquist plot spectra registered at −1.0 V *vs.* Ag|AgCl|$KCl_{sat.}$ in buffer solution (pH 6.8) using a UME positioned at different distances: (A) approaching towards non-polarized graphite; (B) approaching towards polytetrafluoroethylene surface.

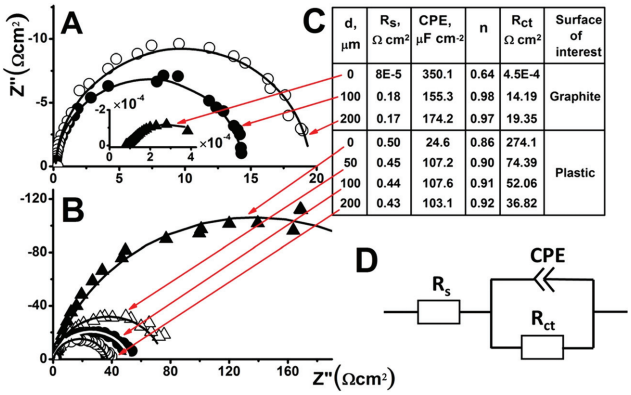

d, μm	Rs, Ω cm²	CPE, μF cm⁻²	n	Rct Ω cm²	Surface of interest
0	8E-5	350.1	0.64	4.5E-4	Graphite
100	0.18	155.3	0.98	14.19	
200	0.17	174.2	0.97	19.35	
0	0.50	24.6	0.86	274.1	Plastic
50	0.45	107.2	0.90	74.39	
100	0.44	107.6	0.91	52.06	
200	0.43	103.1	0.92	36.82	

Fig. 4 FFT-SEIM Nyquist plot spectra registered at −1.2 V *vs.* Ag|AgCl|$KCl_{sat.}$, in buffer solution (pH 6.8) using UME positioned at different distances (*d*, μm): (A) approaching towards non-polarized graphite; (B) approaching towards polytetrafluoroethylene surface. Table (C) represents distances between the UME tip and surfaces of interest and calculated parameters of the equivalent circuit (D), where R_s is the electrolyte resistance, R_{ct} is the charge transfer resistance, and CPE is the constant phase element.

FFT-EIS spectra registered at a potential of −1.2 V *vs.* Ag|AgCl|$KCl_{sat.}$, *i.e.* upon the presence of faradaic currents, are presented in Fig. 4A and B. At such conditions, the influence of hydrogen bubbles on the surface of UME or at least significant interference of this process on the quality of EIS spectra should be avoided. Therefore, in this research, several strategies were applied to avoid the formation of hydrogen bubbles and this interfering effect to get EIS spectra of good quality.

(i) In this research, the advantage of FTT-EIS has been exploited and the EIS spectra were very quickly registered, before the formation of any hydrogen bubbles. Therefore, a significant advantage of FFT-EIS is the capability to register all spectra within few seconds.

(ii) Due to the very small UME surface area and the very initial phase of water electrolysis as is seen from the cyclic voltammogram (Fig. 2), the intensity of the formation of atomic and molecular hydrogen is too less to form hydrogen bubbles during the few seconds of measurement.

(iii) The quality of EIS spectra was checked by an advanced software, *i.e.* the built-in FFT-EIS control software and the EIS data acquisition system. It is very important that during the FFT-EIS experiments, the measured response data could be observed/controlled. If necessary, the 'mismatching' points or even whole EIS spectra, which were wrongly interpreted or were not related to the process of interest, were excluded. This procedure is possible because the used configuration of FFT-EIS spectrometer allows to determine how the EIS response corresponds to the applied perturbation and to evaluate the quality of the registered EIS spectra.

It is seen from the Nyquist plot that the radius of the semicircles strongly depends on the distance between the UME and non-polarized graphite or polytetrafluoroethylene surface. One of the main challenges of these experiments was to ensure stationarity of the measurement conditions by avoiding the effect of possible formation of hydrogen bubbles on the UME surface during the FFT-EIS measurements. The intensity of hydrogen gas bubble formation depends on the solution composition, electrode material and even surface area of the electrode. Fortunately, in our case and with the low measurement time of the FFT-EIS, the chosen UME potential of −1.2 V *vs.* Ag|AgCl|$KCl_{sat.}$ resulted in sufficient current response but had negligible effect on hydrogen generation. Thus, measurements could be completed before the formation of any hydrogen bubbles. Nevertheless, the impedance data validity was checked for each EIS measurement.

Experimental EIS data were fitted to an equivalent circuit model (Fig. 4D) consisting of (i) solution resistance R_s; (ii) constant phase element (CPE),[30–32] which represents a capacitance of the electric double layer (EDL) that forms at the interface between UME and the buffer solution; and (iii) charge transfer resistance R_{ct}, which represents the charge transfer at the interface between UME and the electrolyte. Adequate electrochemical parameters under a selected equivalent circuit model were calculated and are presented in the table in Fig. 4C. The values of charge transfer resistance R_{ct} strongly depend on whether the UME is almost touching the graphite surface ('zero distance') or is positioned at a 100 μm or 200 μm distance from the surface of interest (Fig. 4A). R_{ct} becomes very small (4.5×10^{-4} Ω cm^2) when the UME approaches the conductive surface (Fig. 4A, filled triangles). This result is related to SECM measurements performed in the amperometric mode because the measured current became very high when the UME approached the conductive surface (Fig. 2B). This phenomenon is called as positive feedback, and it is clearly represented by the registered FFT-EIS spectra (Fig. 4A). When the UME was located relatively far from the graphite surface (Fig. 4, opened and filled circles), the R_{ct} became relatively high: 14.19 Ω cm^2 and 19.35 Ω cm^2 at a 100 μm and 200 μm distance, respectively.

FFT-SEIM measurements, performed approaching towards the polytetrafluoroethylene surface (Fig. 4B) shows the 'negative feedback' phenomena, which means that when the UME is located close to the surface of interest then the current becomes very low due to the hindered diffusion of the redox-active species. Therefore, the highest value of R_{ct} was registered at 'zero distance' (274.1 Ω cm^2) when the UME was almost touching the surface of the polytetrafluoroethylene (Fig. 4B, filled triangles), and the resistance became significantly lower when the UME was positioned at higher distances from the insulating surface: 74.39 Ω cm^2, 52.06 Ω cm^2 and 36.82 Ω cm^2 at 50 μm, 100 μm and 200 μm, respectively. In this case, the diffusion of compounds (primarily dissolved oxygen) to UME is hindered by the insulating glass shield of the electrode. Therefore, the retraction of UME from the insulating surface forms a 'free space', which is available for diffusion.

Conclusions

In this research, we have combined the SECM with the FFT electrochemical impedance spectrometer and developed an FFT-SEIM system capable of performing very fast measurements. We have shown that, due to the fast FFT-EIS measurements and the easy data evaluation/validation, it is possible to significantly advance the SECM capabilities and to apply it for the investigation of fast electrochemical processes, which are occurring in a neutral environment without any additional redox probes. The measurement of FFT-EIS spectra in the absence of a redox probe significantly increases the capability of the FFT-EIS and SECM technique because in this way surfaces of samples, which are sensitive or can be contaminated by redox probe, can be evaluated. The ability to perform FFT-EIS experiments very quickly and in the absence of a redox probe is very important for the SECM-based evaluation of living cells or even whole tissues of living organisms. Therefore, this newly designed redox probe-free FFT-SEIM technique introduced here can find specific applications in bioelectrochemistry, biotechnology and cell biology.

Conflicts of interest

There are no conflicts to declare.

Acknowledgements

This research was funded by the European Social Fund according to the activity ''Development of Competences of Scientists, other Researchers and Students through Practical Research Activities'' of Measure No. 09.3.3-LMT-K-712. Project No. 09.3.3-LMT-K-712-02-0137. Coordinated by Lithuanian research council.

References

1 I. Morkvenaite-Vilkonciene, A. Valiūnienė, J. Petroniene and A. Ramanavicius, Hybrid system based on fast Fourier transform electrochemical impedance spectroscopy combined with scanning electrochemical microscopy, *Electrochem. Commun.*, 2017, **83**, 110–112.
2 I. Morkvenaite-Vilkonciene, P. Genys, A. Ramanaviciene and A. Ramanavicius, Scanning electrochemical impedance microscopy for investigation of glucose oxidase catalyzed reaction, *Colloids Surf., B*, 2015, **126**, 598–602.
3 A. S. Bandarenka, K. Eckhard, A. Maljusch and W. Schuhmann, Localized Electrochemical Impedance Spectroscopy: Visualization of Spatial Distributions of the Key Parameters Describing Solid/Liquid Interfaces, *Anal. Chem.*, 2013, **85**(4), 2443–2448.
4 A. Estrada-Vargas, A. Bandarenka, V. Kuznetsov and W. Schuhmann, *In Situ* Characterization of Ultrathin Films by Scanning Electrochemical Impedance Microscopy, *Anal. Chem.*, 2016, **88**(6), 3354–3362.
5 L. Jacobse, S. J. Raaijman and M. T. Koper, The reactivity of platinum microelectrodes, *Phys. Chem. Chem. Phys.*, 2016, **18**(41), 28451–28457.
6 F. Lisdat and D. Schäfer, The use of electrochemical impedance spectroscopy for biosensing, *Anal. Bioanal. Chem.*, 2008, **391**(5), 1555–1567.
7 V. Kuznetsov, A. Maljusch, R. M. Souto, A. S. Bandarenka and W. Schuhmann, Characterisation of localised corrosion processes using scanning electrochemical impedance microscopy, *Electrochem. Commun.*, 2014, **44**, 38–41.
8 K. Eckhard, T. Erichsen, M. Stratmann and W. Schuhmann, Frequency-dependent alternating-current scanning electrochemical microscopy (4D AC-SECM) for local visualisation of corrosion sites, *Chem. – Eur. J.*, 2008, **14**(13), 3968–3976.
9 K. Eckhard, C. Kranz, H. Shin, B. Mizaikoff and W. Schuhmann, Frequency dependence of the electrochemical activity contrast in AC-scanning electrochemical microscopy and atomic force microscopy-AC-scanning electrochemical microscopy imaging, *Anal. Chem.*, 2007, **79**(14), 5435–5438.
10 P. M. Diakowski and Z. F. Ding, Novel strategy for constant-distance imaging using alternating current scanning electrochemical microscopy, *Electrochem. Commun.*, 2007, **9**(10), 2617–2621.
11 C. Gabrielli, F. Huet, M. Keddam, P. Rousseau and V. Vivier, Scanning Electrochemical Microscopy Imaging by Means of High-Frequency Impedance Measurements in Feedback Mode, *J. Phys. Chem. B*, 2004, **108**(31), 11620–11626.
12 A. S. Baranski and P. M. Diakowski, Application of AC impedance techniques to Scanning Electrochemical Microscopy, *J. Solid State Electrochem.*, 2004, **8**(10), 683–692.
13 A. Ramanavicius, I. Morkvenaite-Vilkonciene, A. Kisieliute, J. Petroniene and A. Ramanaviciene, Scanning electrochemical microscopy based evaluation of influence of pH on bioelectrochemical activity of yeast cells - Saccharomyces cerevisiae, *Colloids Surf., B*, 2017, **149**, 1–6.
14 I. Morkvenaite-Vilkonciene, A. Ramanaviciene and A. Ramanavicius, 9,10-Phenanthrenequinone as a redox mediator for the imaging of yeast cells by scanning electrochemical microscopy, *Sens. Actuators, B*, 2016, **228**, 200–206.
15 S. Bergner, J. Wegener and F.-M. Matysik, Simultaneous imaging and chemical attack of a single living cell within a

confluent cell monolayer by means of scanning electrochemical microscopy, *Anal. Chem.*, 2010, **83**(1), 169–174.
16 S. Bergner, P. Vatsyayan and F.-M. Matysik, Recent advances in high resolution scanning electrochemical microscopy of living cells – A review, *Anal. Chim. Acta*, 2013, **775**, 1–13.
17 J. A. Koch, M. B. Baur, E. L. Woodall and J. E. Baur, Alternating Current Scanning Electrochemical Microscopy with Simultaneous Fast-Scan Cyclic Voltammetry, *Anal. Chem.*, 2012, **84**(21), 9537–9543.
18 J. M. Liebetrau, H. M. Miller, J. E. Baur, S. A. Takacs, V. Anupunpisit, P. A. Garris and D. O. Wipf, Scanning electrochemical microscopy of model neurons: imaging and real-time detection of morphological changes, *Anal. Chem.*, 2003, **75**(3), 563–571.
19 X. Zhao, N. O. Petersen and Z. Ding, Comparison study of live cells by atomic force microscopy, confocal microscopy, and scanning electrochemical microscopy, *Can. J. Chem.*, 2007, **85**(3), 175–183.
20 X. Li and A. J. Bard, Scanning electrochemical microscopy of HeLa cells – Effects of ferrocene methanol and silver ion, *J. Electroanal. Chem.*, 2009, **628**(1–2), 35–42.
21 M. Etienne, S. Lhenry, R. Cornut and C. Lefrou, Optimization of the shearforce signal for scanning electrochemical microscopy and application for kinetic analysis, *Electrochim. Acta*, 2013, **88**, 877–884.
22 R. Cornut, P. Hapiot and C. Lefrou, Enzyme-mediator kinetics studies with SECM: Numerical results and procedures to determine kinetics constants, *J. Electroanal. Chem.*, 2009, **633**(1), 221–227.
23 R. Cornut, A. Bhasin, S. Lhenry, M. Etienne and C. Lefrou, Accurate and Simplified Consideration of the Probe Geometrical Defaults in Scanning Electrochemical Microscopy: Theoretical and Experimental Investigations, *Anal. Chem.*, 2011, **83**(24), 9669–9675.
24 F. Ivanauskas, I. Morkvenaite-Vilkonciene, R. Astrauskas and A. Ramanavicius, Modelling of Scanning Electrochemical Microscopy at Redox Competition Mode Using Diffusion and Reaction Equations, *Electrochim. Acta*, 2016, **222**, 347–354.
25 J. S. Daniels and N. Pourmand, Label-free impedance biosensors: Opportunities and challenges, *Electroanalysis*, 2007, **19**(12), 1239–1257.
26 G. Popkirov and R. Schindler, Validation of experimental data in electrochemical impedance spectroscopy, *Electrochim. Acta*, 1993, **38**(7), 861–867.
27 G. Popkirov and R. Schindler, A new impedance spectrometer for the investigation of electrochemical systems, *Rev. Sci. Instrum.*, 1992, **63**(11), 5366–5372.
28 A. Valiūnienė, G. Baltrūnas, R. Valiūnas and G. Popkirov, Investigation of the electroreduction of silver sulfite complexes by means of electrochemical FFT impedance spectroscopy, *J. Hazard. Mater.*, 2010, **180**(1), 259–263.
29 A. Valiūnienė, Ž. Margarian and R. Valiūnas, Electrooxidation of cyanide ion on a platinized Ti electrode, *React. Kinet., Mech. Catal.*, 2015, **115**(2), 449–461.
30 G. Brug, A. Van Den Eeden, M. Sluyters-Rehbach and J. Sluyters, The analysis of electrode impedances complicated by the presence of a constant phase element, *J. Electroanal. Chem. Interfacial Electrochem.*, 1984, **176**(1–2), 275–295.
31 A. Lasia, Electrochemical impedance spectroscopy and its applications, *Modern aspects of electrochemistry*, Springer, 2002, pp. 143–248.
32 J. R. Macdonald and W. R. Kenan, *Impedance Spectroscopy: Emphasizing Solid Materials and Systems*, Wiley, 1987.

ARTICLE 3

Article title: Investigation of Active and Inactivated Yeast Cells by Scanning Electrochemical Impedance Microscopy

Authors: Aušra Valiūnienė, Jūratė Petronienė, Mindaugas Dulkys, Arūnas Ramanavičius

Journal title, edition and volume: *Electroanalysis* 2020, 32, 367–374
ISSN-number: 1040-0397
DOI: 10.1002/elan.201900414

Full Paper

Wiley Online Library

ELECTROANALYSIS

DOI: 10.1002/elan.201900414

Investigation of Active and Inactivated Yeast Cells by Scanning Electrochemical Impedance Microscopy

Aušra Valiūnienė,[a] Jūratė Petronienė,[a] Mindaugas Dulkys,[a] and Arūnas Ramanavičius*[a, b]

Abstract: Scanning electrochemical microscopy (SECM), electrochemical impedance spectroscopy (EIS) and scanning electrochemical impedance microscopy (SEIM) were used to investigate electrochemical activity of active and inactivated yeast *Saccharomyces cerevisiae* cells. SEIM experiment was performed using a unique electrochemical impedance spectrometer with a fast Fourier transform (FFT-EIS) function, which enabled simultaneously perturb/evaluate electrochemical system at 50 frequencies. This allowed very quick observing the differences between impedance spectra, which were taken every few seconds. Therefore, we were able to apply SEIM for relatively fast determination of electrochemical impedance dependence on the distance between ultramicroelectrode (UME) and surface modified by immobilized yeast cells. It was determined that electrochemical activity and 'breathing' (a consumption of dissolved oxygen) of yeast can be electrochemically observed when the distance between UME and surface of yeast cells is in the range from 0 μm to 25 μm. Therefore, 25 μm is the maximum distance suitable for efficient investigation of yeast cell activity when experiments are performed in FFT-SEIM mode. Charge transfer resistance of active and inactivated yeast cells was determined using EIS. It was calculated that charge transfer resistance of active yeast cells is 1.5 times lower than that of inactivated yeast cells. Lipophilic vitamin K_3 (Vit-K_3) and hydrophilic vitamin K_1 (Vit-K_1) were mixtured and used as redox mediators for charge transfer from yeast cells.

Keywords: Scanning Electrochemical Microscopy (SECM) · Fast Fourier Transform Electrochemical impedance spectroscopy (FFT-EIS) · Scanning Electrochemical Impedance Microscopy (SEIM) · Saccharomyces Cerevisiae · Living baker yeast cells

1 Introduction

Recently immobilized cell based systems have been widely investigated and used in different fields of biotechnology, pharmacy, biomedicine, food and environmental technologies [1–5]. In these areas *Saccharomyces cerevisiae* (*S. cerevisiae*) cells, which are also known as baker yeast, are often used as a model system for the imitation of eukaryotic cell behavior. These attractive cells can be used as a biological-recognition unit in cell-based biosensors or as 'electrical current generators' in the design of microbial biofuel cells [6–9]. *S. cerevisiae* is a good model for the evaluation of cytotoxicity studies because: (i) manipulations with them are simple and relatively low cost, (ii) a genome of *S. cerevisiae* is fully sequenced and a survival rate of *S. cerevisiae* under different conditions including harsh aerobic and anaerobic conditions at varying pH is very high [10,11]. Therefore, even if there are some significant differences between *S. cerevisiae* and mammalian cells *S. cerevisiae* in many experiments are replacing mammalian cells, which are very sensitive to environmental factors. There are many reports on manipulations and electrochemical investigations of viable yeast cells [12–16]. However, the number of reports on the immobilization and investigations of nonviable cells is still limited [17–21]. Although, nonviable cells are not able to proliferate, but they can contain some active enzymes, therefore they remain important biosystems for the evaluation of some living cell properties, because active enzymes can perform many catalytic functions even after the losing cell viability [22–24].

There are many different electrochemical methods, which are suitable for the investigation of yeast cells, including scanning electrochemical microscopy (SECM) [15–17] and electrochemical impedance spectroscopy (EIS) [18,19]. SECM is a valuable technique for quantitative investigation and surface analysis of a wide range of processes that occur at electrochemically active interfaces [25]. SECM is growing technique used in scanning probe electrochemistry, which provides ability to analyze, to visualize and to map electrochemical activity of electrochemically active surfaces [10,26,27]. Meanwhile, EIS is a non-destructive method, which is providing useful models on the effect of alternating current (AC) on the sample. EIS enables registering quantitative data, which deter-

[a] A. Valiūnienė, J. Petronienė, M. Dulkys, A. Ramanavičius
Department of Physical Chemistry, Faculty of Chemistry and Geosciences, Vilnius University, Naugarduko 24, LT-03225 Vilnius, Lithuania
E-mail.:
E-mail: arunas.ramanavicius@chf.vu.lt
[b] A. Ramanavičius
Laboratory of Nanotechnology, State Research Institute Center for Physical Sciences and Technology, Sauletekio ave. 3, LT-10257, Vilnius, Lithuania

Supporting information for this article is available on the WWW under https://doi.org/10.1002/elan.201900414

mines properties of electrode/electrolyte boundary [2,28–31]. However, conventional EIS-based technique has a problem because it represents only average response of a whole electrochemical system. Therefore, SECM was combined with EIS in order to perform localized electrochemical impedance spectra measurements of the surfaces and this combined technique is called scanning electrochemical impedance microscopy (SEIM) [15,32–37]. SEIM enables performing localized electrochemical impedance measurements in a wide range of AC frequencies during SECM experiment, when the surface of interest is scanned by ultramicroelectrode (UME) and detailed electrochemical information can be gathered at each point of the measurement [19,21,38,39]. However, the main disadvantage of combined SECM and conventional EIS techniques (SEIM technique) is very low mapping rate of SEIM, therefore, this method is not well suitable for the investigation of electrochemically active interphases with rapidly changing properties, e.g. samples based on living cells. Therefore, seeking advanced application of SEIM for the investigation of biological objects, in our previous researches we have resolved this disadvantage by applying fast Fourier transform based EIS technique (FFT-EIS) [40–43], which allows reducing the duration of EIS signal registration by 5–20 times when compared to duration required for conventional EIS equipment. Recently it was demonstrated that FFT-EIS can be applied in SECM measurements (FFT-SEIM) [2,44] for the fast/localized registration of EIS spectra at several distances from conducting and non-conducting surface in the presence of a redox-couple [2] and in redox-probe-free mode [44]. The application of FFT-SEIM enables to reduce significantly the duration of measurements because the evaluation of the EIS in the frequency range from 1.5 Hz to 50 kHz at any single UME position takes only 1.3 s.

In order to demonstrate the applicability of combined SECM and FFT-EIS based techniques (FFT-SEIM), in this research we have applied FFT-SEIM for the evaluation of electrochemical properties and redox activity of immobilized active and inactivated yeast cells.

2 Experimental

2.1 Materials

All chemicals used in electrochemical experiments were purchased from Merck, Fluka, Carl Roth, AppliChem, Alfa Aesar companies and were highest available purity. Phosphate buffer solution (PBS) of pH 6.75 was used for all electrochemical measurements, and was prepared using 0.05 M NaH_2PO_4, (CAS No.: 7558-80-7; S5011; BioPerformance Certified),0.05 M Na_2HPO_4 (CAS No.: 7758-79-4; 98 + %), 0.05 M CH_3COONa (CAS No.: 127-09-3; extra pure) and 0.1 M KCl (CAS No.: 7747-40-7; suprapur) dissolved in deionized water (with initial conductivity of 0.05 μS). *Saccharomyces cerevisiae* (commonly known as baker's yeast) were bought in granular form from food supplier LALLEMAND (Lublin, Poland), menadione (2-methylnaphthalene-1,4-dione CAS No.: 58-27-5; 98 %), vit K_1 (CAS No.: 130-37-0; 95 %) from Sigma- Aldrich St.Louis, USA.

2.2 Preparation and Immobilization of Yeast Cells

Active yeast cells are those, which can grow, reproduce and carries out metabolism [43]. 0.1 $g\,cm^{-3}$ active yeast suspension was prepared in deionized water. During the preparation this suspension was incubated in 30 °C temperature with stirring for 30 minutes. To prepare inactivated yeast cell sample, the suspension with active cells was stored at 75 °C temperature for 2 hours [45]. After cooling down to ambient temperature such suspension was used for the experiments where inactivated yeast cells were needed.

A plastic petri dish, which was made of poly(methyl methacrylate), was washed with 96 % ethanol solution. Then 0.5 μL of yeast suspension was deposited on the bottom of petri dish and then it was dried out by keeping above 25 % glutaraldehyde solution for 10 minutes.

For the investigations of electrochemical activity of active yeast cells the solution of 12.5 μM mediators Vit-K_1 and 12.5 μM Vit-K_3 was used. Vit-K_1 was prepared by dissolving 0.25 mM sodium 1,4-naphthoquinone-2-sulfonate in deionized water, Vit-K_3 – by dissolving 0.25 mM 2-methyl-1,4-naphthoquinone in 96 % ethanol.

2.3 Electrochemical Equipment and Registration of Electrochemical Signals

Disk-shaped platinum ultramicroelectrode (UME) (diameter 23 μm, calculated geometric surface area 4.15×10^{-6} cm^2) was used as a working electrode, $Ag|AgCl|KCl_{(sat.)}$ was used as a reference and platinum wire – as a counter electrode. Before each electrochemical experiment the UME was polished with polishing paper with grain size of 0.3 μm, then it was washed in ethanol and cleaned in 0.5 M H_2SO_4 solution by cyclic voltammetry until shape of voltammogram curves become constant. Mechanically polished and electrochemically pretreated UME was used for the registration of cycling votammogram in buffer solution, pH 6.75, containing 12.5 μM of Vit-K_1 and 12.5 μM of Vit-K_3 both acting as redox mediators in order to adjust the most proper electrochemical parameters, which were later applied to EIS and SEIM based investigations throughout this work. Scanning electrochemical microscope from Sensolytics (Bochum, Germany) was used for the positioning of UME. It was positioned in several different distances from immobilized yeast cells and electrochemical impedance spectra were registered. In time based experiments EI spectra were registered using impedance spectrometer EIS-128/16 developed and designed in University of Kiel [40] (Kiel, Germany) with fast Fourier transform (FFT) function, which enables registration of whole electrochemical impedance spectrum within 1.3 s when applying alternating current in the range between 50 kHz – 1.5 Hz [41].

Conventional EIS measurements were performed using potentiostat/galvanostat Autolab PGSTAT 30 that registers an EIS spectrum in the same frequency range of 50 kHz – 1.5 Hz, in this case the collection of EIS spectra lasted for 8 min.

To investigate the influence of sodium 1,4-naphthoquinone-2-sulfonate (Vit-K_1) and 2-methyl-1,4-naphthoquinone and (Vit-K_3) on electrochemical activity of active yeast cells, UME was replaced with graphite electrode (which was of 3 mm diameter and of 0.071 cm^2 calculated geometric surface area). Before each experiment graphite electrode was polished with polishing paper and washed in deionized water. Then active yeast cells were immobilized on this electrode during the same procedure as it was applied for the immobilization of yeast cells on the petri dish (as described in section 2.2). Vit-K_1 and Vit-K_3 were introduced into electrochemical cell as redox mediators using two different ways:

(i) in 'System 1' 12.5 μM of Vit-K_1 and 12.5 μM of Vit-K_3 were added into the buffer solution, which was located in the petri dish where yeast cells were immobilized;
(ii) in 'System 2' the same amount of Vit-K_1 and Vit-K_3 was added onto immobilized yeast cells to dry and only after this modification the petri dish was filled with the buffer solution.

Electrochemical impedance spectra depending on the system were registered at certain periods of time: (i) in 'System 1' the EIS registration started instantly after the addition of redox mediators (Vit-K_1 and Vit-K_3) into the buffer solution (ii) in 'System 2' the EIS registration started only after the buffer solution was added to petri dish with immobilized yeast cells, pretreated with redox mediators.

Throughout this work all EIS measurements were carried out at the frequency range of alternating current between 1.5 Hz and 50 kHz. EIS experiments with platinum UME were performed at −1.2 V *vs* Ag|AgCl|$KCl_{(sat.)}$, while EIS spectra of graphite electrode were recorded at −0.84 V *vs* Ag|AgCl|$KCl_{(sat.)}$. The most suitable potentials for EIS measurements were determined from cyclic voltammetry based experiments in the potential range at which Faradaic current was observed. For the impedance measurements AC-perturbation amplitude of 10–15 mV was applied in order to avoid non-linearity of response signal. Gathered EIS spectra were evaluated using EIS data analysis software "ZView" for the determination of electrochemical characteristics using selected equivalent circuit model, in this research EIS data are presented as Nyquist plots.

The thickness of yeast spot was evaluated by atomic force microscope (Bioscope II)/Catalyst from Veeco (Santa Barbara, USA) at room temperature in air using tapping mode, and it was determined as 1.5–2.0 μm (Figure S3), which is in agreement with previuosly published our results [46]. From this experiment the 'zero distance' was set at 1,5 from the surface of Petri dish.

3 Results and Disscusion

3.1 Evaluation of Electrochemical Properties of Immobilized Active and Inactivated Yeast Cells

Before starting SECM, EIS and SEIM measurements, which were performed to investigate electrochemical properties of immobilized active and inactivated yeast cells, some preliminary experiments were carried out. Firstly, cyclic votammogram of mechanically and electrochemically pretreated UME was registered in the buffer solution, pH 6.75, containing 12.5 μM of Vit-K_1 and 12.5 μM of Vit-K_3, which were acting as redox mediators according to the scheme presented in Figure 1.

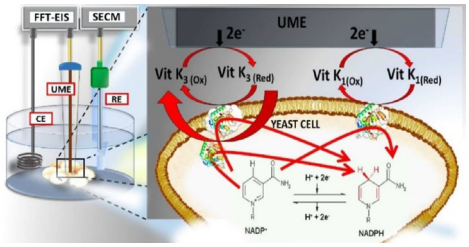

Fig. 1. Interaction of sodium 1,4-naphthoquinone-2-sulfonate (VitK_1) and 2-methyl-1,4-naphthoquinone (VitK_3) with yeast cells and electrode.

As it is shown in Figure 1 Vit-K_1 is able to transfer electrical charge from redox enzymes and other redox-able species, which are localized in the membrane of the cell, while Vit-K_3 is able to penetrate cell membrane and to transfer the charge from redox enzymes and other redox-able species which are localized inside of the cell. Oxidation reduction processes of these enzymes are presented in the Figure 1, which illustrates that significant part of related red-ox processes is based on $NADP^+$/NADPH- based enzymes.

The cyclic voltammogram (Figure 2A) was used for the determination of suitable electrode potential, which is required for the correct registration of EIS spectra at potentiostatic conditions.

For here proposed research it was important to select such UME potential at which Faradaic current is generated on the UME electrode, because it was expected that no significant changes in EIS spectra can be obtained while performing EIS measurements at potentials where'-ideal polarization' of electrode is observed at such conditions when no oxidation and/or reduction processes occur on the electrode. Therefore, we have selected −1.2 V potential *vs* Ag|AgCl|$KCl_{(sat.)}$ for EIS measurements because at this potential significant variation of current density was observed during the registration of cyclic voltammogram (Figure 2A). Before EIS measurements, working UME was used for the registration of

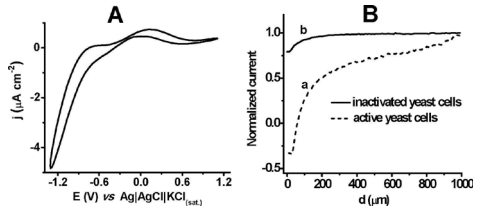

Fig. 2. **A** – cyclic voltammogram of UME in PBS, pH 6.75, containing 12.5 μM of Vit-K_1 and 12.5 μM of Vit-K_3. Potential sweep rate – 0.2 Vs^{-1}. **B** – approach curves registered when UME was approaching towards the surface modified with active (a) and inactivated (b) yeast cells. Approaching was performed at 10 μms^{-1} in PBS, pH 6.75, at −0.5 V potential *vs* Ag|AgCl|KCl$_{(sat.)}$.

approach curves above the petri dish surface modified by active and inactivated yeast cells in order to investigate the process of charge transfer at the interface between UME and the electrolyte when UME is approaching the surface of yeast cells. The registered approach curves are presented in Figure 2B where current is normalized by dividing measured current values by maximally registered one.

The potential of −0.5 V was chosen based on the current density registered in mediator-free PBS. From the obtained current-distance curves (Figures 2B, S1) it is seen that normalized current values decrease significantly when the UME approaches the surface of active yeast cells (Figure 2B, curve a). This result indicates that electrochemical processes at UME are blocked while approaching the surface modified by yeast cells, which is specific indication of negative-feedback behaviour that is usually registered when (i) UME is approaching non-conducting surfaces [2]. Significant decrease of UME current density has been observed when the distance between UME and active yeast cells is below 200 μm. On the one hand, such significant change in current density can be explained by the reduction of dissolved oxygen, which produces current flow at UME, when the electrode is retracted from the cell-modified petri dish surface at the distance, which exceeds 200 μm. But if the electrode is approaching closer to the surface, the concentration of oxygen becomes lower due to consumption of oxygen by metabolic processes, which are taking part in active yeast cells, what is causing significant decrease of UME current.

When UME is approaching the surface modified by inactivated yeast cells, only negligible decrease in current density is observed (Figure 2B, curve b), because inactivated yeast cells are not consuming oxygen. This means if UME positioned above inactivated yeast cells it is only blocked by diffusion limitations for dissolved oxygen when UME is approaching closer than 50 μm towards the inactivated yeast modified surface. When the distance between the electrode and the surface modified by inactivated yeast cells reaches 120 μm, then the electrode current starts to decrease until it becomes very low (below 0.01 nA) at the point when UME is reaching 'zero distance', which was initially determined by approaching cell-modified surface. Comparing currents, which were registered during the approaching of UME to the active yeast cell modified surface (Figure 2B, curve a), with that registered when UME approached the surface modified by inactivated yeast cell (Figure 2B, curve b) it was determined that active yeast cells shows much higher oxygen consumption rate comparing to that of inactivated yeast cells. The registered approach curves (Figure 2B) allow us to gain information about the current flow when the electrode is positioned at 'zero distance' from the yeast cell modified surface. When UME approaches 'zero distance' above either active or inactivated yeast cells, the registered current values do not decrease down to 'zero level'. It means that at 'zero distance' from the yeast cell modified surface the delivery of oxygen towards UME is still blocked only partially, therefore, charge transfer proceeds at the interface between UME and the electrolyte, which still contains some oxygen.

It should be noted that during the registration of approach curves there is a risk to contaminate the conducting part of UME by direct touching the surface of yeast cells. Hence, the UME should be cleaned thoroughly after the registration of each approach curve. Therefore, in this work UME was cleaned in 0.5 M H_2SO_4 solution by potential cycling until the shape of voltammogram curves become constant and only then the electrode was used for EIS measurements.

The registration of significant currents during whole approaching cycle revealed that for both active and inactivated yeast cell modified petri dish surfaces it is possible to perform the measurements of electrochemical impedance spectroscopy and to determine electrochemical characteristics. Firstly, electrochemical impedance spectra were recorded in the buffer solution at −1.2 V potential *vs* Ag|AgCl|KCl$_{(sat.)}$ using UME positioned at'zero distance' from the active and inactivated yeast cells surface. The obtained EIS data are displayed as Nyquist plots in Figure 3A.

A typical equivalent circuit model (Figure 3A, inset) was chosen for the assessment of EIS data using this work and taking into account the fact that in our system the Faraday process occurs under the applied potential of −1.2 V *vs* Ag|AgCl|KCl$_{(sat.)}$ (see Figure 2A). In this case, the equivalent circuit consists of solution resistance (R_s), constant phase element (*CPE*), which represents a capacitance of the electric double layer (EDL) that forms at the interface between UME and buffer solution, and parallel resistance (R_{ct}), which represents the charge transfer at the interface between UME and the electrolyte.

A satisfactory fitting of the experimental EIS data (Figure 3A, symbols) to the equivalent circuit model (Figure 3A, line) was observed and following fitting parameters were calculated for both SEIM experiments: (i) when the electrode was positioned above active yeast

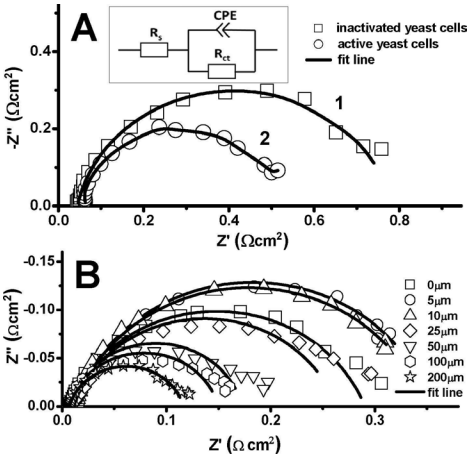

Fig. 3. **A** – electrochemical impedance spectra registered in PBS, pH 6.75, at −1.2 V *vs* Ag|AgCl|KCl$_{(sat.)}$ by using UME positioned at'zero distance' from the active (curve 2) and inactivated (curve 1) yeast cells surface. Inset – equivalent circuit model used for fitting of EIS data: R_s – electrolyte solution resistance; *CPE* – constant phase element; R_{ct} – charge-transfer resistance. **B** - electrochemical impedance spectra registered in FFT-SEIM mode, in PBS, pH 6.75, at −1.2 V *vs* Ag|AgCl|KCl$_{(sat.)}$ when UME was positioned at different distances from the petri dish surface, which was modified by active yeast cells.

cells then $R_s = 57.90\ m\Omega\,cm^2$; $CPE = 30.46\ mF\,cm^{-2}$ (with exponent $n = 0.90$); $R_{ct} = 0.47\ m\Omega\,cm^2$; (ii) when the electrode was positioned above inactivated yeast cells then $R_s = 44.42\ m\Omega\,cm^2$; $CPE = 32.22\ mF\,cm^{-2}$ (with exponent $n = 0.88$); $R_{ct} = 0.74\ m\Omega\,cm^2$ (Table S1). These values of equivalent circuit (Figure 3A, inset) were calculated by analysing EIS data registered by using UME positioned at'zero distance' from petri dish surface modified by active and inactivated yeast cells (Figure 3A). FFT-EIS spectra registered, when UME was approaching towards surface modified by inactivated cells are presented in Figure S2.

The calculated EIS characteristics (Table S2) obviously indicate that charge transfer resistance R_{ct} above the surface modified by active yeast cells is by 0.27 Ωcm^2 lower than that above the surface modified by inactivated yeast cells. This effect can be explained by the formation of oxidized forms of some charge-transfer-able materials as a result of metabolic processes inside of active yeast cells. In opposite, the limited metabolism does not occur on the petri dish surface modified by inactivated yeast cells, thus around inactivated cells there is a lower concentration of oxidized forms of some charge-transfer-able materials close to the surface of cells and it is in agreement with the increase of R_{ct} value.

Further series of EIS experiments were performed in FFT-SEIM configuration, in order to investigate the influence of the distance between UME and surface of active yeast cells on the registered electrochemical impedance spectra. FFT-EIS data registered by using UME positioned at different distances from the surface modified by immobilized cells are presented as Nyquist plots in Figure 3B. By fitting the experimental EIS data to the equivalent circuit model (Figure 3A, inset), the electrochemical characteristics of selected equivalent circuit were calculated and are presented in Table S3.

As it can be expected, due to diffusion limitations, the values of charge transfer resistance (R_{ct}) increase slightly when the UME approaches down from 10 until 5 μm the surface modified by active yeast cells. However, when UME is positioned at higher distances from the surface of active yeast cells (i.e. at 25 μm) the R_{ct} is decreasing when the distance between UME and the surface of interest increases. Summarising it can be concluded, that performing experiments in FFT-SEIM configuration: (i) electrochemical activity and oxygen consumption (breathing) of yeast can be electrochemically observed when the distance between UME and surface of yeast cells is from 0 μm to 25 μm; (ii) 25 μm is the maximum distance suitable for efficient investigation of yeast cell activity.

3.2 Investigations of the Influence of Sodium 1,4-Naphthoquinone-2-Sulfonate (Vit-K$_1$) and 2-Methyl-1,4-Naphthoquinone (Vit-K$_3$) on Electrochemical Activity of Active Yeast Cells

Once the redox activity of immobilized active and inactivated yeast cells was investigated by FFT-SEIM, time based experiments were performed investigating charge transfer between the active yeast cells and lipophilic (Vit-K$_3$) and hydrophilic (Vit-K$_1$) mediators. For this experiment we have applied FFT-EIS, therefore, we were able to monitor EIS almost in real time, and to determine how fast the equilibrium of concentrations of added vitamins (Vit-K$_1$ and Vit-K$_3$) between the solution and immobilized yeast cells is achieved. FFT-EIS spectra were registered at FFT-SEIM mode in PBS at −1.2 V potential *vs* Ag|AgCl|KCl$_{(sat.)}$ when the UME was positioned more than 1 mm away from the petri dish surface, which was modified by yeast cells (Figure 4). FFT-SEIM experiments were carried out with two differently prepared samples in which the same concentration (12.5 μM) of each redox mediator (Vit-K$_1$ and Vit-K$_3$) was formed in electrochemical system by two different ways: (i) in 'System 1', Petri dish, which contained immobilized yeast cells, was filled with 5 ml of buffer solution containing 12.5 μM concentration of each Vit-K$_1$ and Vit-K$_3$ and then FFT-EIS spectra were recorded at different time intervals (Figure 4A); (ii) in 'System 2', 0.5 ml of solution containing 125 μM concentration of each Vit-K1 and Vit-K3 was added into the Petri dish with immobilized yeast cells, incubated at 4 °C for 24 h during which solvent has evaporated and then the petri dish was filled with 5 ml of buffer solution (final concentration of Vit-K$_1$ and Vit-K$_3$ was expected to be the same as it was in the

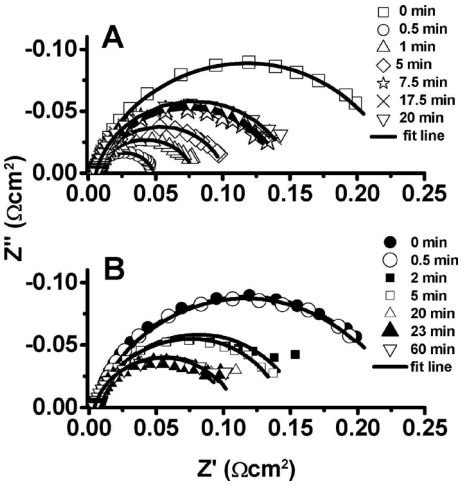

Fig. 4. Time-dependent FFT-EIS spectra registered in FFT-SEIM mode in PBS, pH 6.75, at −1.2 V *vs* Ag|AgCl|KCl$_{(sat.)}$ when UME was positioned above petri dish surface modified by active yeast cells. **A** – 'System 1', the redox mediators (12.5 μM of Vit-K$_1$ and Vit-K$_3$) were added into the buffer solution in the petri dish where active yeast cells were immobilized onto petri dish surface before the addition of Vit-K$_1$ and Vit-K$_3$, **B** – 'System 2', the same amount of Vit-K$_1$ and Vit-K$_3$ was added onto immobilized yeast cells to dry and then the petri dish was filled with the buffer solution.

'System 1'), incubated for 1 h, gently mixed and then FFT-EIS spectra were recorded at different time intervals (Figure 4B). Registered EIS spectra were fitted according to equivalent circuit (Figure 3A, inset) and calculated fit results are presented in Table S3.

In order to investigate kinetics of interactions between the active yeast cells and lipophilic (Vit-K$_3$) and hydrophilic (Vit-K$_1$) mediators, the values of charge transfer resistance are the most important and, therefore, they were analysed very thoroughly (Figure 5). It was found that R_{ct} values become constant: (i) within 20 min for 'System 1' (Vit-K$_1$ and Vit-K$_3$ are added to the buffer solution) (Figure 5A), and within 7.5 min for 'System 2' (Vit-K$_1$ and Vit-K$_3$ are added onto dry immobilized yeast cells) (Figure 5B). These results show that in the case of 'System 2' the equilibrium of Vit-K$_1$ and Vit-K$_3$ concentrations between solution and yeast cells is reached faster. The difference in the duration of reaching steady-state conditions is related to the fact that during the investigation of 'System 1' Vit-K$_1$, which is lipophilic, should diffuse into yeast cell membrane, where it serves as redox mediator between intrinsic redox enzymes and hydrophilic Vit-K$_3$, while in the case of 'System 2' the immobilized yeast cells are pretreated by Vit-K$_1$ containing solution before the petri dish with such modified yeast cells is filled with the buffer solution. Therefore, in the

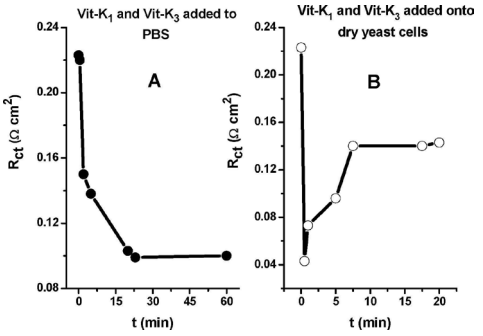

Fig. 5. Evolution of charge transfer resistance (R_{ct}), calculated by fitting FFT-EIS data presented in Figure 4, in time: **A** – 'System 1', Vit-K$_1$ and Vit-K$_3$ are added into the buffer solution in petri dish with immobilized yeast cells; **B** – 'System 2', immobilized yeast cells are modified by Vit-K$_1$ and Vit-K$_3$ before adding the buffer solution.

case of 'System 2' reaching steady-state conditions takes longer, which is reflected by time required for reaching steady-state R_{ct} value.

To investigate the influence of Vit-K$_1$ and Vit-K$_3$, which were acting as redox mediators, on electrochemical activity of active yeast cells, yeast cells were immobilized on the surface of graphite electrode (geometric surface area 0.071 cm^2), and then FFT-EIS spectra were recorded (Figure 6) at −0.84 V potential *vs* Ag|AgCl|KCl$_{(sat.)}$ at which Faradaic current is observed according to cyclic voltammogram data (Figure 6, inset).

Electrochemical characteristics obtained by fitting FFT-EIS data (Figure 6) to equivalent circuit model

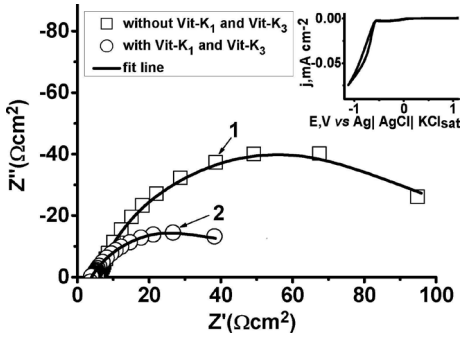

Fig. 6. FFT-EIS spectra of graphite electrode modified by immobilized active yeast cells in PBS, pH 6.75, at −0.84 V *vs* Ag|AgCl|KCl$_{(sat.)}$ without any redox mediators (curve 1) and with 12.5 μM of lipophilic (Vit-K$_3$) and 12.5 μM of hydrophilic (Vit-K$_1$) mediators (curve 2). The inset represents cyclic voltammogram of UME electrode in PBS, pH 6.75. Potential sweep rate 50 mVs^{-1}.

presented in Figure 3A inset were the following: (i) when the experiment was performed in the presence of Vit-K_1 and Vit-K_3, which were serving as redox mediators then $R_s = 3.95\ m\Omega\,cm^2$; $CPE = 2.09\ mF\,cm^{-2}$ (with exponent $n = 0.71$); $R_{ct} = 47.79\ m\Omega\,cm^2$; (ii) when the experiment was performed in the absence of vitamins as redox mediators then $R_s = 5.77\ m\Omega\,cm^2$; $CPE = 0.49\ mF\,cm^{-2}$ (with exponent $n = 0.83$); $R_{ct} = 107.3\ m\Omega\,cm^2$ (Table S4). Comparing FFT-EIS data obtained during the investigation of similar graphite electrode modified by immobilized yeast cells in the absence of redox mediators (Figure 6, curve 1) and in the presence of lipophilic (Vit-K_3) and hydrophilic (Vit-K_1) redox mediators (Figure 6, curve 2), it is obvious that charge transfer resistance, R_{ct}, (Table S4) decreases more than twice (from $107.3\ \Omega cm^2$ down to $47.8\ \Omega cm^2$) in presence of Vit-K_1 and Vit-K_3.

4 Conclusions and Future Trends

Significant difference of charge transfer resistance through the electrode-solution interphase was registered when UME was approaching petri dish surface modified by active and inactivated yeast cells at −1.2 V *vs* Ag|AgCl|$KCl_{(sat.)}$ potential in the phosphate buffer solution, pH 6.75. The charge transfer resistance was $0.74\ \Omega cm^2$ and $0.47\ \Omega cm^2$ in the case of active and inactivated yeast cells, respectively.

While performing experiments in FFT-SEIM configuration, electrochemical activity and oxygen consumption (breathing) by yeast can be electrochemically observed when the distance between UME and surface of yeast cells is from 0 µm to 25 µm. Therefore, 25 µm is the maximum distance, which is still suitable for efficient investigation of yeast cell activity by FFT-SEIM.

The redox-efficiency of applied redox mediators (Vit-K_1 and Vit-K_3) evolved faster when the immobilized yeast cells were pretreated by the solution of Vit-K_1 and Vit-K_3 before adding the buffer solution into the cell.

During future our investigations we are planning to apply FFT-SEIM for the evaluation of stem cells and tissues of mamalians.

Acknowledgements

This research is/was funded by the European Regional Development Fund according to the supported activity 'Research Projects Implemented by World-class Researcher Groups' under Measure No. 01.2.2-LMT-K-718. Authors thanks for AFM imaging, which was performed by Assoc. Prof. Dr. Inga Morkvenaite- Vilkonciene.

References

[1] I. Morkvenaite-Vilkonciene, A. Ramanaviciene, A. Ramanavicius, *Sens. Actuators B* **2016**, *228*, 200–206.
[2] I. Morkvenaite-Vilkonciene, A. Valiūnienė, J. Petroniene, A. Ramanavicius, *Electrochem. Commun.* **2017**, *83*, 110–112.
[3] R. G. Willaert, G. V. Baron, L. De Backer, *Immobilised Living Cell Systems: Modelling and Experimental Methods*, John Wiley & Sons, Chichester, New York, **1996**.
[4] N. Kosaric, 1996. Ethanol-potential source of energy and chemical product in: Biotechnology. Products of Primary Metabolism, 6 ed. Rehm, H. J., Reed, G., Puhler, A., Stadler, P., VCH, Germany, pp. 121–198.
[5] H. Chen, C. K. Heng, P. D. Puiu, X. D. Zhou, A. C. Lee, T. M. Lim, S. N. Tan, *Anal. Chim. Acta* **2005**, *554*, 52–59.
[6] I. Morkvenaite-Vilkonciene, A. Ramanaviciene, P. Genys, A. Ramanavicius, *Electroanalysis* **2017**, *29*, 1532–1542.
[7] S. Ostegaard, L. Olsson, J. Nielsen, *Microbiol. Mol. Biol. Rev.* **2000**, *64*, 34–50.
[8] K. H. R. Baronian, A. J. Downard, R. K. Lowen, N. Pasco, *Appl. Microbiol. Biotechnol.* **2002**, *60*, 108–113.
[9] A. Gunawardena, S. Fernando, F. To, *Int. J. Mol. Sci.* **2008**, *9*, 1893–1907.
[10] A. Ramanavicius, I. Morkvenaite-Vilkonciene, A. Kisieliute, J. Petroniene, A. Ramanaviciene, *Colloids Surf. B* **2017**, *149*, 1–6.
[11] C. E. Rodriguez, M. Shinyashiki, J. Froines, R. C. Yu, J. M. Fukuto, A. K. Cho, *Toxicology* **2004**, *201*, 185–196.
[12] H. Shiku, S. Goto, S. Jung, K. Nagamine, M. Koide, T. Itayama, T. Yasukawa, T. Matsue, *Analyst* **2009**, *134*, 182–187.
[13] M. Tsionsky, J. Zhou, S. Amemiya, F. Fan, A. J. Bard, *Anal. Chem.* **1999**, *71*, 4300–4305.
[14] J. Mauzeroll, A. J. Bard, *PNAS* **2004**, *101*, 7862–7867.
[15] P. M. Diakowski, Z. Ding, *Phys. Chem. Chem. Phys.* **2007**, *9*, 5966–5974.
[16] Sh. Yamashoji, *Biochem. Biophys. Rep.* **2016**, *6*, 88–93.
[17] Y. Huang, R. Holzel, R. Pethig, X. B. Wang, *Phys. Med. Biol.* **1992**, *37*, 1499–1517.
[18] G. H. Markx, M. S. Talary, R. Pethig, *J. Biotechnol.* **1994**, *32*, 29–37.
[19] M. J. Henry-Stanley, R. M. Garni, C. L. Wells, *J. Microbiol. Methods*, **2004**, *59*, 289–292.
[20] D. Brady, A. Stoll, J. R. Duncan, *Environ. Technol.* **1994**, *15*, 429–438.
[21] N. K. Egilmez, J. B. Chen, S. M. Jazwinski, *J. Gerontol.* **1990**, 45, B9–B17.
[22] S. Y. Tang, W. Zhang, S. Baratchi, M. Nasabi, K. Kalantar-zadeh, K. Khoshmanesh, *Anal. Chem.* **2013**, *85*, 6364–6371
[23] E. Herker, H. Jungwirth, K. A. Lehmann, C. Maldener, K. U. Fröhlich, S. Wissing, S. Büttner, M. Fehr, S. Sigrist, F. J. Madeo, *J. Cell Biol.* **2004**, *164*, 501–507.
[24] L. Váchová, Z. J. Palková, *J. Cell Biol.* **2005**, *169*, 711–717.
[25] X. Lu, Q. Wang, X. Liu, *Anal. Chim. Acta* **2007**, *601*, 10–25.
[26] A. J. Bard, M. V. Mirkin, *Scanning Electrochemical Microscopy*, Marcel Dekker, New York, **2001**.
[27] L. P. Bauermann, W. Schuhmann, A. Schulte, *Phys. Chem. Chem. Phys.* **2004**, *6*, 4003–4008.
[28] I. Morkvenaite-Vilkonciene, P. Genys, A. Ramanaviciene, A. Ramanavicius, *Colloids Surf. B* **2015**, *126*, 598–602.
[29] B. Y. Chang, S. M. Park, *Annu. Rev. Anal. Chem.* **2010**, *3*, 207–229.
[30] T. Sabirovas, A. Valiūnienė, G. Valincius, *J. Electrochem. Soc.* **2018**, *165*, G109–G115.
[31] A. Lasia, Electrochemical Impedance Spectroscopy and Its Applications, *Mod. Aspects Electrochem.*, B. E. Conway, J. Bockris, R. E. White, Edts., Kluwer Academic/Plenum Publishers, New York, **1999**, Vol. 32, p. 143–248.
[32] B. B. Katemann, A. Schulte, E. J. Calvo, M. Koudelka-Hep, W. Schuhmann, *Electrochem. Commun.* **2002**, *4*, 134–138.
[33] M. Gębala, W. Schuhmann, F. La Mantia, *Electrochem. Commun.* **2011**, *13*, 689–693.

[34] V. Kuznetsov, A. Maljusch, R. M. Souto, A. S. Bandarenka, W. Schuhmann, *Electrochem. Commun.* **2014**, *44*, 38–41.
[35] P. M. Diakowski, Z. Ding, *Electrochem. Commun.* **2007**, *9*, 2617–2621.
[36] A. S. Baranski, P. M. Diakowski, *J. Solid State Electrochem.* **2004**, *8*, 683–692 DOI: 10.1007/s10008-004-0533-x
[37] C. Gabrielli, F. Huet, M Keddam, P. Rousseau, V. Vivier, *J. Phys. Chem. B* **2004**, *108*, 11620–11626.
[38] A. Estrada-Vargas, A. Bandarenka, V. Kuznetsov, W. Schuhmann, *Anal. Chem.* **2016**, *88*, 3354–3362.
[39] M. A. Alpuche-Aviles, D. O. Wipf, *Anal. Chem.* **2001**, *73*, 4873–4881.
[40] G. Popkirov, R. Schindler, *Electrochim. Acta* **1993**, *38*, 861–867.
[41] A. Valiūnienė, G. Baltrūnas, R. Valiūnas, G. Popkirov, *J. Hazard. Mater.* **2010**, *180*, 259–263.
[42] G. S. Popkirov, R. N. Schindler, *Rev. Sci. Instrum.* **1992**, *63*, 5366–5372.
[43] K. Autio, T. Mattila-Sandholm, *Appl. Environ. Microbiol.* **1992**, *58*, 2153–2157.
[44] A. Valiūnienė, J. Petroniene, I. Morkvenaite-Vilkonciene, G. Popkirov, A. Ramanaviciene, A. Ramanavicius, *Phys. Chem. Chem. Phys.* **2019**, *21*, 9831–9836.
[45] N. Lewpiriyawong, K. Kandaswamy, C. Yang, V. Ivanov, R. Stocker, *Anal. Chem.* **2011**, *83*, 9579–9585
[46] A. Suchodolskis, A. Stirke, A. Timonina, A. Ramanaviciene, A. Ramanavicius, *Advanded Science Letters* **2011**, *4*, 171–173.

Received: July 3, 2019
Accepted: September 11, 2019
Published online on ■■, ■■

FULL PAPER

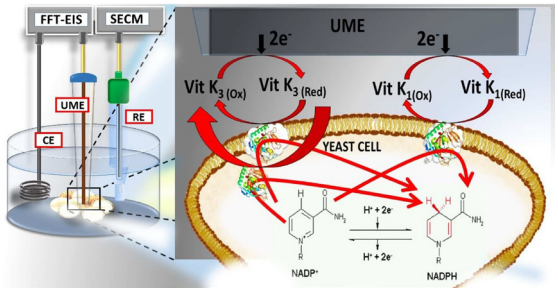

*A. Valiūnienė, J. Petronienė, M. Dulkys, A. Ramanavičius**

ARTICLE 4

Article title: Evaluation of Redox Activity of Human Myocardium Derived Mesenchymal Stem Cells by Scanning Electrochemical Microscopy

Authors: Jurate Petroniene, Inga Morkvenaite-Vilkonciene, Rokas Miksiunas, Daiva Bironaite, Almira Ramanaviciene, Lina Mikoliunaite, Aura Kisieliute, Kestutis Rucinskas, Vilius Janusauskas, Ieva Plikusiene, Siegfried Labeit, Arunas Ramanavicius

Journal title, edition and volume: *Electroanalysis*, 2020, 32, 1-10,
(not final pages number)
DOI: 10.1002/elan.201900723

ELECTROANALYSIS
An International Journal Devoted to Electroanalysis, Sensors and Bioelectronic Devices

Accepted Article

Title: Evaluation of redox activity of human myocardium-derived mesenchymal stem cells by scanning electrochemical microscopy

Authors: Jurate Petroniene, Inga Morkvenaite-Vilkonciene, Rokas Miksiunas, Daiva Bironaite, Almira Ramanaviciene, Lina Mikoliunaite, Aura Kisieliute, Vilius Janusauskas, Kestutis Rucinskas, Ieva Plikusiene, Siegfried Labeit, and Arunas Ramanavicius

To be cited as: *Electroanalysis* 10.1002/elan.201900723

Link to VoR: http://dx.doi.org/10.1002/elan.201900723

WILEY-VCH

Evaluation of redox activity of human myocardium-derived mesenchymal stem cells by scanning electrochemical microscopy

*Jurate Petroniene[a], Inga Morkvenaite-Vilkonciene[b,c], Rokas Miksiunas[d], Daiva Bironaite[d], Almira Ramanaviciene[e], Lina Mikoliunaite[a,f], Aura Kisieliute[a], Kestutis Rucinskas[g], Vilius Janusauskas[g], Ieva Plikusiene[a], Siegfried Labeit[h], Arunas Ramanavicius[a,i]**

[a] Department of Physical Chemistry, Faculty of Chemistry and Geosciences, Vilnius University, Vilnius, Lithuania;
[b] Laboratory of Electrochemical Energy Conversion, State Research Institute Centre for Physical Sciences and Technology, Vilnius, Lithuania;
[c] Department of Mechatronics and Robotics, Faculty of Mechanics, Vilnius Gediminas Technical University, Vilnius, Lithuania
[d] Department of Regenerative medicine, State Research Institute Centre for Innovative Medicine, Vilnius, Lithuania;
[e] Nanotechnas-Centre of Nanotechnology and Materials Science, Faculty of Chemistry and Geosciences, Vilnius University, Vilnius, Lithuania;
[f] Laboratory of Organic Chemistry, State Research Institute Centre for Physical Sciences and Technology, Vilnius, Lithuania ;
[g] Centre of Cardiothoracic Surgery of Vilnius University Hospital Santariskiu Klinikos, Vilnius, Lithuania;
[h] Department of Integrative Pathophysiology, Universitätsmedizin Mannheim, Mannheim, Germany.
[i] Laboratory of Nanotechnology, State Research Institute Centre for Physical Sciences and Technology, Vilnius, Lithuania;

*Corresponding author is Arunas Ramanavicius. e-mail address: arunas.ramanavicius@chf.vu.lt: corresponding author

Accepted: Article accepted on 7 February, 2020

Article ID: ELAN4671

Article DOI: 10.1002/elan.201900723

Internal Article ID: 16687620

Abstract

In this study the redox activity of human myocardium-derived mesenchymal stem cells (hmMSC) were investigated by redox-competition (RC-SECM) and generation-collection (GC-SECM) modes of scanning electrochemical microscopy (SECM), using 2-methylnaphthalene-1,4-dione (menadione, MD) as a redox mediator. The redox activity of human healthy and dilated hmMSCs was evaluated by measuring reduction of MD. Measurements were performed by approaching and retracting the UME from the surface of growing hmMSC cells. The current study shows that the RC-SECM mode can be applied to investigate integrity of cell membranes, whereas the most promising results were observed by using the GC-SECM mode and applying the Hill's equation for the calculation/fitting of dependencies of electrical current *vs* menadione concentration. The calculated apparent Michaelis constant (K_M) for the production of menadiol (MDH_2) in the pathological hmMSC cells was 14.4 folds higher compared to that of the healthy hmMSC revealing the lower redox activity of pathological cells. Moreover, the calculated Hill's coefficient n shows a negative cooperative binding between MD and healthy hmMSC and positive cooperative binding between MD and pathological hmMSC. It means that healthy hmMSC is of lower affinity to MD, which is also related to the better membrane integrity of healthy cells. Data of this study demonstrate that SECM can be applied to investigate intracellular redox and membrane changes ongoing

in human dilated myocardium-derived hmMSC in order to improve their functioning and further regenerative potential.

Keywords: Scanning electrochemical microscopy; Bioelectrochemistry; Mesenchymal stem cells; Redox activity of cells; Redox mediator; Menadione.

DOI: 10.1002/elan. 201900723

1. Introduction

Cardiomyopathies are a heterogeneous group of myocardial diseases associated with mechanical or electrical disorders of cells that cause inappropriate functioning of the left ventricle [1]. Various forms of cardiomyopathies are identified, while dilated cardiomyopathy (DCM) is considered to be the most prevalent and common form of cardiomyopathy in the world leading to heart failure and requirement of heart transplantation [2]. DCM occurs mostly in adults 20 to 60 years old and accounts for 10,000 deaths and 46,000 hospitalizations in the United States annually [3]. Acute myocarditis is the most usual cause of DCM leading to chronic heart failure [4]. DCM can be induced by many prolonged toxic exposures such as stress, diabetes, chemotherapeutic agents, toxins, alcohol intake and other [5]. Treatment of DCM is challenging regarding the complexity of disease and molecular mechanisms directly connecting intracellular and extracellular changes to heart tissue contraction [6]. Therefore, a search for new methods investigating redox changes between healthy and dilated myocardium-derived MSC is of particular importance with the purpose to improve functioning of diseased heart tissue.

Human myocardium-derived MSC (hmMSC) are fibroblast-like, abundant cell type playing a critical role in heart functioning and holding significant promise for the regeneration of injured heart tissue [7,8]. It was shown that fibroblasts and mesenchymal/stromal stem cells are phenotypically indistinguishable and can participate in myogenic regeneration processes [9]. Therefore, the intracellular redox homeostasis of cardiac-resident and non-resident mesenchymal stem cells is extremely important for the proper functioning of muscle tissue [10]. The redox imbalance is mainly caused by the excess of reactive oxygen species (ROS) or declined antioxidant system and is closely related to cardiovascular diseases and aging [11]. Therefore, the investigation of changed intracellular redox environment of human dilated myocardium-derived mesenchymal stem cells MSC, compared to the healthy heart cells, is of further therapeutic importance.

The intracellular activity of redox enzymes is mainly measured in pure enzymatic system, which does not correspond to their catalytic efficiency under regular cell growth conditions *in vivo* [12]. It was also shown that many factors, such as intracellular concentration of the enzymes, their oligomeric state, cell growth conditions and/or diffusion processes can strongly influence catalytic efficiency of enzymes *in vivo* and subsequent final cell response to the extracellular stimuli [13-15]. Therefore, the methods investigating redox status of human myocardium-derived cells should be non-invasive, non-destructive and be able to monitor intracellular redox processes under normal cell growth conditions with high sensitivity.

Scanning electrochemical microscopy (SECM) is a useful tool for the investigation of cells *in vitro* under their natural growth environment [16-21]. In general, SECM could be applied both for the visualization of electrochemically active surfaces and for the determination of reaction kinetics [22-25]. SECM is also suitable for the imaging of chemical gradients in the diffusion layer surrounding the cells and/or tissues and for the investigation of intracellular redox activity of living cells [26-28].

The redox competition mode of scanning electrochemical microscopy (RC-SECM) as well as generation-collection (GC-SECM) mode has been successfully used for the visualization of local catalytic activity in various biological cell systems [29]. RC-SECM at negative potential, registers reduction of mediator in the cells, whereas in GC-SECM mode the reductors of mediator are cells, and collector – UME [30].

In order to investigate the redox activity of healthy and pathological hmMSC by the RC-SECM and GC-SECM modes, a suitable redox mediator should be chosen, which should be able to reach the intracellular redox-active centers, be effectively reduced and released to the extracellular environment for detection. For this purpose, the menadione (MD), which is a synthetic form of K3 vitamin, is often used and being a small lipid soluble molecule (M.W. 172.2 Da) can purely diffusional penetrate cell membrane and simulate generation of intracellular $O_2^{\bullet-}$ [31,32]. It was shown that MD is a membrane-bound electron carrier with structure similar to that of ubiquinone, therefore, easy penetrating the cells [32]. MD can be used as electron carrier between electron-donating and electron-accepting enzyme complexes in the intracellular level [32,33]. It was also shown that menadione (vit. K3) is more enzymatically active comparing to K1 and K2 [34].

The main aim of this study was to investigate and compare redox activity of human healthy and dilated myocardium-derived hmMSC by registering the reduction of menadione using two non-invasive SECM modes, RC-SECM and GC-SECM, and calculation of Hill's parameters. To the best of our knowledge, the investigation of redox activity of human healthy and dilated myocardium-derived hmMSCs by the SECM technique were performed for the first time. The obtained data will allow to develop a new SECM technique-based biomodel system for the investigation of changed intracellular redox status and cell membrane integrity of healthy and diseased human heart primary cells in order to investigate new therapeutical means to regulate their proper functioning. The electrochemical biomodel system in the future will be investigated on other cell types as well.

2. Experimental

2.1. Materials

Phosphate buffer pH 6.5 containing 0.05M NaH_2PO_4, 0.05 M Na_2HPO_4 and 0.1 M KCl was prepared in distilled water. 2-methylnaphthalene-1,4-dione (MD) was dissolved in 96 % ethanol purchased from "UAB Vilniaus Degtine" (Vilnius, Lithuania). All the other chemicals used in the experiments were purchased from Sigma-Aldrich (St. Louis, USA). Iscove's Modified Dulbecco's Medium (IMDM) and fetal bovine serum (FBS) were purchased from Merck (Carrigtohill, Ireland). Fibronectin was purchased from Merck (Carrigtohill, Ireland) and gelatine from Calbiochem (San Diego, USA).

2.2. Isolation of human heart myocardium-derived mesenchymal stem cells from human ventricle myocardium

Human heart muscle biopsies were obtained from the left ventricle of healthy (patients with mitral valve disease, non-dilated left ventricle and with a preserved left ventricle function) and pathological dilated myocardium during clinically indicated (mitral valve surgery, heart transplantation, left ventricle assist device implantation) procedures after informed consent.

Left ventricle tissue specimens were stored on ice and transported to the laboratory for the isolation of the hmMSC. hmMSC were isolated following previously described protocols with some modifications [35]. Briefly, the myocardial specimens were cut into fragments less than 1 mm^3, washed properly with PBS with 2 % of antibiotics and partially digested with trypsin. Tissue fragments were cultured as tissue explants on fibronectin (2 mg/ml) coated 6 well plates in IMDM supplemented with 20% FBS and 100 U/ml penicillin G, 100 U/ml streptomycin. Approximately in 1-3 weeks, a layer of spindle shape cells emerged. Cardiac outgrowth cells, close to the confluence, were lifted with trypsin and transferred to the 75 cm^2 flask coated with gelatine for further growth. The remaining tissues were transferred to the plates coated with the fibronectin for further formation of cardiac outgrowth. Cardiac

outgrowth can be harvested up to four times from the same explants. Isolated hmMSC were identified for the main MSCs markers [36]. For the electrochemical experiments $5x10^3$ of the normal and pathological hmMSC were seeded on 12 mm cover glass and were grown in 3 cm diameter Petri dishes in the IMDM with 10 % of FBS, antibiotics and 25 mM of HEPES for the next 24 hours. Cells attached to the glass surface were placed into an electrochemical SECM cell. The measurement of one cell sample lasted not longer than 30 min, which did not significantly change cell viability (less than by 5 percent) measured by CCK-8 reagent (data not shown).

2.3. Ethical statement

This study was conducted according to principles expressed in the declaration of Helsinki. The study was approved by the local Ethic Committee (license No. 158200-14-741-257). All patients gave written informed consent to include their data in the study for each investigational procedure.

2.4. Investigation of human heart myocardium-derived mesenchymal stem cells by scanning electrochemical microscopy

SECM and a disk-shaped Pt-based UME with Rg value of 10, which represents a ratio between the radius of the insulating and the radius of the conducting part of the UME, both were purchased from Sensolytics (Bochum, Germany) and were used for SECM-based experiments. Measurements were performed using a potentiostat Autolab 80 from Metrohm AG (Herisau, Switzerland). Before the experiment, the UME was cleaned by ethanol, then it was polished with 0.3 μM grain-size polishing paper, after this it was electrochemically pretreated in 0.5 M H_2SO_4 by potential cycling in the potential range between –0.2 V and 1.2 V *vs* Ag/AgCl and lastly it was washed with deionized water. Measurements were performed in a three-electrode electrochemical cells to which the UME was connected as a working electrode, Pt wire was used as an auxiliary/counter electrode and Ag/AgCl in 3M KCl served as a reference electrode. Electrochemical measurements of the hmMSC were performed in IMDM with 10 % of FBS and antibiotics at different concentrations of MD.

The location of the hmMSC was determined by optical microscope CETI from Medline Scientific (Oxford, United Kingdom) with a digital camera (magnification of CETI microscope is SP 40x / 0.65 / 160 / 0.17) and additionally checked by scanning the cells laterally in a horizontal direction using the feedback mode of the SECM (FB-SECM) at 20 μm of vertical distance from the cell's surface. The step length was 1 μm, the scanning speed – 10 μm/s and the applied potential – -500 mV *vs* Ag/AgCl in culture medium. At initial phase of this research, experiments for the determination of cell condition and the distance between the UME and the cell were performed. The distance between UME and cell surface was found in the following way: UME was approached to the plate surface at -500 mV without menadione in order to register current of oxygen reduction at negative feedback mode. The UME then was retracted from the plate surface at 10 μm distance, and horizontal scan in order to find the localization of the cell was performed. The location of cell was detected by diffusion effect: UME was placed above the cell and current was registered by approaching cell at negative feedback mode. The distance between UME and cell surface was determined from approaching curve.

The approaching and retracting curves were registered by moving the UME in a vertical (z) direction, at 1 μm/s speed, 1 μm step. The consumption of MD and reactive oxygen species (ROS) in the cells generated an electrical current, which was measured at -500 mV *vs* Ag/AgCl, while the reduced MD was measured at +400 mV *vs* Ag/AgCl. The experiments were carried out in the following order: the UME was set to a negative potential and brought as close as possible to the cell's bottom surface. Afterwards, the electrochemical cell/bath was switched off immediately (voltage switching mode) [37-39]. After adding a known amount of redox mediator, the media was mixed gently, a positive potential was applied and the UME was retreated at 200 μm from the cell's surface.

2.5. Evaluation of cell morphology

The morphology of human heart biopsies-derived hmMSC were investigated by light microscope Nikon Eclipse TS100 inverted microscope (USA). The cells were also measured by Bioscope Catalyst AFM and Scanasyst-fluid cantilevers from Bruker (Massachusetts, USA). According to the manufacturer's datasheet, the spring constant of the cantilever was 0.7 N/m, the resonance frequency 150 kHz and the tip radius was 20 nm. The cells were examined in culture medium by scanning them horizontally in a contact mode.

2.6. Calculation and statistics

The steady-state diffusion-controlled current, used in order to normalize the experimentally observed current, is related to the initial concentration of the redox active species when the UME is far from the surface [40]:

$$i_{T\infty} = 4\, n_e\, F\, D\, C\, a \qquad [1]$$

where i_T is the current of the UME tip, n_e is the number of electrons involved in the reaction on the UME, F – Faraday's constant, D – diffusion coefficient, C – concentration of the mediator (menadione) and a – radius of the UME.

A modified Hill's equation was used to calculate the cooperativity of menadione towards the cells [41]:

$$i_T = i_{max}[MD]^n/(k^n + [MD]^n) \qquad [2]$$

where i_T – current of the UME tip, n – Hill's number, k – constant, which is equal to the concentration of menadione at which half of the maximal current was registered. According to a physical meaning, the k was similar to apparent Michaelis constant, which is often used in basic enzymatic catalysis described by Michaelis-Menten kinetics.

Statistical analysis was performed using Excel programme at 5% significance level. Data are presented as means ± standard error (Mean ± SEM). *Data were significant at $p \leq 0.05$ by measuring not less than three cells from three independent experiments.

3. Results and discussion

3.1. Identification of hmMSC morphology, location and SECM parameters

The morphology of human heart biopsies-derived hmMSC were investigated by optical microscope and AFM (Fig. 1). The image represented in (Fig. 1a) show hmMSC obtained by outgrowth method. Healthy (Fig. 1b) and pathological (Fig. 1c) hmMSC had fibroblast-like morphology, however, the pathological hmMSC were slightly larger and more flattened compared to the healthy hmMSC. Similar observations were confirmed by AFM (Fig. 1d and 1e).

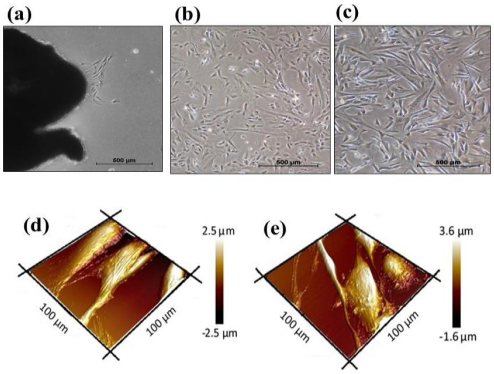

Fig. 1. Morphology images of healthy and pathological hmMSC. (a) Explant outgrowth of hmMSC; (b) Healthy hmMSC; (c) pathological hmMSC; (d) AFM image of healthy hmMSC; (e) AFM image of pathological hmMSC.

Before SECM-based evaluation of hmMSC, the most convenient SECM parameters were chosen: 1 to 200 µM of menadione were added to the cell growth media without the cells and a cyclic voltammetric curve was registered (Fig. 2). The cell growth media with menadione showed most stable current at potential range between -200 and -400 mV. The selected potential of -500 mV was within the Faraday current range and has been used for the further measurements as a negative potential. By the measured sigmoidal cyclic voltammetric curve in positive potential range, the current was mostly stable at potential between +300 mV and +400 mV. The +400 mV potential

was chosen for further evaluation in order to prevent any Faraday process in solution and to record current changes occurring only due to the products released by the cells (Fig. 2). Positive and negative potentials for further experiments were chosen based on CV curves.

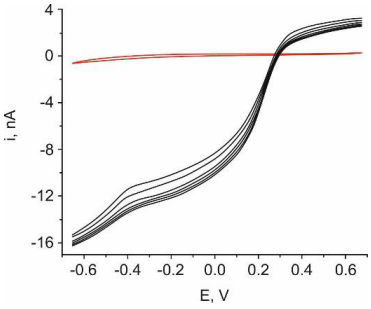

Fig. 2. Cyclic voltammogram (CV) without the cells. Red line - CV in cell growth media. Black line - cell growth media with 10 µM of menadione. Scan speed - 0.01 V/s, potential range was from 0.65 V to -0.65 V, step of potential 0.005 V.

The cell position was firstly determined by the optical microscope (Fig. 3b). After this, the cell location was identified by horizontal scanning at negative feedback mode at the distance of 15 µm without adding additional electrolytes or mediators to the culture medium - cell growth medium contains electrolytes sufficient to perform electrochemical measurements [41]. The lowest current point (Fig. 3a) shows the cell location, i.e. the diffusion of electrolytes from the cell to the UME was blocked due to the close proximity of UME to the cell membrane. The decrease of current value from 1.5 nA to 0.5 nA was reliable to confirm the location of the cell. The point marked by an arrow (Fig. 3a) was chosen for the further vertical cell scans by the SECM. Cell position was also confirmed by light microscope (Fig.3b).

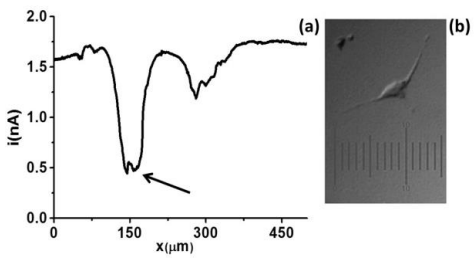

Fig. 3. Determination of hmMSC position. (a) Horizontal scan at feedback mode over cell surface, step - 0.5 µm, approaching rate - 10 µm/s. Arrow points cell position where vertical scan was performed. (b) Light microscope image of selected hmMSC.

3.2. Investigation of intracellular redox conversions by SECM

In a SECM experiment the current is registered by the UME in culture medium containing MD at varying distances from the immobilized cells (Scheme 1). MD diffuses through the cell membrane and is reduced by an intracellular nicotinamide adenine dinucleotide phosphate (NAD(P) NAD(P)H)-depending enzymes that transfer two electrons and two protons to MD [42-45]. The reduced form of MD - menadiol (MH_2) is a lipophilic compound, which can diffuse from the intracellular part of the cell to the extracellular solution. In the RC-SECM mode, the UME registers the current, which is directly proportional to the amount of MD in solution (Scheme 1a). The dependencies of current *vs* distance were registered in the RC-SECM mode by vertical (z-direction) approaching to the cell's surface. The GC-SECM experiments were performed at positive potential retracting the UME from the cell surface in order to evaluate the presence of menadiol.

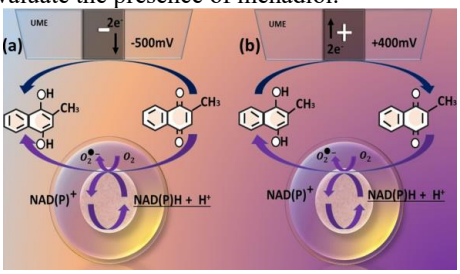

Scheme 1. SECM-based investigations of redox-conversion of menadione to menadiol in both types

of human heart hmMSC. (a) Using RC-SECM mode. (b) Using GC-SECM mode.

The apparent catalytic constant and cooperative binding were calculated from the obtained data registered at different distances from the cell surface that can be used in addition to the redox properties to evaluate many other intracellular parameters: the stability of intracellular processes [46] binding of various ligands to the recipient [31,47-49], an interaction between nucleic acids and proteins, for instant, between DNR and transcription factors [46] and show reversible enzymatic reactions, biochemical switches, function of ion channels, calcium binding to the calmodulin and other [46,50]. However, the cooperative binding during the investigation of intracellular redox processes in human heart myocardium-derived hmMSC has not been studied.

The current changes were registered near the cell's surface, which can be described by the following equations [42]:

RC-SECM mode of detection of MD:

$$MDH_2 + O_2 \leftrightarrows MD^{\bullet-} + O_2^{\bullet-} + 2H^+ \quad [3]$$

$$MD^{\bullet-} + O_2 \leftrightarrows MD + O_2^{\bullet-} \quad [4]$$

$$\mathbf{O_2^{\bullet-} + MD + 1e^- \leftrightarrows O_2 + Semiquinone \leftrightarrows O_2^{\bullet-} + Semiquinone + 1e^- \leftrightarrows O_2 + Hydroquinone} \quad [5]$$

GC-SECM mode of detection of MDH_2:

$$2NAD(P)H + 2H^+ + MD \leftrightarrows 2NAD(P)^+ + MDH_2 \quad [6]$$

$$MDH_2 \leftrightarrows MD + 2H^+ + 2e^- \quad [7]$$

MD - menadione

MDH_2 – menadiol;

$MD^{\bullet-}$ – semiquinone radical of menadione;

FBS adsorption to the electrode might be a problem measuring living cells. Therefore, the measurements in this study were done over three steps: first, an approaching curve was registered at a negative -500 mV potential in the absence of redox mediator in the solution; second, the mediator was added to the solution and finally – retracting curve was registered at a positive +400 mV potential. In such a measurement, the only menadiol, released from the cell, could be detected with minimal influence of FBS.

3.3. Investigation of human heart hmMSC by the RC-SECM mode.

First of all, the cell surface was found in a negative feedback mode using a potential of -500 mV. The potential was further changed to +400 mV and after addition of MD the electrode was withdrawn from the cell in GC mode, identifying a reduced MD. At the distance of 100 μm, the potential has been changed again to -500 mV and the electrode was moved towards the cell in order to ensure that the cell was not pierced or moved, i.e. whether the distance from the electrode to the cell has not been changed or the electrode was not blocked. In addition, change of potential allowed to perform tests without significantly blocking an electrode: the current at the negative potential reduced oxidized forms of some redox/able compounds and repelled negatively charged ions away from the electrode.

Hence, the dependencies of current *vs* distance in healthy hmMSC were registered by RC-SECM mode approaching the UME to the hmMSC (Fig. 4a). The approaching curve at the beginning was done without menadione, where the only breathing products and some amount of electrolytes as a "base line" near the cell surface can be detected. The current was decreasing due to hindered diffusion when UME was close to the cell's surface. At the MD concentration range from 4 μM up to 10 μM, the current generated by the reduction of MD became significantly higher than the diffusion-limited current. The increase of current measured by the RC-SECM mode showed the highest MD concentration close to the cell's surface.

In order to evaluate the rate of MD uptake by healthy hmMSC, the experimental data were

plotted as dependence of current *vs* concentration (Fig. 4b). The MD consumption phenomenon is seen at 0 µm and 1 µm distances. At 0 µm distance the current is decreasing up to 2 µM concentration of MD. At higher than 2 µM concentrations of MD, the current was increasing along with the MD concentration, showing that the measured current was no longer related to the consumption of MD by the cells. When the concentration of MD has reached 4 µM, the increase of the current was no longer dependent on the concentration of MD.

The similar experiment has been performed with the pathological hmMSC. The uptake of MD by the pathological hmMSC has been registered first of all without MD and then with the 1 µM of MD (Fig. 4c). The significant increase of current was observed already at 2 µM of MD compared to the 4 µM for the healthy cells. It shows that the pathological cells are less able to reduce MD. When the concentration of MD reached 5 µM, the current became constant independently of the increasing concentration of MD. So, the best uptake of MD by the pathological cells was observed at MD concentration lower than 5 µM (Fig. 4d).

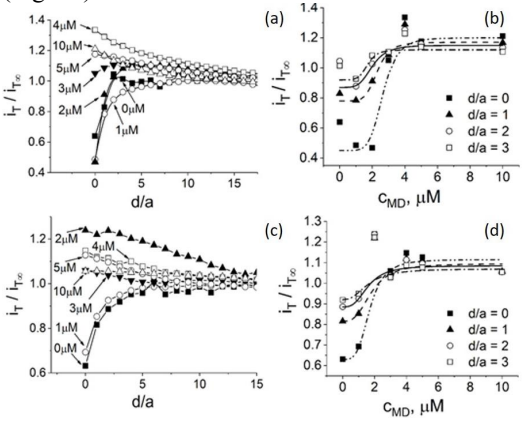

Fig. 4. The investigation of healthy and pathological hmMSC by RC-SECM mode. The dependence of normalized current on the distance between the UME and healthy (a) hmMSC, and between the UME and pathological (c) hmMSC at 500 mV *vs* Ag/AgCl. The dependence of current on MD concentration in healthy (b) and pathological (d) hmMSC.

Fitting of data obtained by RC-SECM (dependence of current *vs* MD concentration) by Hill's function showed a positive cooperative binding n > 1 for both healthy and pathological hmMSC, which means that the affinity of MD for both type of hmMSC is increasing with the increase of MD concentration (Table I). The Hill's coefficients n for the healthy hmMSC were two folds higher than that for the pathological hmMSC (n = 6 for healthy; n = 3 for pathological) revealing that pathological hmMSC can faster take up MD and faster start to release menadiol. It might be also related to the increased permeability of membrane of pathological hmMSC.

Comparing the MD concentrations, at which half of the reaction rate was achieved, we can conclude, that healthy hmMSC cells slower reacted to MD than pathological hmMSC: for healthy hmMSC k = 2.65 - 1.7; for pathological cells k = 1.7 - 1.6.

Table 1. Fitting parameters of the Hill's function for healthy and pathological hmMSC determined by RC-SECM mode.

Healthy hmMSC			**Pathological** hmMSC		
d/a	**k**	**n**	**d/a**	**k***	**n***
0	2.65±0.08	6±0.6	0	1.7±0.08	3.8±0.73
1	2.3±0,07	6±0.6	1	1.8±0.078	3±0,045
2	2±0,06	4.5±0.5	2	1.6±0.056	3±0.078
3	1.7±0,055	6±0.6	3	1.6±0.061	2.5±0.065

***** data are significant at $p \leq 0.05$ comparing healthy and pathological hmMSC.

3.4. Investigation of hmMSC by GC-SECM mode.

Both types of the cells were evaluated by the GC-SECM mode at +400mV *vs* Ag/AgCl potential (Fig. 5), which determines the reduced form of MD. It was determined that the healthy heart-derived hmMSC start to reduce MD immediately after its addition to the solution (Fig. 5a). The

significant increase of UME current in the healthy MSC cells after the addition of 1 μM MD can be explained by a very fast reaction of MD with NAD(P)H. At 5-10 μM of MD, the MD-related current is not decreasing any longer because healthy hmMSC reaches the threshold of MD reduction. The fitting Hills' equation to the dependence of current *vs* concentration did not show a sudden increase of the current at 1μM MD concentration (Fig. 5b).

The reaction of 1 μM MD with NAD(P)H in pathological hmMSC was less intensive than in healthy hmMSC but also very quick (Fig. 5c). It shows that redox capacity of pathological cells is lower compared to the healthy cells. However, at 2 μM of MD the dependence of current *vs* distance in pathological hmMSC showed 'negative feedback' (Fig. 5d). This effect can be related to the uptake of 2 μM of MD by the pathological hmMSC. Higher than 2 μM of MD concentrations (5-10 μM) did not show the increase of UME current. The fitting of the dependence of current *vs* MD concentration showed that 1 μM of MD is too low to generate registerable redox current in pathological hmMSC (Fig. 5d).

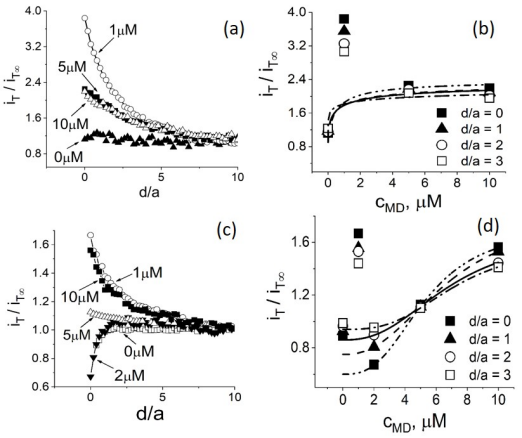

Fig. 5. The investigation of healthy and pathological human myocardium-derived hmMSC by GC-SECM mode. The dependence of normalized current on the distance between UME and healthy (a) hmMSC, and between UME and pathological (c) hmMSC at +400 mV *vs* Ag/AgCl. The dependence of current on MD concentration in healthy (b) and pathological (d) hmMSC.

Hill's coefficient n for the pathological human heart-derived hmMSC was higher than 1 (n > 1) showing the positive cooperative binding between MD and the pathological hmMSC (Table II). It shows that increasing MD concentration increases the affinity between MD and the pathological hmMSC, i.e. MD better penetrated to the pathological compared to the healthy hmMSC. This phenomenon could be explained by possible damage of pathological MSC cell membrane (Table II). The Hill's coefficient n for the healthy hmMSC cells was lower than 1 (n < 1), which means a negative cooperative binding between MD and healthy hmMSC, i.e. the affinity of MD to the healthy hmMSC decreases with the increase of MD concentration. Altogether, the lower MD affinity to the healthy compared to the pathological hmMSC can be related not only to the better redox capacities of healthy hmMSC but also to the more intact membrane of healthy hmMSC.

The data, presented in the Table II show that measurement of healthy and pathological hmMSC by GC-SECM mode allow to distinguish them by two main indications: (i) different cooperative binding, which is negative for the healthy and positive for the pathological hmMSC; (ii) significant difference between reaction rate (Michaelis constant *k* for pathological MSC cells was from 10.6 to 14.4 folds higher than for the healthy hmMSC).

Table 2. Fitting parameters of the Hill's function for healthy and pathological hmMSC determined by GC-SECM mode.

Healthy hmMSC			**Pathological hmMSC**		
d/a	**k**	**n**	**d/a**	**k***	**n***
0	0.5±0.063	0.8±0.062	0	5.3±1.3	2.8±0.074
1	0.5±0.076	0.55±0.078	1	6.7±1.2	2.4±0.067

2	0.5±0.0 52	0.52±0.0 2	2	6.9±1 .5	2.5±0.0 64
3	0.5±0.0 5	0.27±0.0 15	3	7.2±1 .5	3±0.07 2

It can be concluded, that the SECM system is suitable for the identification of membrane integrity and intracellular redox activities of healthy and pathological human heart myocardium-derived MSC and can be used for the selection and/or modification of stem cells for their further regeneration purposes.

4. Conclusions

The SECM technique allows to characterize and to identify electrochemically the redox differences between healthy and pathological left ventricle myocardium-derived MSC. The investigation of hmMSC by two different SECM modes (RC-SECM and GC-SECM) shows three main processes that occur in the hmMSC in the presence of menadiol (MDH2): (i) uptake of MD by the cells; (ii) reduction of MD inside the cells and (iii) release of MD. The investigation of MD uptake by RC-SECM mode additionally shows the integrity of membrane: the membranes of healthy hmMSC were more intact, compared to the pathological hmMSC, therefore, the pathological hmMSC consumed menadione faster.

Data of this study also show that healthy and pathological human myocardium-derived MSC can be characterized by the Hill's equation coefficient n, which shows the affinity between MD and hmMSC and was two folds higher for the healthy hmMSC than for the pathological hmMSC cells in RC-SECM measurements. Additionally, the reduction of menadione, identified by the GC-SECM mode, can be used for the investigation of intracellular redox changes between healthy and pathological hmMSC. The GC-SECM mode allows to distinguish healthy and pathological hmMSC by two main factors – different cooperative binding (n) between redox compound and the cells and apparent Michaelis constant (k), both calculated using Hill's equation of dependencies of current *vs* concentration. Hill's calculations showed that healthy hmMSC, detected by GC-SECM, had a negative binding of redox compound MD to the cells, whereas pathological MSC cells – positive, which suggests that healthy cells were more resistant to MD than pathological hmMSC. However, apparent Michaelis constant for the reduction of MD in pathological hmMSC cells was 10.6 - 14.4 folds higher, compared to that of the healthy hmMSC. It reveals that redox compound MD can better penetrate pathological cell, whereas its reduction is worse due to the reduced redox status of pathological hmMSC.

Hence, SECM is a promising tool for the identification of membrane integrity and reduction potential of healthy and pathological human left ventricle myocardium-derived MSC. The developed electrochemical biomodel system for the identification of intracellular redox status will be further exploited while applying modes of scanning electrochemical impedance microscopy for the investigation of other types of living cells for further purposeful regulation of their intracellular homeostasis.

3. Acknowledgements

Support by Lithuanian Research Council, Project No S-MIP-17-13 is acknowledged.

4. References

1. B. Maisch, M. Noutsias, V. Ruppert, A. Richter, S. Pankuweit, *Heart Fail. Clin.* **2012**, *8*, 53.
2. B. J. Maron, J. A. Towbin, G. Thiene, C. Antzelevitch, D. Corrado, D. Arnett, A. J. Moss, C. E. Seidman, J. B. Young, *Circulation*. **2006**, *113*, 1807
3. Mahmaljy, H., Singhal, M. *Dilated cardiomyopathy.* StatPearls. StatPearls Publishing StatPearls Publishing LLC., Treasure Island (FL), **2018**.
4. L. T. Cooper, *N. Engl. J. Med.* **2009**, *360*, 1526.
5. Hantson, P.,Clin. Toxic., **2019**. 57(1): p. 1-9.
6. K. Dadson, L. Hauck, F. Billia, *Clin. Sci.* **2017**, *131*, 1375.
7. S. A. Doppler, C. Carvalho, H. Lahm, M.-A. Deutsch, M. Dreßen, N. Puluca, R. Lange, M. Krane, *J. Thorac. Dis.* **2017**, *9*, S36.
8. Rossini, A., Frati, C., Lagrasta, C., Graiani, G., Scopece, A., Cavalli, S., Musso, E., Baccarin, M., Di Segni, M., Fagnoni, F. Germani, A., Cardiovascular research, **2010**, 89, 3, 650-660.
9. Denu, R.A., Nemcek, S., Bloom, D.D., Goodrich, A.D., Kim, J., Mosher, D.F. and Hematti, P., Acta haematologica, **2016**, 136 2, 85-97.

10. B. Subramani, S. Subbannagounder, C. Ramanathanpullai, S. Palanivel, R. Ramasamy, *Exp. Biol. Med.* **2017**, *242*, 645.
11. G. K. Sakellariou, A. P. Lightfoot, K. E. Earl, M. Stofanko, B. McDonagh, *J. Cachexia. Sarcopenia Muscle*. **2017**, *8*, 881.
12. A. Zotter, F. Bäuerle, D. Dey, V. Kiss, *J. Biol. Chem*. **2017,** *292*, 15838.
13. García-Contreras, R., Vos, P., Westerhoff, H.V., Boogerd, The FEBS journal, **2012**, 279, 22, 4145.
14. D. Davidi, E. Noor, W. Liebermeister, A. Bar-Even, A. Flamholz, K. Tummler, U. Barenholz, M. Goldenfeld, T. Shlomi, R. Milo, *Proc. Natl. Acad. Sci. U.S.A.* **2016,** *113***,** 3401.
15. Y. Phillip, V. Kiss, G. Schreiber, *Proc. Natl. Acad. Sci. U.S.A.* **2012,** *109*, 1461.[16] I. Morkvenaite-Vilkonciene, A. Ramanaviciene, A. Ramanavicius, *Sens. Actuat., B Chem.* **2016**, *228*, 200.
16. I. Morkvenaite-Vilkonciene, A. Ramanaviciene, A. Ramanavicius, *Sens. Actuat., B Chem.* **2016**, *228*, 200.
17. L. R. Giam, M. D. Massich, L. Hao, L. S. Wong, C. C. Mader, C. A. Mirkin, *Proc. Natl. Acad. Sci.* **2012**, *109*, 4377.
18. P. Sun, F. O. Laforge, T. P. Abeyweera, S. A. Rotenberg, J. Carpino, M. V. Mirkin, *Proc. Natl. Acad. Sci. U. S. A.* **2008**, *105*, 443.
19. B. Liu, W. Cheng, S. A. Rotenberg, M. V. Mirkin, *J. Electroanal. Chem.* **2001**, *500*, 590.
20. T. Murata, T. Yasukawa, H. Shiku, T. Matsue, *Biosens. Bioelectron.* **2009**, *25*, 913.
21. T. Kaya, Y. Torisawa, D. Oyamatsu, M. Nishizawa, T. Matsue, *Biosens. Bioelectron.* **2003**, *18*, 1379.
22. I. Morkvenaite-Vilkonciene, A. Ramanaviciene, A. Kisieliute, V. Bucinskas, A. Ramanavicius, *Biosens. Bioelectron.* **2019**, *141*, 111411.
23. R. Astrauskas, F. Ivanauskas, I. Morkvenaite‐Vilkonciene, A. Ramanavicius, *Electroanalysis*. **2019**, *31*, 2214.
24. S. A. Rotenberg, M. V Mirkin, *J. Mammary Gland Biol. Neoplasia*. **2004**, *9*, 375.
25. L. Yao, F. P. Filice, Q. Yang, Z. Ding, B. Su, *Anal. Chem.* **2019**, *91*, 1548.
26. I. Beaulieu, S. Kuss, J. Mauzeroll, M. Geissler, *Anal. Chem.* **2011***, 83,* 1485.
27. L. P. Bauermann, W. Schuhmann, A. Schulte, *Phys. Chem. Chem. Phys.* **2004**, *6*, 4003.
28. A. Ueda, O. Niwa, K. Maruyama, Y. Shindo, K. Oka, K. Suzuki, *Angew. Chemie-International Ed.* **2007**, *46*, 8238.
29. Conzuelo, F., A. Schulte, Schuhmann, W., Proc. of the Royal Soc. A: Math., Phys. and Eng. Sc., **2018**, *474*, 2218, 20180409.
30. Eckhard, K., Chen, X., Turcu, F. Schuhmann, W., *phys. chem. chem. phys*., **2006**, *8*,45, 5359.
31. J. Mauzeroll, A. J. Bard, *Proc. Natl. Acad. Sci. U. S. A.* **2004**, *101*, 7862.
32. V. Shneyvays, D. Leshem, Y. Shmist, T. Zinman, A. Shainberg, *J. Mol. Cell. Cardiol.* **2005**, *39*,149.
33. Jan, J.R. Richardson, A.A. Baker, V., Mishin, D.E. Heck, D.L. Laskin, J.D. Laskin, *Toxic. Appl. Pharm.* **2015**, *288,* 114.
34. Okayasu, H., Ishihara, M., Satoh, K., Sakagami, H., Anticancer research, **2001**, *21*,4A, 2387 .Y.H.
35. D. R. Davis, Y. Zhang, R. R. Smith, K. Cheng, J. Terrovitis, K. Malliaras, T.-S. Li, A. White, R. Makkar, E. Marbán, *PLoS One*. **2009**, *4*, e7195.
36. Garikipati, V.N.S., Singh, S.P., Mohanram, Y., Gupta, A.K., Kapoor, D., Nityanand, S., PLoS One, **2018,** *8*, 13, 2, e0192244
37. Y. Takahashi, A. I. Shevchuk, P. Novak, B. Babakinejad, J. Macpherson, P. R. Unwin, H. Shiku, J. Gorelik, D. Klenerman, Y. E. Korchev, et al., *Proc. Natl. Acad. Sci.* **2012**, *109*, 11540.
38. Y. Takahashi, *Electrochemistry*. **2016**, *84*, 662.
39. H. Yamada, D. Haraguchi, K. Yasunaga, *Anal. Chem.* **2014**, *86*, 8547.
40. A. J. Bard, M. V Mirkin, *Scanning Electrochemical Microscopy*, Marcel Dekker, NY, **2001**.
41. A. Ramanavicius, I. Morkvenaite-Vilkonciene, A. Kisieliute, J. Petroniene, A. Ramanaviciene, *Colloids Surf. B*. **2017**, *149*, 1.
42. S H. (Helmut) Sies, L. Packer, *Quinones and Quinone Enzymes. Part B*, *Vol 382* Elsevier Academic Press **2004**, pp.423,359.
43. A. Heiskanen, J. Emnéus, *Monitoring of Cellular Dynamics with Electrochemical Detection Techniques,* Springer **2011**.
44. D. Koley, A. J. Bard, *Proc. Natl. Acad. Sci. U. S. A.* **2012**, *109*, 11522.
45. W. Ying, *Antioxid. Redox Signal.* **2008**, *10*, 179.
46. M. I. Stefan, N. Le Novère, *PLoS Comput. Biol.* **2013**, *9*, e1003106.
47. J. A. Mezick, C. Thomas Settlemire, G. P. Brierley, K. P. Barefield, W. N. Jensen, D. G. Cornwell, *Biochim. Biophys. Acta.* **1970**, *219*, 361.
48. J.J. Tyson, K.C. Chen, B. Novak, *Current opinion in cell biology* **2003***, 15,* 221.
49. J. J. Feher, Quantitative human physiology: an introduction. Academic press, **2017**, 859.
50. J. Keener, J. Sneyd, *Mathematical Physiology: I: Cellular Physiology*, Springer-Verlag, New York **2009.**

Vilniaus universiteto leidykla
Saulėtekio al. 9, LT-10222 Vilnius
El. p. info@leidykla.vu.lt,
www.leidykla.vu.lt
Tiražas 15 egz.